Order Number 9003490

Numerical study of the onset of instability in the flow past a sphere

Kim, Inchul, Ph.D.

The University of Arizona, 1989

U·M·I

300 N. Zeeb Rd.
Ann Arbor, MI 48106

NUMERICAL STUDY OF THE ONSET OF INSTABILITY IN THE FLOW PAST A SPHERE

by

Inchul Kim

A Dissertation Submitted to the Faculty of the

DEPARTMENT OF AEROSPACE AND MECHANICAL ENGINEERING

In Partial Fulfillment of the Requirements
For the Degree of

DOCTOR OF PHILOSOPHY
WITH A MAJOR IN AEROSPACE ENGINEERING

In the Graduate College

THE UNIVERSITY OF ARIZONA

1 9 8 9

THE UNIVERSITY OF ARIZONA
GRADUATE COLLEGE

As members of the Final Examination Committee, we certify that we have read the dissertation prepared by Inchul Kim

entitled NUMERICAL STUDY OF THE ONSET OF INSTABILITY IN THE FLOW PAST A SPHERE

and recommend that it be accepted as fulfilling the dissertation requirement for the Degree of Doctor of Philosophy.

Arne J. Pearlstein	Date 8/7/89
Chuan F. Chen	Date 7/19/89
Edward J. Kerschen	Date 7/31/89
Wilfred M. Greenlee	Date 7/18/89
Bruce J. Bayly	Date 17 July 1989

Final approval and acceptance of this dissertation is contingent upon the candidate's submission of the final copy of the dissertation to the Graduate College.

I hereby certify that I have read this dissertation prepared under my direction and recommend that it be accepted as fulfilling the dissertation requirement.

Dissertation Director	Date 8/7/89

STATEMENT BY AUTHOR

This dissertation has been submitted in partial fulfillment of requirements for an advanced degree at The University of Arizona and is deposited in the University Library to be made available to borrowers under rules of the Library.

Brief quotations from this dissertation are allowable without special permission, provided that accurate acknowledgment of source is made. Requests for permission for extended quotation from or reproduction of this manuscript in whole or in part may be granted by the head of the major department or the Dean of the Graduate College when in his or her judgment the proposed use of the material is in the interests of scholarship. In all other instances, however, permission must be obtained from the author.

SIGNED: Inchul Kim

DEDICATION

To my parents, wife Seunghee, and son Sungjun

ACKNOWLEDGMENTS

I am deeply grateful to my advisor, Professor Arne J. Pearlstein, for his advice and guidance in performing this work. Without his profound knowledge and help, this work would not have been completed. I also thank my other committee members, Professors C. F. Chen, Edward Kerschen, Wilfred Greenlee, and Bruce Bayly for their interest and suggestions concerning the dissertation. The willingness of Professor Chen and Professor Bayly to serve on my committee with relatively short notice is greatly appreciated.

I also wish to thank Professor Sadatoshi Taneda for providing copies of original figures from his 1956 paper in order that the comparison in Table 12 could be made.

Finally, I would like to thank my wife, Seunghee, for her endless love and support, and our son, Sungjun, who always brings joy to the family.

This work was performed with the support of NSF Grant MSM-8451157. I appreciate the provision of computing services at the Center for Computing and Information Technology in the University of Arizona and at the San Diego Supercomputer Center (CRAY X-MP/48) which is supported by the National Science Foundation.

TABLE OF CONTENTS

TABLE OF CONTENTS--continued

Page

LIST OF ILLUSTRATIONS

LIST OF ILLUSTRATIONS--continued

LIST OF TABLES

LIST OF TABLES--continued

ABSTRACT

Experiment shows that the steady axisymmetric flow past a sphere becomes unstable in the range $120 < Re < 300$. The resulting time-dependent nonaxisymmetric flow gives rise to nonaxisymmetric vortex shedding at higher Reynolds numbers. The present work reports a computational investigation of the linear stability of the axisymmetric base flow.

When the sphere is towed, fixed, or otherwise constrained, stability is determined solely by the Reynolds number. On the other hand, when the sphere falls due to gravity, the present work shows that a additional parameter, the ratio of fluid density to sphere density ($\beta = \rho_f/\rho_s$) is involved.

We use a spectral technique to compute the steady axisymmetric flow, which is in closer agreement with experiment than previous calculations. We then perform a linear stability analysis of the base flow with respect to axisymmetric and nonaxisymmetric disturbances. A spectral technique similar to that employed in the base flow calculation is used to solve the linear disturbance equations in streamfunction form for axisymmetric disturbances, and in a modified primitive variable form for nonaxisymmetric disturbances.

For the density ratio $\beta = 0$, which corresponds to a fixed sphere, the analysis shows that the axisymmetric base flow undergoes a Hopf bifurcation at $Re = 175.1$, with the critical disturbance having azimuthal wavenumber $m = 1$. The results are favorably compared to previous experimental work.

CHAPTER 1

INTRODUCTION

1.1 Motivation

Flow past a sphere is a classical problem in hydrodynamics, and is among other things, the simplest example of flow past a three-dimensional bluff body. When the Reynolds number is small enough, the flow past a sphere is laminar, steady, attached, and axisymmetric. As the Reynolds number increases, the flow becomes separated from the rear part of the sphere, and a secondary flow appears in the form of a standing eddy. Experiment shows that the laminar, steady, separated, axisymmetric wake behind a fixed sphere in a uniform flow becomes unstable at a Reynolds number (based on diameter) somewhere above 120, and eventually gives rise to temporally periodic nonaxisymmetric vortex shedding at a higher Reynolds number.

However, as discussed in §1.2, the details of the transition are not at all clear, with different investigators reporting different transition Reynolds numbers. For freely falling spheres, where one might expect the transition Reynolds number to depend on the fluid/sphere density ratio, no real conclusion can be drawn due to the limited amount of data and the fact that most previous investigators have been unaware of the potential importance of the density ratio, and so have reported neither the density ratio nor enough information to allow its calculation.

Current knowledge of transition in flow past a sphere is limited to the conclusions obtained from trajectory measurements for freely falling spheres, and flow

visualization experiments for fixed and falling spheres. As stated by Nakamura (1976) in reference to the previous analytical and numerical calculations of the steady axisymmetric solution, "None of the theoretical workers, however, has predicted the critical Reynolds number at which the wake behind a sphere becomes unstable."

In addition to the fundamental fluid mechanical interest of the present work, there are many applications in which the development of the more complicated unsteady, nonaxisymmetric velocity field can have an important influence on the rates of heat and mass transfer to and from the sphere, as well as a profound effect on the trajectory of the sphere in the event that it is not fixed. Among such applications are a number in which the range of relevant Re overlaps the transition range $100 < Re < 300$, including

a) the dissolution and motion of dye crystals in flow visualization experiments (Harms & Wiegel 1979)

b) heat and mass transfer to particles entrained in a high temperature gas in the production of molybdenum, zirconium, and titanium from their ores or concentrates, as well as in the production of ferro-alloys such as ferrovanadium and ferrocolumbium. The short contacting times require accurate knowledge of heat and mass transfer to and from the particles in the design, operation, and optimization of these electrometallurgical process (Sayegh & Gauvin 1979)

c) the motion of metal particles added to solid propellant rocket fuels to increase the specific impulse (Zarin & Nicholls 1971)

d) the motion of sedimenting particles in natural waters, for which the settling rate "is one of the most important factors affecting the erodibility and movement of earth material" (Stringham, Simons & Guy 1969)

e) the motion of small particles in numerous gas-solid fluidization processes (Cheremisinoff & Cheremisinoff 1984)

f) the settling of particles in clarifiers, sedimentation processes, and other unit operations in the chemical and process industries.

There are also many situations involving the motion of small liquid droplets in a gas for which the deformation and internal circulation of the drop are unimportant, and the motion of the drop, as well as the wake behind it do not differ significantly from the rigid sphere case (Beard 1976). The velocity field in the wake region and the effect of instability on droplet motion are important factors in the

g) "rotation, oscillation, spinning, and swerving of falling burning drops" (Natarajan 1974)

h) spray deposition of refractory and erosion resistant coatings (Vardelle et al. 1983)

i) determination of collision frequencies, coalescence and breakup, rates of scavenging of pollutant gases (such as oxides of sulfur in acid rain formation), evaporation/condensation, and particulate capture for both cloud and precipitation drops, as well as related problems in the spray scrubbing of effluent gases (Wang & Pruppacher 1977, Suneja 1973)

j) analysis of heat and mass transfer in spray column heat exchangers (Letan and Kehat 1968)

k) study of transport phenomena and motion of "Significant portions of the droplets in sprays to quench fires, nuclear reactor emergency core cooling sprays, and high temperature sprays (which) can have Reynolds numbers on the order of 100" (Harpole 1977).

1.2 Previous Work

At sufficiently small Reynolds numbers, flow about bluff bodies is known to be attached and steady. At higher Reynolds numbers, the flow becomes separated, unsteady, and ultimately turbulent.

In recent years, the process by which this transition occurs has been extensively studied for two-dimensional bodies, both experimentally (Provansal, Mathis & Boyer 1987) and theoretically (Monkewitz & Nguyen 1987, Monkewitz 1988a). In the case of a circular cylinder (Thoman & Szewczyk 1969, Lin, Pepper & Lee 1976, Jackson 1987, Zebib 1987), the first stage in the transition is found to be a wake instability of the separated steady flow, leading to a time-periodic two-dimensional flow with considerable concentration of bound vorticity in the near wake adjacent to the body. As Re is increased, this flow may in turn give rise to the shedding of fluid parcels with concentrated vorticity ("vortex shedding"), and eventually to turbulence.

For axisymmetric bodies, the transition is less well understood, despite the considerable experimental progress that has been made for axisymmetric wakes of slender (Hama & Peterson 1976, Peterson & Hama 1978, Sato & Okada 1966) and bluff (Achenbach 1974, Fuchs, Mercker & Michel 1979, Goldburg & Florsheim 1966, Jayaweera & Mason 1965, Kim & Durbin 1988, Masliyah 1972, Willmarth, Hawk & Harvey 1964) bodies of revolution. We note that for nonspherical bodies of revolution, experiments may be plagued by the need for extremely precise alignment of the body's axis with the flow direction (Hama et al. 1977).

On the theoretical side, there have been several studies of the stability of axisymmetric parallel velocity profiles as models of axisymmetric wakes (Batchelor & Gill 1962, Gold 1963, Lessen & Singh 1973, Monkewitz 1988b). Batchelor & Gill

performed an inviscid stability analysis of a family of parallel axisymmetric velocity profiles appropriate to jets and wakes, and found the critical azimuthal wavenumber to be m = 1. Gold extended this approach to compressible flows, and found the same critical azimuthal wavenumber. Lessen and Singh extended the approach of Batchelor & Gill by including the viscous terms in the disturbance equations, and also found m = 1 to be the critical azimuthal wavenumber. More recently, Monkewitz (1988b) has also considered, on a viscous basis, the linear stability of incompressible axisymmetric parallel wake profiles, including those appropriate to bluff bodies of revolution. Monkewitz has established conditions under which these parallel flows are absolutely unstable with respect to m = 1 disturbances.

The prototypical axisymmetric flow is that generated by a sphere in a uniform flow. At low Reynolds numbers, the flow is steady, axisymmetric, and remains attached. In the classical experiments of Taneda (1956), separation is first observed at Re $\cong$ 24. (All Reynolds numbers referred to herein are based on diameter.) As Re increases, the downstream extent of the recirculating wake becomes progressively longer, and the separation circle on the sphere moves forward from the rear stagnation point. At values of Re in the range 120 < Re < 300, experiment shows that the steady axisymmetric flow loses its stability (henceforth referred to as the first transition, with corresponding Reynolds number Re_1) and the motion becomes unsteady and nonaxisymmetric. There is considerable uncertainty in the experimental value of Re_1 (Goldburg & Florsheim 1966, Möller 1938, Nakamura 1976, Roos & Willmarth 1971, Taneda 1956, Toulcova & Podzimek 1968, Zikmundova 1970).

The experimental determination of Re_1 in conventional wind/water tunnel facilities is complicated by three factors. First, the presence of a sting or other

support is known to have a strong influence on the stability of the sphere wake (Roos 1968, Roos & Willmarth 1971). This leads to the hypothesis that Re_1 depends rather delicately on the details of the base flow. Second, because the onset of unsteadiness occurs as a weak, low-frequency oscillation, the instability may not be easily discernible. Third, free-stream turbulence is known to have a influence on the Reynolds number at which vortex shedding occurs (Zarin 1970), and may also effect Re_1. The first of these problems can be avoided by use of a magnetic suspension balance or some other noninterfering support (Zarin 1970). The third can be avoided by towing the sphere through otherwise quiescent fluid (Möller 1938, Roos & Willmarth 1971). The first problem can be avoided and the third can in large part be eliminated by using freely falling or rising spheres. Unfortunately, this introduces a possible coupling of the rigid body motion of the sphere to the nonaxisymmetric instability of the wake (through the no-slip boundary condition on the surface of the sphere). This may in turn lead to a reduction in Re_1 for freely falling/rising spheres. For either fixed or falling/rising spheres, the weakness of the oscillations at the onset of instability presents a formidable challenge to the experimental determination of Re_1.

The stability of the steady axisymmetric flow is especially important because the breakdown to nonaxisymmetric vortex shedding at higher Re appears to occur via an intermediate stage involving nonaxisymmetric wake oscillations. Although the recent work of Kim & Durbin (1988) has substantially clarified the previously muddled (Achenbach 1974, MacCready & Jex 1964, Möller 1938, Preukschat 1962, Shafrir 1965, Sheth 1970, Stringham, Simons & Guy 1969, Viets 1971, Viets & Lee 1971) nature of the vortex shedding at higher Re, there is still relatively little known about the

mechanism by which the transition from nonaxisymmetric wake oscillations to vortex shedding occurs. Obviously, a first step in unravelling the transition process is the determination of the Re at which the first transition occurs.

In the one previous theoretical investigation of the problem, Kawaguti (1955) used a Galerkin approximation to the steady axisymmetric base flow. A Galerkin calculation showed that the base flow became unstable with respect to axisymmetric disturbances at $Re_1 = 51$, which is at variance with both the range of experimentally determined Re_1, and with the nonaxisymmetric nature of the flow above Re_1 (Kendall 1964, Goldburg & Florsheim 1966, Roos & Willmarth 1971).

1.3 Development of the Governing Equations

In this section, we present the Navier-Stokes equations for the flow of a viscous incompressible fluid about a sphere, along with the rigid body equations of motion for the sphere.

We begin with the equations of motion for a constant property, incompressible Newtonian fluid

$$\nabla \cdot \mathbf{V}_f = 0 \tag{1.1a}$$

$$\frac{\partial \mathbf{V}_f}{\partial t} + (\mathbf{V}_f \cdot \nabla)\,\mathbf{V}_f = -\frac{1}{\rho_f}\nabla p + \nu \nabla^2 \mathbf{V}_f - g\mathbf{k} \tag{1.1b}$$

and a sphere that falls (or rises) freely through the fluid due to gravity (Happel & Brenner 1965, p. 30, and Likins 1973, p. 440)

$$m_s \frac{d\mathbf{V}_s}{dt} = -m_s g\mathbf{k} + \int_{S_t} d\mathbf{S} \cdot \boldsymbol{\sigma} \tag{1.1c}$$

$$\mathbf{I} \cdot \frac{d\Omega}{dt} + \Omega \times \mathbf{I} \cdot \Omega = \int_{S_t} \mathbf{r} \times (d\mathbf{S} \cdot \sigma) \tag{1.1d}$$

$$\mathbf{V}_f = \mathbf{V}_s + \Omega \times \mathbf{r} \qquad \text{on } S_t. \tag{1.1e}$$

Here, we have defined the velocities in an inertial reference frame for which the fluid is at rest far away from the sphere. Equation (1.1e) is the no-slip boundary condition at the surface of the sphere. We have used the notation:

- $\mathbf{V}_f$ - local fluid velocity
- $\mathbf{V}_s$ - center of mass velocity of the sphere
- p - pressure
- g - gravitational acceleration
- $\mathbf{k}$ - unit vector in vertical direction (positive upwards)
- m_s - mass of the sphere
- $\mathbf{I}$ - inertia tensor of the sphere
- ν - kinematic viscosity of the fluid
- ρ_f - density of the fluid
- σ - stress tensor
- Ω - angular velocity of the sphere
- $\mathbf{r}$ - position vector from the center of the sphere
- $d\mathbf{S}$ - surface element on the sphere
- S_t - instantaneous locus of points on the sphere

If we define a hydrodynamic pressure $P = p + \rho_f gz$, we then have

$$\nabla \cdot \mathbf{V}_f = 0$$

$$\frac{\partial V_f}{\partial t} + (V_f \cdot \nabla)\, V_f = -\frac{1}{\rho_f}\nabla P + \nu\nabla^2 V_f$$

$$m_s \frac{dV_s}{dt} = (\rho_f \forall_s - m_s)gk + \int_{S_t} dS \cdot H$$

$$I \cdot \frac{d\Omega}{dt} + \Omega \times I \cdot \Omega = \int_{S_t} r \times (dS \cdot H)$$

$$V_f = V_s + \Omega \times r \qquad \text{on } S_t,$$

where $\forall_s$ is the sphere volume, $H = \sigma - \rho_f gzE$, and E is the isotropic unit tensor.

This formulation has the decided disadvantage that the sphere's location is an unknown function of time, to be determined as a part of the solution of, say, an initial value problem. We therefore refer the fluid velocity to a nonrotating, noninertial frame moving with the center of mass of the sphere. Thus, $V_{fm} = V_f - V_s$ is the fluid velocity in the moving frame. Hence, the location of the sphere is known, and we have

$$\nabla \cdot V_{fm} = 0$$

$$\frac{dV_s}{dt} + \frac{\partial V_{fm}}{\partial t} + (V_{fm} \cdot \nabla)\, V_{fm} = -\frac{1}{\rho_f}\nabla P + \nu\nabla^2 V_{fm}$$

$$m_s \frac{dV_s}{dt} = (\rho_f V_s - m_s)gk + \int_{S_o} dS \cdot H$$

$$I \cdot \frac{d\Omega}{dt} + \Omega \times I \cdot \Omega = \int_{S_o} r \times (dS \cdot H)$$

$$\mathbf{V}_{fm} = \Omega \times \mathbf{r} \qquad \text{on } S_o,$$

$$\mathbf{V}_{fm} \to -\mathbf{V}_s \qquad \text{as } |\mathbf{r}| \to \infty ,$$

where S_o is the (known) surface of the sphere.

Introducing the nondimensionalization

$$t = \frac{a}{V_o}t' \qquad \Omega = \frac{V_o}{a}\Omega' \qquad \mathbf{V}_s = V_o\mathbf{U}_s \qquad \mathbf{V}_{fm} = V_o\mathbf{U}_f$$

$$\mathbf{I} = \frac{2}{5}\, m_s a^2 \mathbf{I}' \qquad \mathbf{r} = a\mathbf{r}' \qquad P = \rho_f V_o^2 \Phi \qquad \mathbf{H} = \rho_f V_o^2 \mathbf{H}' ,$$

where a is the radius of the sphere, and V_o is the steady downward velocity at which the sphere will fall according to the "standard drag curve", we obtain

$$\nabla \cdot \mathbf{U}_f = 0 \tag{1.2a}$$

$$\frac{d\mathbf{U}_s}{dt} + \frac{\partial \mathbf{U}_f}{\partial t} + (\mathbf{U}_f \cdot \nabla)\,\mathbf{U}_f = -\nabla\Phi + \frac{2}{Re}\nabla^2\mathbf{U}_f \tag{1.2b}$$

$$\frac{d\mathbf{U}_s}{dt} = -C_D\,\frac{3\beta}{8}\mathbf{k} + \frac{3\beta}{4\pi}\int_{S_o} d\mathbf{S} \cdot \mathbf{H} \tag{1.2c}$$

$$\mathbf{I} \cdot \frac{d\Omega}{dt} + \Omega \times \mathbf{I} \cdot \Omega = \frac{15\beta}{8\pi}\int_{S_o} \mathbf{r} \times (d\mathbf{S} \cdot \mathbf{H}) \tag{1.2d}$$

$$\mathbf{U}_f = \Omega \times \mathbf{r} \qquad \text{on } S_o \tag{1.2e}$$

$$\mathbf{U}_f \to -\mathbf{U}_s \qquad \text{as } |\mathbf{r}| \to \infty , \tag{1.2f}$$

where Re is the Reynolds number for steady fall ($Re = 2V_o a/\nu$), $\beta = \rho_f/\rho_s$, C_D is the

drag normalized by the dynamic pressure associated with the steady velocity V_0 and the projected area of the sphere, and we have dropped the primes.

1.4 Overview of Present Work

It is the purpose of the present work to computationally investigate the first stage in the transition process for the geometrically simplest axisymmetric body, namely the sphere. In contrast to the work of Gold (1963), Lessen & Singh (1973), and Monkewitz (1988b), our work uses a numerically computed base flow which is a converged nonparallel solution of the Navier-Stokes equations. The disturbance equations are exact linearizations of the three-dimensional Navier-Stokes equations, with full treatment of the viscous and (on a linear basis) the inertial terms. To the best of our knowlege, this is the first viscous three-dimensional stability analysis of a nonparallel axisymmetric flow. The only previous attempt to compute Re_1 for a sphere is that of Kawaguti (1955).

CHAPTER 2

Accurate Computation of Steady Axisymmetric Flow

2.1 Motivation and Introduction

The steady axisymmetric viscous flow past a sphere in a uniform stream has been investigated analytically and numerically by many authors. In this chapter, we present a method which is ideally suited for accurate calculation of the flow near the sphere, and in particular, in the near wake. Accurate computation of the flow is a necessary prerequisite for the determination of the stability of the steady axisymmetric flow, which is the first step in the transition to turbulence for this simplest three-dimensional bluff body flow. In addition, accurate knowledge of the flow near the body is of interest in a number of situations in which heat or mass transfer occurs between a dispersed phase (particles or droplets) and a fluid medium. A problem of current interest is the scavenging of gaseous pollutants (e.g., oxides of sulfur and nitrogen) by raindrops.

The length of the separation bubble and the angle of separation are important features of the near wake, so it is natural to use the accuracy of these quantities to infer the accuracy of the computed velocity, vorticity, and streamfunction fields in the region near the sphere. The accuracy of the computed length of the separation bubble and the angle at which it separates from the sphere can be assessed by comparison to experiment, as well as by checking convergence (as the size of the domain and the resolution of the computation are increased).

In the present work, we present the results of a new calculation of the steady

axisymmetric flow. A useful technique for extrapolating the results to infinite resolution is proposed and demonstrated. The superiority to previous results is demonstrated by comparison to experiment. The results allow for an assessment of the accuracy of previous solutions.

2.2 Previous Computations

When the Reynolds number is sufficiently low, approximate theoretical calculations of the flow past a sphere can be made by the methods of Stokes and Oseen, or by the extension of Proudman & Pearson (1957), employing linearizing approximations. These solutions begin to diverge from experiment (e.g., Maxworthy 1965) for $Re \geq 1.3$.

Jenson (1959) obtained numerical solutions of a vorticity-streamfunction formulation of the Navier-Stokes equations using a finite difference method for $5 \leq Re \leq 40$. He used a desk calculator and a relaxation method to obtain an approximate solution of the finite-difference equations. Hamielec, Hoffman & Ross (1967) and Le Clair, Hamielec & Pruppacher (1970) followed Jenson's approach, and used a similar relaxation technique and a digital computer to solve the problem on a finer mesh. They extended the range of Reynolds number to $0.1 \leq Re \leq 100$ and $0.01 \leq Re \leq 400$, respectively. Numerical solutions of a time-dependent vorticity-streamfunction formulation were obtained by Rimon & Cheng (1969) using the Dufort-Frankel method for $1 \leq Re \leq 1000$. Another finite-difference solution of the unsteady equations was given by Lin & Lee (1973) for $5 \leq Re \leq 300$. In all of these finite-difference calculations, the far-field boundary conditions were enforced relatively close to the sphere ($r_\infty \leq 20$ for $Re \geq 40$). As per the observation of Tiwary & Reethof (1986), it appears that this has been done in order to match numerical results

to the experimentally observed drag on the sphere and to render the relaxation scheme stable.

Dandy & Leal (1986) transformed the unbounded physical domain to a finite computational domain and used an alternating-direction-implicit technique for $20 \leq Re \leq 180$. More recently, Fornberg (1988) obtained steady solutions for $100 \leq Re \leq 5000$, using Newton's method to solve the nonlinear equations arising from a finite-difference discretization. A rectangular computational domain was obtained by conformal transformation of a physical domain chosen to concentrate grid points in the wake. The location of the most remote grid point (in the wake) was at $r_\infty = 148$.

Dennis & Walker (1971) used a series truncation method in the polar direction, followed by finite-difference discretization of the resulting system of ordinary differential equations in the radial coordinate, to solve a vorticity-streamfunction formulation in the range $0.1 \leq Re \leq 40$. Similarly, Oliver & Chung (1987) used a combined series/finite-element method to solve a fourth-order streamfunction formulation for $0.5 \leq Re \leq 50$. Dennis & Walker (1971) and Oliver & Chung (1987) used $r_\infty = 148$ and $r_\infty = 300$, respectively, as the radius at which the far-field boundary condition was enforced.

Cliffe & Lever (1983) solved a vorticity-streamfunction formulation for $1 \leq Re \leq 100$ using finite-element methods. They used $r_\infty = 37$, except for $Re = 1$, for which $r_\infty = 67$ was used. In a later paper, Cliffe & Lever (1986) used a finite-element technique to solve both a primitive variables formulation, as well as a vorticity-streamfunction formulation in the same range of Re.

A spectral Galerkin method was used by Kawaguti (1955) to solve a fourth-order streamfunction formulation for $1 \leq Re \leq 80$. As noted by Flumerfelt & Slattery

(1965), Kawaguti's results are incorrect. Another spectral Galerkin method was used by Zebib (1984) to solve the fourth-order streamfunction formulation for $1 \leq Re \leq 10$.

2.3 Governing Equations and Numerical Solution

Our first task is to compute the basic state, so we specialize (1.2a-f) to the case of steady axisymmetric flow, corresponding to a purely vertical motion of the sphere, for which $\mathbf{U}_s = -\mathbf{k}$, $\mathbf{U}_f = \bar{\mathbf{U}}_f(r,\theta)$, $\Phi = \bar{\Phi}(r,\theta)$, and $\Omega = 0$. This yields

$$\nabla \cdot \bar{\mathbf{U}}_f = 0 \tag{2.1a}$$

$$(\bar{\mathbf{U}}_f \cdot \nabla)\, \bar{\mathbf{U}}_f = -\nabla\bar{\Phi} + \frac{2}{Re}\nabla^2 \bar{\mathbf{U}}_f \tag{2.1b}$$

$$\bar{\mathbf{U}}_f = \mathbf{0} \qquad \text{on } S_o \tag{2.1c}$$

$$\bar{\mathbf{U}}_f \to \mathbf{k} \qquad \text{as } |\mathbf{r}| \to \infty\,, \tag{2.1d}$$

where an overbar denotes a steady, axisymmetric quantity.

Because the base flow is axisymmetric, we use a streamfunction formulation of the Navier-Stokes equations (2.1b), which we write as

$$\frac{1}{r^2}\left\{ \frac{\partial\Psi}{\partial r}\frac{\partial}{\partial\zeta} - \frac{\partial\Psi}{\partial\zeta}\frac{\partial}{\partial r} + \frac{2\zeta}{1-\zeta^2}\frac{\partial\Psi}{\partial r} + \frac{2}{r}\frac{\partial\Psi}{\partial\zeta}\right\} D^2\Psi - \frac{2}{Re} D^4\Psi = 0\,, \tag{2.2}$$

with boundary conditions

$$\Psi(1,\zeta) = 0 \qquad \frac{\partial\Psi(1,\zeta)}{\partial r} = 0\,. \tag{2.3a,b}$$

At large r, we have the asymptotic boundary condition

$$\lim_{r \to \infty} \quad \Psi(r,\zeta) \to \frac{1}{2} r^2 (1-\zeta^2) \quad . \tag{2.4}$$

In (2.2), we have defined $\zeta = \cos\theta$, and

$$D^2 \equiv \frac{\partial^2}{\partial r^2} + \frac{1-\zeta^2}{r^2} \frac{\partial^2}{\partial \zeta^2} .$$

Since the solution must be symmetric about $\theta = 0$ and π, we also impose the conditions

$$\Psi(r,1) = 0 \qquad \Psi(r,-1) = 0 . \tag{2.5a,b}$$

The radial coordinate is transformed to the finite domain $-1 \le \eta \le 1$ according to

$$r = \exp\left[\frac{a(\eta+1)}{2}\right] . \tag{2.6}$$

Equations (2.2, 2.3, and 2.5) are straightforwardly transformed into a finite domain. If the far-field boundary condition (2.4) is satisfied at $\eta = 1$ (i.e., at finite r), then it is of the "hard" type discussed by Fornberg (1980). The fourth-order streamfunction formulation requires two far-field conditions on the function $\psi(\eta,\zeta) = \Psi(r,\zeta)$, which we take to be the "soft" conditions

$$\frac{\partial\psi(\eta,\zeta)}{\partial\eta} = \frac{1}{2} (1-\zeta^2)\, a\, e^{a(\eta+1)} \qquad \frac{\partial^3\psi(\eta,\zeta)}{\partial\eta^3} = \frac{1}{2} (1-\zeta^2)\, a^3\, e^{a(\eta+1)} \tag{2.7a,b}$$

applied at $\eta = 1$.

We follow the approach of Zebib (1984) and expand the highest η-derivative of ψ in terms of the fourth radial derivative of the uniform flow and complete sets of functions in the η- and ζ-coordinates

$$\frac{\partial^4 \psi(\eta,\zeta)}{\partial \eta^4} = \frac{1}{2}(1-\zeta^2)\, a^4\, e^{a(\eta+1)} + \sum_{i=1}^{\infty} W_i(\zeta)\, \frac{d^4 H_i(\eta)}{d\eta^4} \quad , \tag{2.8}$$

where the radial functions are in turn expanded in terms of Chebyshev polynomials

$$\frac{d^4 H_i(\eta)}{d\eta^4} = \sum_{j=0}^{\infty} A_{ij}\, T_j(\eta) \quad , \tag{2.9a}$$

and the angular functions

$$W_i(\zeta) = \int_{\zeta}^{1} P_i(\zeta')\, d\zeta' \tag{2.9b}$$

individually satisfy the symmetry conditions (2.5a,b), where $P_i(\zeta)$ is the i-th Legendre polynomial.

We next truncate (2.8) and (2.9a) to K and L+1 terms in the polar and radial directions, respectively, and integrate with respect to η to obtain expressions for ψ and its first three η-derivatives as

$$\frac{\partial^4 \psi(\eta,\zeta)}{\partial \eta^4} = \frac{1}{2}(1-\zeta^2)\, a^4\, e^{a(\eta+1)} + \sum_{i=1}^{K} W_i(\zeta) \sum_{j=0}^{L} A_{ij}\, T_j(\eta)$$

$$\frac{\partial^3 \psi(\eta,\zeta)}{\partial \eta^3} = \frac{1}{2}(1-\zeta^2)\, a^3\, e^{a(\eta+1)} + \sum_{i=1}^{K} W_i(\zeta) \sum_{j=0}^{L} A_{ij} \sum_{q=0}^{L+1} f_{qj}^{(3)}\, T_q(\eta) + C_1(\zeta)\, T_0(\eta)$$

$$\frac{\partial^2 \psi(\eta,\zeta)}{\partial \eta^2} = \frac{1}{2}(1-\zeta^2)\, a^2\, e^{a(\eta+1)} + \sum_{i=1}^{K} W_i(\zeta) \sum_{j=0}^{L} A_{ij} \sum_{q=0}^{L+2} f_{qj}^{(2)}\, T_q(\eta) + C_1(\zeta)\, T_1(\eta)$$

$$+ C_{2(\zeta)}\, T_0(\eta)$$

$$\frac{\partial\psi(\eta,\zeta)}{\partial\eta} = \frac{1}{2}(1-\zeta^2)\, a\, e^{a(\eta+1)} + \sum_{i=1}^{K} W_i(\zeta) \sum_{j=0}^{L} A_{ij} \sum_{q=0}^{L+3} f_{qj}^{(1)}\, T_q(\eta) + \frac{1}{4} C_1(\zeta)\, T_2(\eta)$$

$$+ C_2(\zeta)\, T_1(\eta) + C_3(\zeta)\, T_0(\eta)$$

$$\psi(\eta,\zeta) = \frac{1}{2}(1-\zeta^2)\, e^{a(\eta+1)} + \sum_{i=1}^{K} W_i(\zeta) \sum_{j=0}^{L} A_{ij} \sum_{q=0}^{L+4} f_{qj}^{(0)}\, T_q(\eta) + \frac{1}{24} C_1(\zeta)\, T_3(\eta)$$

$$+ \frac{1}{4} C_2(\zeta)\, T_2(\eta) + \left[C_3(\zeta) - \frac{1}{8} C_1(\zeta) \right] T_1(\eta) + C_4(\zeta)\, T_0(\eta)$$

where the coefficients $f_{qj}^{(n)}$ are defined in the Appendix. The constants of integration are chosen so that $\psi(\eta,\zeta)$ satisfies all of the boundary conditions (2.3a,b) and (2.7a,b), and are evaluated as

$$C_1 = -\sum_{i=1}^{K} W_i(\zeta) \sum_{j=0}^{L} A_{ij} \sum_{q=0}^{L+1} f_{qj}^{(3)}$$

$$C_2 = -\frac{1}{2} \sum_{i=1}^{K} W_i(\zeta) \sum_{j=0}^{L} A_{ij} \sum_{q=0}^{L+3} [1 - (-1)^q]\, f_{qj}^{(1)} + \frac{1}{2}(1-\zeta^2)\, \frac{a}{2}$$

$$C_3 = -\frac{1}{2} \sum_{i=1}^{K} W_i(\zeta) \sum_{j=0}^{L} A_{ij} \left\{ \sum_{q=0}^{L+3} [1 + (-1)^q]\, f_{qj}^{(1)} - \frac{1}{2} \sum_{q=0}^{L+1} f_{qj}^{(3)} \right\} - \frac{1}{2}(1-\zeta^2)\, \frac{a}{2}$$

$$C_4 = -\sum_{i=1}^{K} W_i(\zeta) \sum_{j=0}^{L} A_{ij} \left\{ \sum_{q=0}^{L+4} (-1)^q\, f_{qj}^{(0)} + \frac{1}{8} \sum_{q=0}^{L+3} [3 + 5(-1)^q]\, f_{qj}^{(1)} - \frac{1}{3} \sum_{q=0}^{L+1} f_{qj}^{(3)} \right\}$$

$$+ \frac{1}{2}(1-\zeta^2) \left[-\frac{5}{8} a - 1 \right]$$

The final result is

$$\frac{d^n\psi}{d\eta^n} = \frac{1}{2}(1-\zeta^2)\left\{a^n\, e^{a(\eta+1)} + \sum_{p=0}^{2} B_p^{(n)}\, T_p(\eta)\right\}$$

$$+ \sum_{i=1}^{K} W_i(\zeta) \sum_{j=0}^{L} A_{ij} \sum_{q=0}^{L+4-n} G_{qj}^{(n)} T_q(\eta)\,, \qquad 0 \le n \le 3\,, \qquad (2.10)$$

where the coefficients $B_p^{(n)}$ and $G_{qj}^{(n)}$ are defined in the Appendix.

That the boundary and symmetry conditions are automatically satisfied by any linear combination of the functions in (2.10) allows further consideration to be restricted to the partial differential equation (2.2). Rewriting this as

$$N(\psi) - \frac{2}{Re} D^4\psi = 0\,, \qquad (2.11)$$

we formulate a weighted residuals procedure whereby the residual of the discretization of (2.11) is made orthogonal to the trial functions according to

$$\int_1^{e^a} \int_0^{\pi} \left[N(\psi) - \frac{2}{Re} D^4\psi \right] V_i(\theta)\, S_j(r)\, r^k \sin\theta \, d\theta \, dr = 0$$

for $1 \le i \le K$ and $0 \le j \le L$, where

$$V_i(\theta) = W_i(\zeta)\,, \qquad S_j(r) = \sum_{q=0}^{L+4} G_{qj}^{(0)}\, T_q(\eta)\,.$$

Thus, the problem is reduced to a system of K(L+1) nonlinear equations, which we solve by Newton-Raphson iteration.

The computational technique applied above borrows from an idea due to

Zebib (1984, 1987). Zebib (1984) expanded the streamfunction in terms of Legendre polynomials in the angular direction

$$\Psi(r,\theta) = \sum_{n=1}^{N_\theta} r\, f_n(r)\, P_n(\cos\theta) \tag{2.12}$$

and obtained a system of nonlinear ordinary differential equations

$$\frac{2}{Re} D_l^2(f_l) = \sum_{n=1}^{N_\theta}\sum_{m=1}^{N_\theta} C_{nlm}\, \frac{(f_n\, D_m f_m)'}{r} + C_{lnm}\, \frac{(rf_n)'\, D_m f_m}{r^2} \quad , \quad 1 \le l \le N_\theta \tag{2.13}$$

in the radial direction, where the differential operator D_m is given by

$$D_m = \frac{d^2}{dr^2} + \frac{2}{r}\frac{d}{dr} - \frac{m(m+1)}{r^2} \, . \tag{2.14}$$

Zebib then expanded the fourth derivative of the solution of (2.13) in terms of a set of Chebyshev polynomials, such that each term in (2.12) satisfies the radial boundary conditions at $r = 1$ and r_∞.

In our technique, we have decomposed the streamfunction into a uniform flow and a Galerkin series. In the latter, the i-th angular trial function is an integral of the i-th Legendre polynomial and satisfies the proper symmetry conditions (2.9a,b). We have also used a correct asymptotic implementation of the "soft" far-field boundary conditions of Fornberg (1980) at the outer boundary of the computational domain. Finally, our Galerkin integrations are done with weightings of the form $r^k \sin\theta$. (We have used $k = 1$ herein; essentially identical results, requiring the same number of Newton iterations to solve the nonlinear algebraic equation system, are obtained for $k = 0, 1, 2$.).

2.4 Results

We divide this section into two parts. In the first, we establish the convergence of the present results, with respect to changes in the size of the computational domain and the number of spectral functions retained in the expansion. In the second part, we compare our results to previous work (experimental and theoretical), and assess the errors in the latter.

The results are presented in terms of the drag coefficient (C_D), the length of the separation bubble (l_s), measured from the rear stagnation point in units of sphere radii, and the separation angle (θ_s), also measured relative to the rear stagnation point.

The total drag on the sphere consists of two parts.

$$\text{Drag} = D_p + D_v$$

where D_p is the pressure or form drag caused by normal stresses, and D_v is the viscous drag caused by shear stresses on the body surface. Recalling the nondimensionalization in §1.3, we have

$$D_p = 2\pi \int_0^{\pi} (\sigma_{rr})_{r=1} \cos\theta \sin\theta \, d\theta$$

$$D_v = -2\pi \int_0^{\pi} (\tau_{r\theta})_{r=1} \sin^2\theta \, d\theta \, .$$

The expressions for these two components of the stress tensor are

$$\sigma_{rr} = -\Phi + \frac{4}{Re}\frac{\partial u_r}{\partial r}$$

$$\tau_{r\theta} = \frac{2}{Re}\left[r\frac{\partial}{\partial r}\left(\frac{u_\theta}{r}\right) + \frac{1}{r}\frac{\partial u_r}{\partial \theta}\right],$$

where the continuity equation requires that $\partial u_r/\partial r$ is zero on the surface of the sphere, and pressure is evaluated from the θ-component of the momentum equation (2.1b). The drag coefficient is defined as the drag force divided by the product of the free-stream dynamic pressure and the projected area of the sphere.

As the Reynolds number increases, the flow may separate from the rear part of the sphere, with a secondary flow appearing in the form of a standing eddy. If the Reynolds number is not too large, the recirculating wake remains laminar and is confined within the streamline $\psi = 0$. The dimensionless radial distance r_s from the sphere center to the downstream end of the eddy is obtained by letting $u_r = 0$ at $\theta = 0$. The root of the corresponding nonlinear algebraic equation is found by Newton-Raphson iteration. We note that l_s, defined before, corresponds to $r_s - 1$.

When the flow becomes separated, the ϕ-component of vorticity on the surface of the sphere changes sign on a circle on the rear of the sphere surface, indicating a change in direction of the surface streamline. This separation circle marks the surface streamline bounding the wake. The exact position of separation is determined as follows. The ϕ-component of vorticity may be expressed in terms of the streamfunction as

$$\omega_\phi = -\frac{D^2\Psi}{r\sin\theta}. \qquad (2.15)$$

By setting the right hand side of (2.15) to zero on the sphere, we get a nonlinear

algebraic equation, which is again solved by the Newton-Raphson method. We denote the location of the separation circle by θ_s, measured relative to the rear stagnation point.

Figures 2-10 show the streamlines at Reynolds numbers 0.1, 5, 20, 40, 70, 100, 140, 180, and 200. The contour values are 0.0, 0.125, 0.5, 1.125, 2.0, 3.125, and -0.006, -0.02, -0.04 (in the recirculating wake).

We choose Reynolds numbers 0.1, 40 and 180 to show the convergence of our scheme for the length and angle of the separation bubble and the drag coefficient. The flows at these values of Re are representative of, respectively, flows at low Re, intermediate Re, and at the upper range of Re for which the steady axisymmetric flow is stable (Kim & Pearlstein, 1989).

For Re = 0.1 and twenty expansion functions in each of the radial and polar directions, Table 1 shows the variation of the drag coefficient (C_D) as the size of the computational domain ($r_\infty = e^a$) increases. The error falls below one percent only for r_∞ in excess of 40. The drag coefficient converges monotonically. For r_∞ chosen sufficiently large for finite domain effects to be unimportant (according to Table 1) at Re = 0.1, Table 2 shows that C_D converges quite rapidly as the number of spectral functions increases. We note that for small numbers of expansion functions, C_D varies nonmonotonically with the number of terms retained.

For Re = 40 and twenty expansion functions in the radial and polar directions, Table 3 shows the dependence of l_s, θ_s, and C_D on the size of the computational domain. In this case, none of the computed quantities is a monotonic function of the domain size. Moreover, the magnitude of the relative errors also depends nonmonotonically on r_∞. This is the source of the "false convergence" of l_s at

$r_\infty = e^{2.5}$ and e^3, for which one might deduce that l_s has converged (to values nearly identical to the fully converged result at $r_\infty = e^5$), even though the results for the intervening values of r_∞ ($e^{3.5}$ and e^4) differ significantly. We also note that the values of θ_s and C_D converge considerably faster than the value of l_s. Table 4 shows the dependence of l_s, θ_s, and C_D on the number of expansion functions. We note that the drag coefficient converges monotonically, whereas l_s and θ_s do not. Table 5 shows that when K (the number of angular terms retained) is equal to twenty, C_D is essentially independent of L (the number of radial functions), even though l_s and θ_s still depend significantly on L. Table 5 also shows that for K = 20, C_D is essentially independent of L, even though Table 4 shows that C_D is not fully converged. From this it is clear that for sufficiently large K and L, the drag coefficient depends primarily on K. The dependence of l_s and θ_s on K and L is more complex.

For Re = 180, Table 6 shows a similar nonmonotonic dependence of l_s, θ_s, and C_D on the size of the computational domain. As noted for Re = 40, this nonmonotonic dependence can easily give rise to false convergence. In this case, we see that θ_s converges faster than l_s and C_D with increasing r_∞. None of the computed quantities converges monotonically as r_∞ increases. For Re = 180, Table 7 shows that as K and L are increased, l_s and θ_s converge faster than does C_D.

Finally, Table 8 shows l_s and θ_s near the Reynolds number (Re_s) at which the flow separates from the sphere at the rear stagnation point. At Re_s, we would have $l_s = \theta_s = 0$. We note that as the Reynolds number approaches Re_s, the absolute errors in l_s and θ_s are nearly constant, thus rendering a precise estimate of Re_s rather difficult. However, when we plot θ_s versus 1/K = 1/L, we find that the points nearly lie on a straight line. This plot has the obvious advantage of requiring extrapolation

to the origin rather than to infinity (Domb & Sykes 1957, Van Dyke 1975). More important, the extrapolation is often nearly linear as in the present work. Thus, the converged result can be estimated by extrapolation, rather than by using increasingly large expansions, which would require excessive computing time and storage. In Table 8, we show $\theta_{s\infty}$ obtained by this extrapolation, along with the standard deviation of the computed points from the straight line obtained by a linear least squares fit. The fit to a straight line is excellent. Table 9 shows the effect of the location of the outer computational boundary for Re = 20 with K = L = 28. We see that $r_\infty = e^6$ is sufficiently large. On the basis of the results shown in Table 8, we estimate $Re_s = 20.49$.

For Re = 0.1 Table 10 shows a comparison of the values of C_D computed by our spectral technique and by previous authors. In particular, we note that the pressure contribution to C_D is slightly more than one-half the viscous contribution, in agreement with results at higher Re (Jenson 1959, Dennis & Walker 1971, Lin & Lee 1973). (At Re = 0, the ratio of the pressure and viscous contributions is exactly one-half; we expect it to decrease monotonically with increasing Re.) We note that in the calculation of Le Clair et al. (1970), the ratio of pressure to viscous contributions was in excess of one-half, thus indicating a problem in their algorithm or code.

There have been many previous experimental and computational estimates of the Reynolds number at which the flow separates from the sphere at the rear stagnation point. Table 11 shows a fairly wide range of measured and computed values of Re_s between 10 and 24. In fact, the experimental determination of Re_s by flow visualization is very difficult due to the very small size of the separation bubble. Thus, it is not surprising that the most definitive estimate of Re_s is by a mass transfer

measurement, in which Garner et al. (1959) measured the rate of dissolution in a fluid of a slightly soluble solid sphere. Our results definitively confirm two previous fortuitous estimates of Re_s. Kalra & Uhlherr (1973) estimated $Re_s = 20$, on the basis of measurements of l_s for $Re > 27$ (with considerable scatter) and extrapolation to $l_s = 0$. Lin & Lee (1973) computed the axisymmetric steady flow as a long-time solution of the unsteady Navier-Stokes equations for Re = 5, 20, 40, 100, 200, and 300. They found that the steady flow exhibited a small separated region for Re = 20.

Table 12 provides a detailed comparison of our computed values of l_s and θ_s with previous calculations for the entire range of Re over which the steady axisymmetric flow is stable. (The corresponding computational domains and truncation levels are shown in Table 13.) The present results are in closer agreement with the classical experiments of Taneda (1956) than are any previous calculations. Table 14 shows the detailed convergence of l_s and θ_s at the Reynolds numbers used in Table 12 and 13, as well as the extrapolated result.

2.5 Comparison to Experiment and Previous Computations

The present work provides very accurate results over the entire range of Reynolds numbers in which the steady axisymmetric flow is stable and hence physically realizable, and gives closer agreement with the classical experiments of Taneda (1956) than any previous calculations, as shown in Table 12. Our extrapolation technique improves the agreement even more, and confirms two previous fortuitous estimates of Re_s.

CHAPTER 3

Stability of Flow Past a Fixed Sphere

We first consider the incompressible flow of a constant property Newtonian fluid past a fixed rigid sphere, which is governed by a special case of equations (1.2a-f) for the fluid/sphere density ratio $\beta = 0$. The governing equations are

$$\nabla \cdot \mathbf{U}_f = 0$$

$$\frac{\partial \mathbf{U}_f}{\partial t} + (\mathbf{U}_f \cdot \nabla)\,\mathbf{U}_f = -\nabla\Phi + \frac{2}{Re}\nabla^2\mathbf{U}_f$$

$$\mathbf{U}_f = \mathbf{0} \qquad \text{on } S_o$$

$$\mathbf{U}_f \to \mathbf{k} \qquad \text{as } |\mathbf{r}| \to \infty\ .$$

3.1 Linear Disturbance Equations

We consider infinitesimally small disturbances to the steady axisymmetric flow and decompose the dimensionless velocity and pressure into

$$\mathbf{U}_f(r,\theta,\phi,t) = \bar{\mathbf{U}}_f(r,\theta) + \mathbf{u}_f(r,\theta,\phi,t)$$
$$\Phi(r,\theta,\phi,t) = \bar{\Phi}(r,\theta) + \Pi(r,\theta,\phi,t)\ .$$

In what follows, we shall only retain terms to first order in the disturbance quantities and obtain the following linear disturbance equations.

$$\nabla \cdot \mathbf{u}_f = 0 \tag{3.1a}$$

$$\frac{\partial \mathbf{u}_f}{\partial t} + (\mathbf{u}_f \cdot \nabla)\,\bar{\mathbf{U}}_f + (\bar{\mathbf{U}}_f \cdot \nabla)\,\mathbf{u}_f = -\nabla\Pi + \frac{2}{Re}\nabla^2\mathbf{u}_f \tag{3.1b}$$

$$\mathbf{u}_f = 0 \quad \text{on } S_o \tag{3.1c}$$

$$\mathbf{u}_f \to 0 \qquad \text{as } r \to \infty\ . \tag{3.1d}$$

The disturbances can be Fourier decomposed into azimuthal components according to

$$\mathbf{u}_f(r,\theta,\phi,t) = \sum_{m=-\infty}^{\infty} \mathbf{u}_m(r,\theta,t)\ e^{im\phi} \tag{3.2a}$$

and

$$\Pi(r,\theta,\phi,t) = \sum_{m=-\infty}^{\infty} p_m(r,\theta,t)\ e^{im\phi}\ . \tag{3.2b}$$

The remainder of this chapter is devoted to discussions of the fates of axisymmetric ($m = 0$) and nonaxisymmetric ($m \neq 0$) disturbances to the steady axisymmetric base flow. For each azimuthal wavenumber, we will then seek to determine whether, at fixed Re, any disturbances grow in time. The critical Reynolds number for the axisymmetric base flow, Re_1, is the Re for which no distrubances grow, and one or more disturbances are neutral.

3.2 Axisymmetric (m = 0) disturbances

We begin by considering axisymmetric disturbances with arbitrary time dependence. Because the base flow and disturbance are axisymmetric, we can use a streamfunction formulation of the Navier-Stokes equations, which we write as

$$\frac{\partial(D^2\Psi')}{\partial t} + \frac{1}{r^2}\left\{\frac{\partial\Psi_s}{\partial r}\frac{\partial}{\partial\zeta} - \frac{\partial\Psi_s}{\partial\zeta}\frac{\partial}{\partial r} + \frac{2\zeta}{1-\zeta^2}\frac{\partial\Psi_s}{\partial r} + \frac{2}{r}\frac{\partial\Psi_s}{\partial\zeta}\right\}D^2\Psi'$$

$$+ \frac{1}{r^2}\left\{\frac{\partial\Psi'}{\partial r}\frac{\partial}{\partial\zeta} - \frac{\partial\Psi'}{\partial\zeta}\frac{\partial}{\partial r} + \frac{2\zeta}{1-\zeta^2}\frac{\partial\Psi'}{\partial r} + \frac{2}{r}\frac{\partial\Psi'}{\partial\zeta}\right\}D^2\Psi_s - \frac{2}{Re}D^4\Psi' = 0 \qquad (3.3)$$

with boundary conditions

$$\Psi'(1,\zeta,t) = 0 \qquad \frac{\partial\Psi'(1,\zeta,t)}{\partial r} = 0\,, \qquad (3.4a,b)$$

where the subscript s denotes a base flow quantity and the prime denotes a disturbance quantity. At large r, we have the asymptotic boundary condition

$$\lim_{r\to\infty} \Psi'(r,\zeta,t) \to 0\,. \qquad (3.5)$$

In (3.3), we have defined $\zeta = \cos\theta$, and

$$D^2 \equiv \frac{\partial^2}{\partial r^2} + \frac{1-\zeta^2}{r^2}\frac{\partial^2}{\partial\zeta^2}\,.$$

Since the solution must be symmetric about $\theta = 0$ and π, we also impose the conditions

$$\Psi'(r,1,t) = 0 \qquad \Psi'(r,-1,t) = 0\,. \qquad (3.6a,b)$$

The determination of Re_1 is thus equivalent to computing the largest value of Re for which no solution of (3.3-3.6) grows in time. As (3.3-3.6) are linear and time-invariant, we investigate modal solutions of the form

$$\Psi'(r,\zeta,t) = \psi'(r,\zeta)\,e^{\sigma t}$$

where σ is the temporal eigenvalue. Thus, we consider the eigenvalue problem

$$\sigma\, D^2\psi' + \frac{1}{r^2}\left\{\frac{\partial\Psi_s}{\partial r}\frac{\partial}{\partial\zeta} - \frac{\partial\Psi_s}{\partial\zeta}\frac{\partial}{\partial r} + \frac{2\zeta}{1-\zeta^2}\frac{\partial\Psi_s}{\partial r} + \frac{2}{r}\frac{\partial\Psi_s}{\partial\zeta}\right\} D^2\psi'$$

$$+ \frac{1}{r^2}\left\{\frac{\partial\psi'}{\partial r}\frac{\partial}{\partial\zeta} - \frac{\partial\psi'}{\partial\zeta}\frac{\partial}{\partial r} + \frac{2\zeta}{1-\zeta^2}\frac{\partial\psi'}{\partial r} + \frac{2}{r}\frac{\partial\psi'}{\partial\zeta}\right\} D^2\Psi_s - \frac{2}{Re} D^4\psi' = 0 \qquad (3.7)$$

subject to the boundary conditions

$$\psi'(1,\zeta) = 0 \qquad \frac{\partial\psi'(1,\zeta)}{\partial r} = 0 \ , \qquad (3.8a,b)$$

$$\lim_{r\to\infty} \psi'(r,\zeta) \to 0 \ , \qquad (3.9)$$

and the symmetry conditions

$$\psi'(r,1) = 0 \qquad \psi'(r,-1) = 0 \ . \qquad (3.10a,b)$$

We have solved the linear eigenvalue problem for axisymmetric disturbances by a numerical technique akin to that used in the base flow calculation, in which the radial coordinate is transformed to the finite domain $-1 \le \eta \le 1$ according to

$$r = \exp\left[\frac{a(\eta+1)}{2}\right] . \qquad (3.11)$$

Equations (3.7, 3.9, and 3.10) are straightforwardly transformed into the finite domain. If the far-field boundary condition (3.9) is satisfied at $\eta = 1$ (i.e., at finite r), then it is of the "hard" type discussed by Fornberg (1980). The fourth-order streamfunction formulation for the axisymmetric disturbances requires two far-field conditions on the function $\tilde{\psi}(\eta,\zeta) = \psi'(r,\theta)$, which we take to be the "soft" conditions

$$\frac{\partial \tilde{\psi}(\eta,\zeta)}{\partial \eta} = 0 \qquad \frac{\partial^3 \tilde{\psi}(\eta,\zeta)}{\partial \eta^3} = 0 \tag{3.12a,b}$$

applied at $\eta = 1$.

As in the calculation of the base flow, we have followed the approach of Zebib (1987) and expanded the highest η-derivative of $\tilde{\psi}$ in terms of complete sets of functions in the η- and ζ-coordinates

$$\frac{\partial^4 \tilde{\psi}(\eta,\zeta)}{\partial \eta^4} = \sum_{i=1}^{\infty} W_i(\zeta) \frac{d^4 H_i(\eta)}{d\eta^4} , \tag{3.13}$$

where the radial functions are expanded in terms of Chebyshev polynomials

$$\frac{d^4 H_i(\eta)}{d\eta^4} = \sum_{j=0}^{\infty} A_{ij} T_j(\eta) , \tag{3.14a}$$

and the angular functions

$$W_i(\zeta) = \int_{\zeta}^{1} P_i(\zeta') \, d\zeta' \tag{3.14b}$$

individually satisfy the symmetry conditions, where $P_i(\zeta)$ is the i-th Legendre polynomial.

We next truncate (3.13) and (3.14a) to I and J+1 terms in the polar and radial directions, respectively, and integrate with respect to η to obtain expressions for ψ and its first three η-derivatives. The constants of integration are chosen so that each radial function $H_i(\eta)$ satisfies all of the boundary conditions. The result is

$$\frac{d^n H_i}{d\eta^n} = \sum_{j=0}^{J} A_{ij} \sum_{q=0}^{J+4-n} G_{qj}^{(n)} T_q(\eta) , \qquad 0 \le n \le 3 , \tag{3.15}$$

where the coefficients $G_{qj}^{(n)}$ are shown in the Appendix.

That the boundary and symmetry conditions are automatically satisfied by any linear combination of the functions in (3.13) allows further consideration to be restricted to the partial differential equation (3.7). Rewriting this as

$$\sigma D^2\tilde{\psi} + L(\tilde{\psi}) - \frac{2}{Re} D^4\tilde{\psi} = 0 , \tag{3.16}$$

we formulate a weighted residuals procedure whereby the residual of the discretized (3.16) is made orthogonal to the trial functions according to

$$\int_1^{e^a} \int_0^{\pi} \left[\sigma D^2\tilde{\psi} + L(\tilde{\psi}) - \frac{2}{Re} D^4\tilde{\psi} \right] V_i(\theta)\, S_j(r)\, r^k \sin\theta \, d\theta \, dr = 0$$

for $1 \le i \le I$ and $0 \le j \le J$, where

$$V_i(\theta) = W_i(\zeta) , \qquad S_j(r) = \sum_{q=0}^{J+4} G_{qj}^{(0)}\, T_q(\eta) .$$

Thus, the problem is reduced to a I(J+1) x I(J+1) matrix eigenvalue problem

$$A\,x = \sigma\, C\,x , \tag{3.17}$$

which is solved using standard numerical software (Garbow et al. 1977). That (3.17) is nonsingular and has no spurious eigenvalues (Gottlieb & Orszag 1977) is guaranteed by satisfying the boundary and symmetry conditions (which do not involve σ) on a term-by-term basis in (3.14a,b) rather than by inclusion in (3.17) (Zebib 1984).

3.3 Nonaxisymmetric ($m \neq 0$) disturbances

The linear analysis of the stability of nonaxisymmetric disturbances (i.e., $m \neq 0$) proceeds from the Fourier decompositions (3.2a,b). Because of the axisymmetry of the base flow and the linearity of the disturbance equations, the individual Fourier modes are uncoupled and can be investigated separately. Because the disturbance variables $\mathbf{u}_f$ and Π must be real, we require that $\mathbf{u}_{-m} = \mathbf{u}_m^*$ and $p_{-m} = p_m^*$, where * denotes a complex conjugate. As the case $m = 0$ has been treated in §3.2, attention will be restricted to $m \geq 1$.

We have found it convenient to use the primitive variable form of (3.1a,b) in this part of the analysis. The m-th Fourier component of the disturbance is then governed by

$$\nabla \cdot \mathbf{u}_m' = 0 \tag{3.18}$$

$$\frac{\partial \mathbf{u}_m'}{\partial t} + (\mathbf{u}_m' \cdot \nabla)\,\bar{\mathbf{U}} + (\bar{\mathbf{U}} \cdot \nabla)\,\mathbf{u}_m' = -\nabla p_m' + \frac{2}{Re}\nabla^2 \mathbf{u}_m' \tag{3.19}$$

with the no-slip boundary condition

$$\mathbf{u}_m'(1,\theta,\phi,t) = 0\ , \tag{3.20}$$

where $\mathbf{u}_m'(r,\theta,\phi,t) = \mathbf{u}_m(r,\theta,t)\, e^{im\phi}$ and $p_m'(r,\theta,\phi,t) = p_m(r,\theta,t)\, e^{im\phi}$.

We then make the change of variables $\zeta = \cos\theta$ and eliminate the pressure and azimuthal velocity component as follows. We first note that $\partial u_m'/\partial\phi = imu_m'$ and use (3.18) to eliminate $u_{m\phi}$ from (3.18, 3.19). In the same manner, we can solve the azimuthal momentum equation for p_m', and hence eliminate p_m.

As with axisymmetric disturbances, we consider modal solutions of the form

$$u_{mr}(r,\zeta,t) = e^{\sigma t}\,\hat{u}_{mr}(r,\zeta) \tag{3.21a}$$

$$u_{m\zeta}(r,\zeta,t) = e^{\sigma t}\,\hat{u}_{m\zeta}(r,\zeta)\,, \tag{3.21b}$$

leading to two coupled equations in r and ζ which constitute an eigenvalue problem for σ.

The final result is a pair of partial differential equations for the r- and ζ-components of the velocity of the form

$$\sigma\left[m^2\,\hat{u}_{mr} + \sin^2\theta\,\frac{\partial}{\partial r}(r\,h_m)\right]$$

$$+ m^2\left[\frac{\partial}{\partial r}(\bar{U}_r\hat{u}_{mr}) - \frac{\sin\theta}{r}\left[\frac{\partial\bar{U}_r}{\partial\zeta}\,\hat{u}_{m\zeta} + \bar{U}_\zeta\,\frac{\partial\hat{u}_{mr}}{\partial\zeta}\right] - \frac{2}{r}\,\bar{U}_\zeta\hat{u}_{m\zeta}\right]$$

$$+ \sin^2\theta\,\frac{\partial}{\partial r}\left[r\,\bar{U}_r\,\frac{\partial h_m}{\partial r} - \bar{U}_\zeta\,\frac{\partial}{\partial\zeta}(h_m\sin\theta) + \bar{U}_r h_m + h_m\,\bar{U}_\zeta\cot\theta\right]$$

$$+ \frac{2}{Re}\left\{\frac{m^2}{r^2}\left[-\frac{\partial}{\partial r}\left[r^2\,\frac{\partial\hat{u}_{mr}}{\partial r}\right] - \frac{\partial}{\partial\zeta}\left[\sin^2\theta\,\frac{\partial\hat{u}_{mr}}{\partial\zeta}\right] + 2\,\hat{u}_{mr} + \frac{m^2}{\sin^2\theta}\,\hat{u}_{mr}\right]\right.$$

$$- \sin\theta\,\frac{\partial}{\partial r}\left[\frac{\sin\theta}{r}\,\frac{\partial}{\partial r}\left[r^2\,\frac{\partial h_m}{\partial r}\right] + \frac{1}{r}\,\frac{\partial}{\partial\zeta}\left[\sin^2\theta\,\frac{\partial}{\partial\zeta}(h_m\sin\theta)\right]\right]$$

$$\left. + (1+m^2)\,\frac{\partial}{\partial r}\left[\frac{h_m}{r}\right] + 2m^2\left[\cot\theta\,\frac{\partial}{\partial r}\left[\frac{\hat{u}_{m\zeta}}{r}\right] - \frac{3}{r^2}\,\hat{u}_{mr}\right]\right\} = 0 \tag{3.22a}$$

$$\sigma \left[m^2 \hat{u}_{m\zeta} - \sin\theta \frac{\partial}{\partial \zeta} (h_m \sin^2\theta) \right]$$

$$+ m^2 \left[\hat{u}_{mr} \left(\frac{\partial}{\partial r} + \frac{1}{r} \right) \bar{U}_\zeta + \bar{U}_r \left(\frac{\partial}{\partial r} + \frac{1}{r} \right) \hat{u}_{m\zeta} - \frac{\sin\theta}{r} \frac{\partial}{\partial \zeta} (\bar{U}_\zeta \hat{u}_{m\zeta}) \right]$$

$$- \sin\theta \frac{\partial}{\partial \zeta} \left[\sin^2\theta \left(\bar{U}_r \frac{\partial h_m}{\partial r} - \frac{\bar{U}_\zeta}{r} \frac{\partial}{\partial \zeta} (h_m \sin\theta) + \frac{\bar{U}_r}{r} h_m + \frac{\bar{U}_\zeta}{r} h_m \cot\theta \right) \right]$$

$$+ \frac{2}{Re} \left\{ \frac{m^2}{r^2} \left[-\frac{\partial}{\partial r} \left(r^2 \frac{\partial \hat{u}_{m\zeta}}{\partial r} \right) - \frac{\partial}{\partial \zeta} \left(\sin^2\theta \frac{\partial \hat{u}_{m\zeta}}{\partial \zeta} \right) + \frac{1+m^2}{\sin^2\theta} \hat{u}_{m\zeta} - 2 \sin\theta \frac{\partial}{\partial \zeta} (\hat{u}_{m\zeta} \cot\theta) \right] \right.$$

$$+ \frac{\sin\theta}{r^2} \frac{\partial}{\partial \zeta} \left[\sin^2\theta \frac{\partial}{\partial r} \left(r^2 \frac{\partial h_m}{\partial r} \right) + \sin\theta \frac{\partial}{\partial \zeta} \left(\sin^2\theta \frac{\partial}{\partial \zeta} (h_m \sin\theta) \right) \right]$$

$$\left. - \frac{1+m^2}{r^2} \sin\theta \frac{\partial h_m}{\partial \zeta} + \frac{2m^2}{r^2} h_m \cot\theta \right\} = 0 , \qquad (3.22b)$$

where

$$h_m = \frac{\partial}{\partial \zeta} (\hat{u}_{m\zeta} \sin\theta) - \frac{1}{r} \frac{\partial}{\partial r} (r^2 \hat{u}_{mr}) \ .$$

Here, the velocity components must satisfy the boundary conditions

$$\hat{u}_{mr}(1,\zeta) = 0 \qquad \hat{u}_{m\zeta}(1,\zeta) = 0 \qquad (3.23a,b)$$

on the sphere. Following Batchelor & Gill (1962), the disturbance must also satisfy the kinematic conditions

$$\hat{u}_{mr}(r,\pm 1) = 0, \qquad m \geq 1 \qquad (3.23c)$$

$$\hat{u}_{1\zeta}(r,\pm 1) \quad \text{bounded} \qquad (3.23d)$$

$$\hat{u}_{m\zeta}(r,\pm 1) = 0, \qquad m > 1 \tag{3.23e}$$

on the coordinate axes $\zeta = \pm 1$.

As in §3.2, the numerical treatment begins with the transformation (3.11) of the radial variable. The transformed counterparts of (3.22a,b) contain fourth derivatives of $\tilde{u}_{m\eta}(\eta,\zeta) = \hat{u}_{mr}(r,\zeta)$ and third derivatives of $\tilde{u}_{m\zeta}(\eta,\zeta) = \hat{u}_{m\zeta}(r,\zeta)$ with respect to η. The boundary conditions satisfied by $\hat{u}_{m\eta}$ and $\hat{u}_{m\zeta}(r,\zeta)$ are then

$$\tilde{u}_{m\eta}(-1,\zeta) = 0 \qquad \frac{\partial \tilde{u}_{m\eta}(-1,\zeta)}{\partial \eta} = 0 \tag{3.24a,b}$$

and

$$\tilde{u}_{m\zeta}(-1,\zeta) = 0 \tag{3.24c}$$

at the surface of the sphere. Here (3.24a,c) follow directly from (3.23a,b), whereas (3.24b) is a direct consequence of the continuity equation.

The η- and ζ-components of the velocity are then required to satisfy two far-field boundary conditions at $\eta = 1$. As in the calculation of the base flow and the investigation of axisymmetric disturbances, there is a degree of choice available in the selection of these far-field conditions. We have chosen to require that each of the disturbance velocity components satisfy a "hard" and a "soft" boundary condition at $\eta = 1$. These are

$$\tilde{u}_{m\eta}(1,\zeta) = 0 \qquad \tilde{u}_{m\zeta}(1,\zeta) = 0 \tag{3.24d,e}$$

and

$$\frac{\partial \tilde{u}_{m\eta}(1,\zeta)}{\partial \eta} = 0 \qquad \frac{\partial \tilde{u}_{m\zeta}(1,\zeta)}{\partial \eta} = 0\,, \tag{3.24f,g}$$

where the hard conditions (3.24d,e) ensure that the disturbance inflow is axisymmetric

on the outer boundary of the computational domain.

We now consider solution of an eigenvalue problem consisting of the partial differential equations (3.22a,b) and the boundary and kinematic conditions (3.23, 3.24). This time, we expand the disturbance quantities directly in terms of a complete set of functions. (A similar procedure had earlier been attempted for the base flow calculation, but was abandoned due to slow convergence of the Newton iteration required to solve the nonlinear algebraic equation system.) The expansion for m = 1

$$\tilde{u}_{1\eta}(\eta,\zeta) = \sum_{i=1}^{I} W_i(\zeta) \sum_{j=0}^{J} B_{ij}\, e^{-a(\eta+1)/2}\, (\eta^2-1)^2\, \eta^j \tag{3.25a}$$

$$\tilde{u}_{1\zeta}(\eta,\zeta) = \sum_{i=0}^{I} P_i(\zeta) \sum_{j=0}^{J} Q_{ij}\, e^{-a(\eta+1)/2}\, (\eta^2-1)\, (\eta-1)\, \eta^j \,. \tag{3.25b}$$

differs from the general case on account of the kinematic condition (3.23e), and will be treated first. We denote by $R_1(\eta,\zeta)$ and $\Theta_1(\eta,\zeta)$ the residuals that result when the expansions (3.25a,b) are substituted into the differential equations (3.22a) and (3.22b), respectively. We then make these residuals orthogonal to the trial functions according to

$$\int_{-1}^{1}\int_{-1}^{1} R_1(\eta,\zeta)\, W_i(\zeta)\, (\eta^2-1)^2\, \eta^j\, d\zeta\, d\eta = 0 \,, \qquad 1 \le i \le I,\ 0 \le j \le J \tag{3.26a}$$

$$\int_{-1}^{1}\int_{-1}^{1} \Theta_1(\eta,\zeta)\, P_i(\zeta)\, (\eta^2-1)\, (\eta-1)\, \eta^j\, d\zeta\, d\eta = 0 \,, \qquad 0 \le i \le I,\ 0 \le j \le J \,. \tag{3.26b}$$

These linear equations constitute a matrix eigenvalue problem of the form (3.17),

where **C** is again nonsingular. In the nonaxisymmetric case, the order of the eigenvalue problem is (J+1)(2I+1). Again, the eigenproblem is solved using standard EISPACK software. No spurious eigenvalues were found.

For m > 1, the linear disturbance equations are still (3.22a,b) and (3.23c, 3.24), with (3.23d) replaced with (3.23e). We employ the expansions

$$\tilde{u}_{m\eta}(\eta,\zeta) = \sum_{i=1}^{I} W_i(\zeta) \sum_{j=0}^{J} F_{ij}\, e^{-a(\eta+1)}\, (\eta^2-1)^2\, \eta^j$$

$$\tilde{u}_{m\zeta}(\eta,\zeta) = \sum_{i=1}^{I} W_i(\zeta) \sum_{j=0}^{J} X_{ij}\, e^{-a(\eta+1)}\, (\eta^2-1)\, (\eta-1)\, \eta^j \ .$$

As before, these expressions are substituted into (3.26a,b), and the residuals are made orthogonal to the trial functions. The resulting set of 2I(J+1) homogeneous linear algebraic equations again constitutes an eigenvalue problem of the form (3.24), which is solved as before.

3.4 Results

Table 15 shows, for m = 0, the least stable temporal eigenvalue of (3.17) for (I, J) = (10, 10), (14, 14), and (18, 18). These values were computed with a = 5, corresponding to a computational domain consisting of a spherical annulus with radii 1 and $r_\infty \equiv e^a = 148$. Additional calculations show that when the base flow and disturbance equations are solved on a smaller domain ($r_\infty = 90.0$), the computed temporal eigenvalues (with I = J = 14) differ by 4.5% and 3.3% at Re = 130 and 190, respectively. The results clearly indicate that for Re ≤ 190, all of the eigenvalues σ of the discretization are in the left half-plane. We therefore conclude that the flow is

stable with respect to axisymmetric disturbances for Re $\leq$ 190. For m = 0, we also plot the real part of the least stable temporal eigenvalue as a function of Reynolds number in figure 11.

The stability of the flow with respect to axisymmetric disturbances at higher Re was not investigated because of the discovery of an instability with respect to nonaxisymmetric disturbances with azimuthal wavenumber m = 1 at Re = 175.1.

Table 16 shows, for m = 1 and 160 $\leq$ Re $\leq$ 190, the temporal eigenvalue σ having the largest real part, for r_∞ = 148 and (I, J) = (12, 12), (14, 14), (16, 16), and (14, 16). (We have considered I = J and I $\neq$ J in order to examine the possible dependence of Re_1 and the disturbance eigenfunction on the truncation scheme employed (Steen & Aidun, 1988).) As in the m = 0 case, calculations using r_∞ = 90.0 gave least stable (most unstable) temporal eigenvalues differing only modestly from the results for r_∞ = 148 at Re = 130 and 190 (6.5% and 9.5%, respectively). For m = 1, we also plot the real part of the least stable temporal eigenvalue as a function of Reynolds number in figure 12.

The results indicate that disturbances with azimuthal wavenumber m = 1 become unstable at Re $\cong$ 175.1 with an imaginary part of approximately ω = 0.300. This corresponds to a Hopf bifurcation, and indicates that the onset of instability occurs *via* oscillatory disturbances. If the frequency is nondimensionalized in the same way as a Strouhal number (based on sphere diameter), we obtain $St_1 = \omega/\pi = 0.0955$. The computed values of Re_1 and St_1 are both in excellent agreement with experiment, as will be discussed in §3.5.

Figures 14(a-b) show the distribution of the temporal eigenvalues at Re = 175 with I = J = 14 and r_∞ = 148. From figure 14(a), we note that the eigenvalues cluster

along a curve which passes near to the origin of the σ-plane. Figure 14(b) shows that although a pair of eigenvalues with $Im(\sigma) = 0.300$ is the least stable at Re = 175, there are many other eigenvalues having real parts which are only slightly negative.

The number of functions retained in the expansion of the base flow in the computation of the above results for m = 1 was 28. Table 17 shows that this number is sufficient.

The results shown in Table 18 clearly indicate that the flow is stable for disturbances with m = 2 for $Re < Re_1$. For m = 2, we also plot the real part of the least stable temporal eigenvalue as a function of Reynolds number in figure 13. Table 19 suggests that the flow becomes increasingly stable with respect to disturbances having larger azimuthal wavenumbers, at least near Re_1.

Here, we make a few remarks regarding the interpretation of our analysis. We note that for either axisymmetric or nonaxisymmetric disturbances, the problem reduces to one of deciding whether the spectra of certain linear partial differential operators lie entirely in the left half-plane. We have approximated the linear operators by finite-dimensional matrices, the eigenvalues of which are taken to approximate those of the corresponding differential operators. This approach leaves in some doubt the status of the continuous spectrum of the original operator. Although we cannot prove that the continuous spectra (if in fact they exist) lie entirely in the left half-plane for all of the combinations of Re and m investigated, there is every reason (based on the reasonable agreement with experiment and the distribution of eigenvalues shown in figures 14(a-b)) to believe that the present results are in fact not corrupted by the discretization.

In order to better understand the three-dimensional character of the

nonaxisymmetric disturbance that becomes unstable at Re_1, we have examined an approximation to the oscillating wake. In particular, we have considered a composite flow consisting of the axisymmetric base flow to which is added some multiple of the eigenfunction of the linear stability problem, i.e.,

$$u_c(r,\theta,\phi,t) = \bar{U}_f(r,\theta) + u_1(r,\theta,\phi,t) \ , \tag{3.27}$$

with the amount of the linear eigenfunction added to the base flow chosen so that the maximum speed of the disturbance flow ($|u_1|$) is 0.0174, where the characteristic velocity of the base flow is unity, corresponding to the uniform flow. Equation (3.27) consists of a system of ordinary differential equations as follows:

$$\frac{dr}{dt} = u_{cr} = \bar{U}_{fr}(r,\theta) + u_{1r}(r,\theta,\phi,t)$$

$$r\,\frac{d\theta}{dt} = u_{c\theta} = \bar{U}_{f\theta}(r,\theta) + u_{1\theta}(r,\theta,\phi,t)$$

$$r\sin\theta\,\frac{d\phi}{dt} = u_{c\phi} = u_{1\phi}(r,\theta,\phi,t) \ ,$$

where the r-component of the perturbation velocity is expressed as

$$u_{1r}(r,\theta,\phi,t) = [\ \hat{u}_{1rR}(r,\theta)\cos(\phi + \sigma_I t) - \hat{u}_{1rI}(r,\theta)\sin(\phi + \sigma_I t)\ ]\exp(\sigma_R t) \ ,$$

and the subscripts R and I denote the real and imaginary parts of the complex eigenfunction and eigenvalue. The θ-component of the perturbation velocity has a similar expression and the ϕ-component is obtained from the continuity equation.

Although (3.27) is no longer a numerical solution of the full Navier-Stokes equations, it should be a good approximation to the actual flow just above Re_1 if instability sets in *via* oscillations of small amplitude (infinitesimal amplitude at the

bifurcation point).

For this composite flow, we have selected Re = 175, and computed the pathline for a fluid particle having an initial position r = 1.2 and θ = 30°. This point lies within the recirculating flow region for the base flow with Re = 175. Figure 15 shows two perspective views of the pathlines at a sequence of dimensionless times. We observe that the pathline resembles a trajectory on a torus having a noncircular, ϕ-dependent cross-section. In fact, the perimeter of the cross-section of the torus closely approximates a pathline (in a constant ϕ-plane) of the steady axisymmetric base flow. The helical nature of the disturbance is clearly evident. At larger Re (corresponding to a larger azimuthal velocity component), the pathlines will be less tightly wound. We can easily show that the particle trajectories will not be temporally periodic unless Re is chosen so that the number of times the pathline winds around the toroidal cross-section during a 2π change in ϕ is an integer.

The m = 1 eigenfunction can also be characterized in terms of the disturbance vorticity field. Figures 16(a-c) show the r- and θ-dependence of the azimuthal, polar, and radial components of the disturbance vorticity, with the real and imaginary parts in the upper and lower halves, respectively, of each figure. We note that the disturbance is strongest near the equator of the sphere, upstream of the separation point, which is located at θ = 63° for Re = 175. In each of the six cases (real and imaginary part of the three vorticity components), inspection of the entire field out to r = 148 revealed no other vorticity contours with level equal to or exceeding the contours shown. It is thus clear that although the disturbance manifests itself as a helical motion in the wake, its origin is in the instability of the boundary layer flow on the sphere.

3.5 Comparison to Experiment

In this section, our computational results are compared to a number of previous experiments. As discussed below, the experimental determination of Re_1 is complicated by the fact that the wake oscillations have a very low frequency. In light of this problem, we believe that the comparisons presented here are very good.

Möller (1938) vertically towed spheres equipped with dye ports through water in tanks of square cross-section. He found that the flow was steady below Re = 170, and that at Re = 200, the wake oscillated with a very low frequency. The ratio of tank width to sphere diameter was eight at Re = 170 and twenty at Re = 200. In light of the rather large blockage factor, we consider the agreement between Möller's experiment and our calculation to be very good.

Taneda (1956) reported that when a "Reynolds number of about 130 is reached, however, the faint periodic pulsatile motion with a very long period occurs at the rear of the vortex-ring". A possible explanation for the observation of unsteadiness at an Re below our computed Re_1 is given by Taneda, who noted "that a slight asymmetry of the flow pattern was caused by the presence of the support; namely the separation point just behind the support was moved slightly forward." The fact that the spheres were suspended by a single vertical support (with the base flow being primarily in the horizontal direction) means that, *per force*, the disturbance to the base flow had a substantial m = 1 component, which is the azimuthal mode with respect to which the flow is most unstable. In addition, Taneda's use of a thin piano wire (with diameter 0.3 mm or 0.5 mm and aspect ratios of 50 and 30, respectively) to support a much larger sphere (diameters between 9.52 mm and 19.82 mm) may allow considerable coupling between disturbances in the flow and the rigid body motion of

the sphere. It seems likely that Re_1 for a fixed (i.e., rigidly supported) sphere will be greater than or equal to the Re_1 for a sphere which is allowed to respond to flow disturbances, because the disturbances to which the latter sphere are subject are less constrained than those to which the former are subject. Thus, the lack of rigidity of the support may also contribute to Taneda's observation of instability at a lower Re than predicted by us.

Goldburg & Florsheim (1966) observed that the wake behind a falling sphere lost its axisymmetry at an Re of about 210, although they did not detect the loss of steadiness until Re = 270. We consider our results to be in good agreement with these, given the low frequency nature of the instability, which renders more difficult the discernment of unsteadiness.

Toulcova & Podzimek (1968) dropped aluminum alloy spheres through various solutions of glycerol and water, and reported that the transition to unsteadiness occurred at Re = 130. In a later study with the same spheres, Zikmundova (1970) reported a transition to unsteadiness in the range $130 < Re < 150$. Since Re_1 for falling spheres approaches the fixed-sphere value when the sphere/fluid density ratio ($\beta = \rho_f/\rho_s$) in the freely falling case approaches zero, we might expect Re_1 to be significantly lower for these experiments, in which $\beta = 0.46$. (Although neither the composition nor the density of the solutions was given, subsequent inquiry (private communication, J. Goodman (formerly J. Toulcova and J. Zikmundova) 1984) revealed that in all cases, the glycerol mass fraction was in excess of 0.99.)

Roos & Willmarth (1971) found that for a sphere towed through water and supported by a sting in the rear, a side force first became apparent at $Re \cong 290$, corresponding to a nonaxisymmetric force exerted on the sphere by the flow. They

also found that if a weighted sphere was supported by two fine threads, the onset of the side force occurred at Re ≅ 215. Roos (1968) concluded that the presence of a sting in the near wake had the effect of "tying down the tail of the wake bubble through the no-slip condition at the sting surface", and that this prevented oscillation of the wake under conditions where it otherwise would have been unstable (i.e., for $215 \leq Re \leq 290$). We think that our computed value of $Re_1 = 175.1$ is in good agreement with the value (Re ≅ 215) of Roos & Willmarth (1971).

Nakamura (1976) observed the trajectories of falling spheres to be vertical for Re < 190, with meandering at higher Re. Since it can be shown that the trajectory of a freely falling sphere subject to disturbances containing an m = 1 azimuthal component cannot be vertical, the onset of meandering corresponds to the onset of an m = 1 instability. Thus, we consider our results to be in excellent agreement with Nakamura's flow visualization experiments.

As for the frequency of the wake oscillations near the onset of instability, there is relatively little quantitative data with which our results can be compared. Probably the best data at low Re (below the onset of vortex shedding) is that of Roos (1968), who towed a 3 in (7.62 cm) diameter sphere supported by a side-sting in a 380 in (9.6 m) long tank having a 24 inch x 26 inch (60.96 cm x 66.04 cm) cross section, and found $St_1 \cong 0.087$. (This is an average of measurements at the six lowest Re, in the range 250 < Re < 450, with all values lying between 0.084 and 0.095.) We consider this to be in excellent agreement with our computed value $St_1 = 0.0955$.

In connection with the observations of Möller (1938) and Taneda (1956) regarding the low frequency nature of the wake oscillations, it is of interest to note that the dimensional frequency

$$f = \frac{\omega \nu Re}{4\pi R_0^2} \tag{3.28}$$

corresponding to $\omega = 0.300$ is very low in most of the previous experimental work in which Re_1 was estimated. Table 20 shows the sphere radii, fluids, and dimensional frequencies (calculated according to (3.28) with Re = 175.1) for previous experiments. The low frequencies undoubtedly contribute to the difficulty in observing the wake oscillations, especially at or near Re_1. (The experimental work of Stringham et al. (1969) is not included in Table 20 because their measured viscosity data for aqueous glycerol solutions are in serious disagreement with accepted sources (Segur & Oberstar 1951). We cannot correct for this by interpolating from the data of Segur & Oberstar because it is not known whether the discrepancy is due to poor viscometry or the absorption of atmospheric water by the extremely hygroscopic glycerol. We have also not used the data of Toulcova & Podzimek (1968) because of uncertainty about the degree to which the velocity of the falling sphere had approached its terminal value.)

3.6 Discussion

The present work provides the first accurate calculation of the critical Reynolds number at which the nonparallel flow past any body of revolution becomes unstable. Our results for a sphere are in good agreement with previous experimental work, for both Re_1 as well as the frequency of the wake oscillations. The predicted instability mode (m = 1) is the same as that observed experimentally at higher Re.

Our results are also in good agreement with the theoretical prediction by Monkewitz (1988b) of local absolute instability for a class of parallel axisymmetric wake profiles. His results are for the m = 1 azimuthal mode and are parameterized

by a centerline reversed flow parameter (Λ) and a shape parameter. In light of the fact that both the degree of reversed flow on the centerline, as well as the wake shape depend on downstream distance (due to the nonparallel nature of the flow), we have not attempted a direct comparison of our results for the sphere to Monkewitz's theory. However, we do note that our computed value $Re_1 = 175.1$, lies in the range ($10^2 < Re < 10^3$) in which Monkewitz has predicted the occurrence of local absolute instability for two values of Λ.

Since our analysis is a linear one that finds the smallest Re at which infinitesimally small disturbances will grow, the possibility remains that disturbances of finite amplitude might lead to the onset of subcritical instability at smaller Re. That the onset of instability in the steady axisymmetric base flow probably occurs by a linear mechanism is suggested by the agreement with experiment. First, the computed value of Re_1 and the associated Strouhal number are in good agreement with previous experimental values. (In those cases where the agreement between computed and experimental values of Re_1 leaves something to be desired, differences between experiment and the ideal situation considered in our analysis are such as to justify the magnitudes and signs of the discrepancies.) Moreover, the predicted azimuthal wavenumber ($m = 1$) is the same as that observed in experiments at higher Re.

Since in the two-dimensional case transition from steady flow to vortex shedding seems to be the result of a Hopf bifurcation, it would be interesting to determine whether the transition to vortex shedding in the three-dimensional case also proceeds *via* a linear mechanism. This question could be investigated by introducing disturbances into a three-dimensional time-dependent numerical simulation.

CHAPTER 4

Stability of the Motion of a Falling Sphere

4.1 Motivation

When a sphere falls (or rises) due to gravity, dimensional analysis and existing experimental data show that an additional parameter, the ratio of fluid density to sphere density, is involved if the flow is unsteady. This is because the sphere may be subjected to lateral forces due to nonaxisymmetric pressure and velocity distributions; the resulting acceleration and rigid body motion of an unconstrained sphere will depend on the sphere's mass (or in dimensionless terms, on the ratio of the fluid density to the sphere density).

In §1.3, we presented the Navier-Stokes equations for the flow of a viscous incompressible fluid about a sphere, along with the rigid body equations of motion for the sphere. We now specialize them to a form useful in the linear stability analysis for general small disturbances. In so doing, we combine the Navier-Stokes equations and the no-slip boundary condition in such a way that the linear stability problem does not explicitly involve the dynamic variables associated with the sphere's rigid body motion (i.e., $\mathbf{U}_s$ and Ω).

4.2 Linear Disturbance Equations

The linear stability of the steady axisymmetric flow can be investigated by expanding the pressure and velocity about their nominally steady axisymmetric values and retaining only the terms that are linear in the disturbance quantities. The zeroth order terms satisfy the steady equations (2.1a-d). Thus,

$$U_s = -k + u_s \qquad \Omega = 0 + \omega_\alpha \qquad \Phi = \bar{\Phi} + \Pi$$

$$U_f = \bar{U}_f + u_f \qquad H = \bar{H} + h$$

and we obtain the linear perturbation equations

$$\nabla \cdot u_f = 0 \tag{4.1a}$$

$$\frac{du_s}{dt} + \frac{\partial u_f}{\partial t} + (u_f \cdot \nabla)\,\bar{U}_f + (\bar{U}_f \cdot \nabla)\,u_f = -\nabla\Pi + \frac{2}{Re}\nabla^2 u_f \tag{4.1b}$$

$$\frac{du_s}{dt} = \frac{3\beta}{4\pi}\int_{S_o} dS \cdot h \tag{4.1c}$$

$$I \cdot \frac{d\omega_\alpha}{dt} = \frac{15\beta}{8\pi}\int_{S_o} r \times (dS \cdot h) \tag{4.1d}$$

$$u_f = \omega_\alpha \times r \qquad \text{on } S_o \tag{4.1e}$$

$$u_f \to -u_s \qquad \text{as } r \to \infty\,, \tag{4.1f}$$

Clearly, (4.1b,c) can be combined to eliminate u_s and (4.1d,e) can be combined to eliminate ω_α, leaving a boundary value problem involving only the disturbance pressure Π and velocity u_f as independent variables.

The resulting integro-differential equations are

$$\nabla \cdot u_f = 0 \tag{4.2a}$$

$$\frac{3\beta}{4\pi}\int_{S_o} dS \cdot h + \frac{\partial u_f}{\partial t} + (u_f \cdot \nabla)\,\bar{U}_f + (\bar{U}_f \cdot \nabla)\,u_f = -\nabla\Pi + \frac{2}{Re}\nabla^2 u_f \tag{4.2b}$$

$$\mathbf{I} \cdot \frac{\partial \mathbf{u}_f}{\partial t} = \frac{15\beta}{8\pi}\left[\int_{S_o} \mathbf{r} \times (d\mathbf{S} \cdot \mathbf{h})\right] \times \mathbf{r} \qquad \text{on } S_o \tag{4.2c}$$

$$\frac{\partial \mathbf{u}_f}{\partial t} \to -\frac{3\beta}{4\pi}\int_{S_o} d\mathbf{S} \cdot \mathbf{h} \qquad \text{as } r \to \infty \,. \tag{4.2d}$$

As in Chapter 3, the disturbances can be Fourier decomposed into azimuthal components according to

$$\mathbf{u}_f(r,\theta,\phi,t) = \sum_{m=-\infty}^{\infty} \mathbf{u}_m(r,\theta,t)\, e^{im\phi} \tag{4.3a}$$

and

$$\Pi(r,\theta,\phi,t) = \sum_{m=-\infty}^{\infty} p_m(r,\theta,t)\, e^{im\phi} \,. \tag{4.3b}$$

The Fourier decompositions are substituted into the equations (4.2a-d). Because of the axisymmetry of the base flow and the linearity of the disturbance equations, the individual Fourier modes are uncoupled and can be investigated separately.

4.2.1 Boundary Conditions

We now evaluate the force and torque on the sphere due to perturbation stresses, which appear in the boundary conditions (4.2c,d) and the first term in the momentum equation (4.2b). The forces due to σ_{rr}, $\tau_{r\theta}$, and $\tau_{r\phi}$ are calculated separately. By using the Fourier decompositions (4.3a,b) and Cartesian unit base vectors converted from the unit base vectors in a spherical coordinate system, we can perform the ϕ-integrations in the surface integrals and get force components in the x-,

y-, and z-directions. After summing the contributions from σ_{rr}, $\tau_{r\theta}$, and $\tau_{r\phi}$ in the x-, y-, and z-directions, we obtain

$$\int_{S_o} dS \cdot \mathbf{h} = F_x(t)\, \mathbf{e}_x + F_y(t)\, \mathbf{e}_y + F_z(t)\, \mathbf{e}_z \ ,$$

which can be rewritten as

$$\begin{aligned} \int_{S_o} dS \cdot \mathbf{h} = & [\ F_x(t) \sin\theta \cos\phi + F_y(t) \sin\theta \sin\phi + F_z(t) \cos\theta\ ]\, \mathbf{e}_r \\ & + [\ F_x(t) \cos\theta \cos\phi + F_y(t) \cos\theta \sin\phi - F_z(t) \sin\theta\ ]\, \mathbf{e}_\theta \\ & + [\ -F_x(t) \sin\phi + F_y(t) \cos\phi\ ]\, \mathbf{e}_\phi \ , \end{aligned} \tag{4.4}$$

in which F_x, F_y, and F_z are the components of the perturbation force acting on the sphere and are given by

$$\begin{aligned} F_x(t) = \pi \int_0^\pi \sin\theta \Big\{ & [\ f_1(\theta,t)+f_{-1}(\theta,t)\ ]\sin\theta + [\ g_1(\theta,t)+g_{-1}(\theta,t)\ ]\cos\theta \\ & - i[\ b_1(\theta,t)-b_{-1}(\theta,t)\ ] \Big\}\, d\theta \end{aligned}$$

$$\begin{aligned} F_y(t) = i\pi \int_0^\pi \sin\theta \Big\{ & [\ f_1(\theta,t)-f_{-1}(\theta,t)\ ]\sin\theta + [\ g_1(\theta,t)-g_{-1}(\theta,t)\ ]\cos\theta \\ & - i[\ b_1(\theta,t)+b_{-1}(\theta,t)\ ] \Big\}\, d\theta \end{aligned}$$

$$F_z(t) = 2\pi \int_0^{\pi} \sin\theta \, [\, f_o(\theta,t) \cos\theta - g_o(\theta,t) \sin\theta \,] \, d\theta \,,$$

where we have used the Fourier decompositions, and defined

$$f_m(\theta,t) = - p_m(1,\theta,t) + \frac{4}{Re} \frac{\partial u_{mr}(1,\theta,t)}{\partial r} \tag{4.5a}$$

$$g_m(\theta,t) = \frac{2}{Re} \left[\frac{\partial u_{m\theta}(1,\theta,t)}{\partial r} - u_{m\theta}(1,\theta,t) + \frac{\partial u_{mr}(1,\theta,t)}{\partial \theta} \right] \tag{4.5b}$$

$$b_m(\theta,t) = \frac{2}{Re} \left[\frac{im}{\sin\theta} u_{mr}(1,\theta,t) + \frac{\partial u_{m\phi}(1,\theta,t)}{\partial r} - u_{m\phi}(1,\theta,t) \right] . \tag{4.5c}$$

Next, we evaluate the torque acting on the sphere due to perturbation stresses, according to the boundary condition (4.2c). The torques due to $\tau_{r\theta}$ and $\tau_{r\phi}$ are calculated, separately. Again, by using the Fourier decompositions (4.3a,b) and Cartesian unit base vectors converted from the unit base vectors in a spherical coordinate system, we can perform the ϕ-integrations in the components of (4.2c) to obtain the torque components in the x-, y-, and z-directions. Summing the contributions from $\tau_{r\theta}$ and $\tau_{r\phi}$ in the x-, y-, and z-directions, we get

$$\int_{S_o} \mathbf{r} \times (d\mathbf{S} \cdot \mathbf{h}) = M_x(t)\, \mathbf{e}_x + M_y(t)\, \mathbf{e}_y + M_z(t)\, \mathbf{e}_z \,, \tag{4.6}$$

where M_x, M_y, and M_z are the components of the perturbation torque acting on the sphere. These are evaluated as

$$M_x(t) = -\pi \int_0^{\pi} \sin\theta \left\{ i[\, g_1(\theta,t)-g_{-1}(\theta,t)\,] + [\, b_1(\theta,t)+b_{-1}(\theta,t)\,]\cos\theta \right\} d\theta$$

$$M_y(t) = \pi \int_0^{\pi} \sin\theta \left\{ [\, g_1(\theta,t)+g_{-1}(\theta,t)\,] - i[\, b_1(\theta,t)-b_{-1}(\theta,t)\,]\cos\theta \right\} d\theta$$

$$M_z(t) = 2\pi \int_0^{\pi} b_0(\theta,t)\, \sin^2\theta \, d\theta \,,$$

where we have used the Fourier decompositions, and g_m and b_m are given in (4.5b) and (4.5c), respectively.

Using (4.6), we can evaluate the boundary condition (4.2c). The right hand side of (4.2c) is evaluated on the sphere as

$$\left[\int_{S_o} \mathbf{r} \times (d\mathbf{S} \cdot \mathbf{h}) \right] \times \mathbf{r} = [\, -M_x(t)\, \sin\phi + M_y(t)\, \cos\phi\,]\, \mathbf{e}_\theta$$

$$\{\, -[\, M_x(t)\, \cos\phi + M_y(t)\, \sin\phi\,]\, \cos\theta + M_z(t)\, \sin\theta\, \}\, \mathbf{e}_\phi \,. \qquad (4.7a)$$

The left hand side of (4.2c) is evaluated as

$$\mathbf{I} \cdot \frac{\partial \mathbf{u}_f}{\partial t} = \sum_{m=-\infty}^{\infty} e^{im\phi} \left[\frac{\partial u_{mr}}{\partial t}\, \mathbf{e}_r + \frac{\partial u_{m\theta}}{\partial t}\, \mathbf{e}_\theta + \frac{\partial u_{m\phi}}{\partial t}\, \mathbf{e}_\phi \right]. \qquad (4.7b)$$

By equating the right hand sides of (4.7a) and (4.7b), we evaluate the boundary condition represented by (4.2c) on the surface of the sphere. The result is decoupled about the azimuthal wavenumber m and is expressed as

$$\frac{\partial u_{mr}(1,\theta,t)}{\partial t} = 0 \qquad \text{for all } m \tag{4.8a}$$

$$\frac{\partial u_{m\theta}(1,\theta,t)}{\partial t} = 0 \qquad \text{for } m \neq 1 \tag{4.8b}$$

$$\frac{\partial u_{1\theta}(1,\theta,t)}{\partial t} = \frac{15\beta}{16\pi}\left[M_y(t) + i\, M_x(t) \right] \tag{4.8c}$$

$$\frac{\partial u_{0\phi}(1,\theta,t)}{\partial t} = \frac{15\beta}{8\pi} M_z(t) \sin\theta \tag{4.8d}$$

$$\frac{\partial u_{1\phi}(1,\theta,t)}{\partial t} = i\, \frac{15\beta}{16\pi} \cos\theta \left[M_y(t) + i\, M_x(t) \right] \tag{4.8e}$$

$$\frac{\partial u_{m\phi}(1,\theta,t)}{\partial t} = 0 \qquad \text{for } m \geq 2 \tag{4.8f}$$

$$\frac{\partial^2 u_{mr}(1,\theta,t)}{\partial t \partial r} = 0 \qquad \text{for all } m\,, \tag{4.8g}$$

where (4.8g) is obtained by taking the time derivative of (4.2a), and

$$M_y(t) + i\, M_x(t) = \frac{4\pi}{Re} \int_0^{\pi} \sin\theta \left[(1+\cos^2\theta) \left[\frac{\partial u_{1\theta}}{\partial r} - u_{1\theta} \right]_{r=1} + \sin\theta \cos\theta \left[\frac{\partial^2 u_{1\theta}}{\partial r \partial \theta} + \frac{\partial^2 u_{1r}}{\partial r^2} \right]_{r=1} \right] d\theta\,. \tag{4.8h}$$

By using (4.4), we evaluate the boundary condition at infinity (4.2d). The result is again decoupled about the azimuthal wavenumber m, and is written as

$$\frac{\partial u_{0r}(r,\theta,t)}{\partial t} \rightarrow -\frac{3\beta}{4\pi} F_z(t) \cos\theta \tag{4.9a}$$

$$\frac{\partial u_{1r}(r,\theta,t)}{\partial t} \to -\frac{3\beta}{8\pi} \sin\theta \, [\, F_x(t) - i\, F_y(t) \,] \tag{4.9b}$$

$$\frac{\partial u_{mr}(r,\theta,t)}{\partial t} \to 0 \qquad \text{for } m \geq 2 \tag{4.9c}$$

$$\frac{\partial u_{0\theta}(r,\theta,t)}{\partial t} \to \frac{3\beta}{4\pi} F_z(t) \sin\theta \tag{4.9d}$$

$$\frac{\partial u_{1\theta}(r,\theta,t)}{\partial t} \to -\frac{3\beta}{8\pi} \cos\theta \, [\, F_x(t) - i\, F_y(t) \,] \tag{4.9e}$$

$$\frac{\partial u_{m\theta}(r,\theta,t)}{\partial t} \to 0 \qquad \text{for } m \geq 2 \tag{4.9f}$$

$$\frac{\partial u_{1\phi}(r,\theta,t)}{\partial t} \to -\frac{3\beta}{8\pi} i \, [\, F_x(t) - i\, F_y(t) \,] \tag{4.9g}$$

$$\frac{\partial u_{m\phi}(r,\theta,t)}{\partial t} \to 0 \qquad \text{for } m \neq 1 \tag{4.9h}$$

as $r \to \infty$, where

$$F_x(t) - i\, F_y(t) = \frac{4\pi}{(1-\beta)\,\mathrm{Re}} \int_0^{\pi} [\, -i \sin^3\theta \, A_f(1,\theta,t) + B_f(1,\theta,t) \,]\, d\theta \tag{4.10a}$$

$$F_z(t) = \frac{4\pi}{(1-\beta)\,\mathrm{Re}} \int_0^{\pi} \left[\sin\theta \cos\theta \, D_f(1,\theta,t) - \sin^2\theta \, \frac{\partial u_{0\theta}}{\partial r}(1,\theta,t) \right] d\theta \tag{4.10b}$$

$$A_f(1,\theta,t) = -i \left[\sin\theta \left\{ 6 \frac{\partial^2 u_{1r}}{\partial r^2} + \frac{\partial^3 u_{1r}}{\partial r^3} \right\}_{r=1} + \cos\theta \left\{ 2 \frac{\partial u_{1\theta}}{\partial r} + \frac{\partial^2 u_{1\theta}}{\partial r^2} \right\}_{r=1} \right.$$
$$\left. + \sin\theta \left\{ 2 \frac{\partial^2 u_{1\theta}}{\partial r \partial \theta} + \frac{\partial^3 u_{1\theta}}{\partial r^2 \partial \theta} \right\}_{r=1} - 2 \cos\theta \, (u_{1\theta})_{r=1} \right]$$

$$B_f(1,\theta,t) = 2 \sin\theta \cos\theta \left\{ \frac{\partial u_{1\theta}}{\partial r} - u_{1\theta} \right\}_{r=1} + \sin^2\theta \left\{ \frac{\partial^2 u_{1r}}{\partial r^2} + \frac{\partial^2 u_{1\theta}}{\partial r \partial \theta} \right\}_{r=1}$$

$$C_f(1,\theta,t) = -\left[2\frac{\partial u_{0\theta}}{\partial r} + \frac{\partial^2 u_{0\theta}}{\partial r^2}\right]_{r=1}$$

and

$$D_f(1,\theta,t) = \int^{\theta} C_f(1,\theta',t)\, d\theta' .$$

Finally, we notice that the boundary conditions used for the stability of flow past a fixed sphere in Chapter 3 are recovered when the density ratio β approaches zero in (4.8) and (4.9).

4.2.2 Navier-Stokes Equations

In this section, we rewrite the linearization of the momentum equation (4.2b). First, we use the Fourier decompostion (4.3a,b), and resolve (4.2b) into three scalar components, using (4.4) to represent the rigid body coupling term. Because of the axisymmetry of the base flow and the linearity of the disturbance equations, the individual Fourier modes are uncoupled and can be investigated separately.

For axisymmetric (m = 0) disturbances, we can eliminate the pressure and rigid body coupling term by subtracting the r-derivative of the θ-component of the momentum equation multiplied by r, from the θ-derivative of the r-component of the momentum equation. The combined equation does not involve $u_{0\phi}$, and we define a streamfunction-like variable $\psi_{ps}(r,\theta,t)$ such that

$$u_{0r} = \frac{1}{r^2 \sin\theta}\frac{\partial \psi_{ps}}{\partial \theta}, \qquad u_{0\theta} = -\frac{1}{r \sin\theta}\frac{\partial \psi_{ps}}{\partial r}$$

satisfies the axisymmetric continuity equation. The final expression is

$$\frac{\partial(D^2\psi_{ps})}{\partial t} + \frac{1}{r^2}\left\{\frac{\partial\Psi_s}{\partial r}\frac{\partial}{\partial\zeta} - \frac{\partial\Psi_s}{\partial\zeta}\frac{\partial}{\partial r} + \frac{2\zeta}{1-\zeta^2}\frac{\partial\Psi_s}{\partial r} + \frac{2}{r}\frac{\partial\Psi_s}{\partial\zeta}\right\}D^2\psi_{ps}$$

$$+ \frac{1}{r^2}\left\{\frac{\partial\psi_{ps}}{\partial r}\frac{\partial}{\partial\zeta} - \frac{\partial\psi_{ps}}{\partial\zeta}\frac{\partial}{\partial r} + \frac{2\zeta}{1-\zeta^2}\frac{\partial\psi_{ps}}{\partial r} + \frac{2}{r}\frac{\partial\psi_{ps}}{\partial\zeta}\right\}D^2\Psi_s - \frac{2}{Re}D^4\psi_{ps} = 0 \quad , \quad (4.11a)$$

where the subscript s denotes a base flow quantity. In (4.11a), we have defined $\zeta = \cos\theta$, and

$$D^2 \equiv \frac{\partial^2}{\partial r^2} + \frac{1-\zeta^2}{r^2}\frac{\partial^2}{\partial\zeta^2} .$$

The ϕ-component of the momentum equation is expressed as

$$\frac{\partial u_{0\phi}}{\partial t} + \bar{U}_r\frac{\partial u_{0\phi}}{\partial r} + \frac{\bar{U}_\theta}{r}\frac{\partial u_{0\phi}}{\partial\theta} + \frac{\bar{U}_r u_{0\phi}}{r} + \frac{\bar{U}_\theta u_{0\phi}}{r}\cot\theta = \frac{2}{Re}\left[\nabla^2 u_{0\phi} - \frac{u_{0\phi}}{r^2\sin^2\theta}\right] ,$$

which is decoupled from the r- and θ-components of the momentum equation, and can be solved separately. This equation is further simplified to

$$\frac{Du_{0\phi}}{Dt} = \frac{2}{Re}\nabla^2 u_{0\phi} - \frac{2u_{0\phi}}{r^2 Re\sin^2\theta}\left[1 + \frac{Re}{2}r\sin\theta\,(\bar{\mathbf{U}}\cdot\mathbf{i}_\omega)\right] , \qquad (4.11b)$$

where $\mathbf{i}_\omega$ is the unit vector normal to the symmetry axis.

We observe that (4.11a,b) do not involve the density ratio β. The differential equation (4.11a) is identical to (3.3), but is subject to boundary conditions at infinity derived from (4.9a,d). On the other hand, the differential equation (4.11b) is a convective diffusion equation. Thus, its solution will decay if the quantity inside the square brackets in (4.11b) is nonnegative.

Because the disturbance variables $\mathbf{u}_f$ and Π must be real, we require that $\mathbf{u}_{-m} = \mathbf{u}_m^*$ and $p_{-m} = p_m^*$, where * denotes a complex conjugate. As the case $m = 0$

has been treated above, attention will be restricted to $m \geq 1$.

For $m \geq 1$, we can use the continuity equation (4.2a) to eliminate $u_{m\phi}$, and the ϕ-component of the momentum equation (4.2b) to eliminate p_m, where we note that $\partial u'_{m\phi}/\partial\phi = imu'_{m\phi}$ and $\partial p'_m/\partial\phi = imp'_m$. When the expression for p_m (obtained from the ϕ-component of the momentum equation) is substituted into the r- and θ-components of the momentum equation, the rigid body coupling term cancels in each equation. The final result is a pair of partial differential equations for the r- and ζ-components of the velocity

$$\frac{\partial}{\partial t}\left[m^2\, u_{mr} + \sin^2\theta\, \frac{\partial}{\partial r}(r\, h_m)\right]$$

$$+ m^2\left[\frac{\partial}{\partial r}(\bar{U}_r u_{mr}) - \frac{\sin\theta}{r}\left[\frac{\partial \bar{U}_r}{\partial \zeta}\, u_{m\zeta} + \bar{U}_\zeta\, \frac{\partial u_{mr}}{\partial \zeta}\right] - \frac{2}{r}\,\bar{U}_\zeta u_{m\zeta}\right]$$

$$+ \sin^2\theta\, \frac{\partial}{\partial r}\left[r\,\bar{U}_r\, \frac{\partial h_m}{\partial r} - \bar{U}_\zeta\, \frac{\partial}{\partial \zeta}(h_m \sin\theta) + \bar{U}_r h_m + h_m\, \bar{U}_\zeta \cot\theta\right]$$

$$+ \frac{2}{Re}\left\{\frac{m^2}{r^2}\left[-\frac{\partial}{\partial r}\left[r^2\, \frac{\partial u_{mr}}{\partial r}\right] - \frac{\partial}{\partial \zeta}\left[\sin^2\theta\, \frac{\partial u_{mr}}{\partial \zeta}\right] + 2\, u_{mr} + \frac{m^2}{\sin^2\theta}\, u_{mr}\right]\right.$$

$$- \sin\theta\, \frac{\partial}{\partial r}\left[\frac{\sin\theta}{r}\, \frac{\partial}{\partial r}\left[r^2\, \frac{\partial h_m}{\partial r}\right] + \frac{1}{r}\, \frac{\partial}{\partial \zeta}\left[\sin^2\theta\, \frac{\partial}{\partial \zeta}(h_m \sin\theta)\right]\right]$$

$$\left. + (1+m^2)\, \frac{\partial}{\partial r}\left[\frac{h_m}{r}\right] + 2m^2\left[\cot\theta\, \frac{\partial}{\partial r}\left[\frac{u_{m\zeta}}{r}\right] - \frac{3}{r^2}\, u_{mr}\right]\right\} = 0 \qquad (4.12a)$$

and

$$\frac{\partial}{\partial t}\left[m^2 u_{m\zeta} - \sin\theta\ \frac{\partial}{\partial \zeta}\left(h_m \sin^2\theta\right)\right]$$

$$+ m^2\left[u_{mr}\left(\frac{\partial}{\partial r} + \frac{1}{r}\right)\bar{U}_\zeta + \bar{U}_r\left(\frac{\partial}{\partial r} + \frac{1}{r}\right)u_{m\zeta} - \frac{\sin\theta}{r}\frac{\partial}{\partial \zeta}\left(\bar{U}_\zeta u_{m\zeta}\right)\right]$$

$$- \sin\theta\ \frac{\partial}{\partial \zeta}\left[\sin^2\theta\left[\bar{U}_r\ \frac{\partial h_m}{\partial r} - \frac{\bar{U}_\zeta}{r}\frac{\partial}{\partial \zeta}\left(h_m \sin\theta\right) + \frac{\bar{U}_r}{r}h_m + \frac{\bar{U}_\zeta}{r}h_m \cot\theta\right]\right]$$

$$+ \frac{2}{Re}\left\{\frac{m^2}{r^2}\left[-\frac{\partial}{\partial r}\left[r^2\ \frac{\partial u_{m\zeta}}{\partial r}\right] - \frac{\partial}{\partial \zeta}\left[\sin^2\theta\ \frac{\partial u_{m\zeta}}{\partial \zeta}\right] + \frac{1+m^2}{\sin^2\theta}u_{m\zeta} - 2\sin\theta\ \frac{\partial}{\partial \zeta}\left(u_{m\zeta}\cot\theta\right)\right]\right.$$

$$+ \frac{\sin\theta}{r^2}\frac{\partial}{\partial \zeta}\left[\sin^2\theta\ \frac{\partial}{\partial r}\left[r^2\ \frac{\partial h_m}{\partial r}\right] + \sin\theta\ \frac{\partial}{\partial \zeta}\left[\sin^2\theta\ \frac{\partial}{\partial \zeta}\left(h_m \sin\theta\right)\right]\right]$$

$$\left. - \frac{1+m^2}{r^2}\sin\theta\ \frac{\partial h_m}{\partial \zeta} + \frac{2m^2}{r^2}h_m \cot\theta\right\} = 0\ , \qquad (4.12b)$$

where

$$h_m = \frac{\partial}{\partial \zeta}\left(u_{m\zeta}\sin\theta\right) - \frac{1}{r}\frac{\partial}{\partial r}\left(r^2\ u_{mr}\right)\ .$$

Finally, we notice that, as in the case $m = 0$, (4.12a,b) do not involve the density ratio β. Thus, for any m, the linear disturbance forms of the momentum equation are identical for spheres which are fixed or falling under gravity. However, they are subject to different boundary conditions, as will be shown in the next section.

4.3 Solution Procedure

For $m = 0$, we use a streamfunction-like variable for the r- and θ-component of the linear disturbance equations, given as (4.11a) in the previous section. We again investigate modal solutions of the form

$$\psi_{ps}(r,\zeta,t) = \psi'(r,\zeta)\, e^{\sigma t} \ , \tag{4.13}$$

where σ is the temporal eigenvalue. As mentioned in the previous section, the differential equation (4.11a) after (4.13) is substituted into it is identical to (3.7), but is subject to the boundary conditions

$$\psi'(1,\zeta) = 0 \qquad \frac{\partial \psi'(1,\zeta)}{\partial r} = 0 \ , \tag{4.14a,b}$$

$$\lim_{r \to \infty} \quad \sigma\, \psi'(r,\zeta) \to -\, \frac{3\beta}{4\pi}\, \hat{F}_z\, \frac{r^2}{2} \sin^2\theta \ , \tag{4.15}$$

where (4.14a,b) are obtained from (4.8a,b), (4.15) is obtained from (4.9a,d), and $\hat{F}_z$ is found from (4.10b) after substituting the modal solution (4.13).

For $m \geq 1$, we use a modified primitive variables formulation (4.12a,b). As with axisymmetric disturbances, we consider modal solutions of the form

$$u_{mr}(r,\zeta,t) = e^{\sigma t}\, \hat{u}_{mr}(r,\zeta) \tag{4.16a}$$

$$u_{m\zeta}(r,\zeta,t) = e^{\sigma t}\, \hat{u}_{m\zeta}(r,\zeta) \ , \tag{4.16b}$$

leading to two coupled equations in r and ζ which constitute an eigenvalue problem for σ. The final result is a pair of partial differential equations for the r- and ζ-components of the velocity, exactly as in (3.22a,b) for the stability of flow past a fixed sphere, but subject to different boundary conditions.

For $m = 1$, the boundary conditions to be satisfied are

$$\hat{u}_{1r}(1,\theta) = 0 \qquad \frac{\partial \hat{u}_{1r}}{\partial r}(1,\theta) = 0 \tag{4.17a,b}$$

$$\sigma\, \hat{u}_{1\theta}(1,\theta) = \frac{15\beta}{16\pi} [\, \hat{M}_y + i\, \hat{M}_x \,] \tag{4.17c}$$

on the sphere, where (4.17a,b) are obtained from (4.8a,g), (4.17c) is obtained from (4.8c), and $[\, \hat{M}_y + i\, \hat{M}_x \,]$ is found by substituting the modal solution (4.16a,b) into (4.8h). The far-field boundary conditions to be satisfied are

$$\sigma\, \hat{u}_{1r}(r,\theta) \to -\frac{3\beta}{8\pi} \sin\theta\, [\, \hat{F}_x - i\, \hat{F}_y \,] \tag{4.18a}$$

$$\sigma\, \hat{u}_{1\theta}(r,\theta) \to -\frac{3\beta}{8\pi} \cos\theta\, [\, \hat{F}_x - i\, \hat{F}_y \,] \tag{4.18b}$$

as $r \to \infty$, where (4.18a,b) are obtained from (4.9b) and (4.9e), and $[\, \hat{F}_x - i\, \hat{F}_y \,]$ is found by substituting the modal solution (4.16a,b) into (4.10a).

For $m \geq 2$, the boundary conditions to be satisfied are

$$\hat{u}_{mr}(1,\theta) = 0 \qquad \frac{\partial \hat{u}_{mr}}{\partial r}(1,\theta) = 0 \tag{4.19a,b}$$

$$\hat{u}_{m\theta}(1,\theta) = 0 \tag{4.19c}$$

on the sphere and

$$\hat{u}_{mr}(r,\theta) \to 0 \tag{4.20a}$$

$$\hat{u}_{m\theta}(r,\theta) \to 0 \tag{4.20b}$$

as $r \to \infty$. Here (4.19a,b,c) and (4.20a,b) are consequences of (4.8a,b,g) and (4.9c,f), respectively.

We note that for $m \geq 2$, the boundary conditions as well as the differential equations are exactly the same as in the case of the stability of flow past a fixed sphere. Thus, the stability of the motion of a falling/rising sphere with respect to

disturbances having azimuthal wavenumber $m \geq 2$ does not need to be considered further.

CHAPTER 5

Conclusions

We have presented a new spectral Galerkin technique for the steady axisymmetric flow past a sphere, which is well-suited for accurate calculation of the flow near the sphere, and in particular, in the near wake for the entire range of Reynolds numbers for which the steady axisymmetric flow is stable and hence physically realizable. The new technique also gives closer agreement with the classical experiments of Taneda (1956) than does any previous calculation.

We have performed a linear stability analysis of the steady axisymmetric base flow with respect to axisymmetric and nonaxisymmetric disturbances. The analysis shows that, for a fixed sphere, the axisymmetric base flow undergoes a Hopf bifurcation at Re = 175.1 with the critical disturbance having azimuthal wavenumber m = 1 and Strouhal number St = 0.0955. The computed value of Re_1 and the associated Strouhal number are in good agreement with previous experimental values. Moreover, the predicted azimuthal wavenumber (m = 1) is the same as that observed in experiments at higher Reynolds numbers.

We have also derived the differential equations and boundary conditions for a sphere falling under gravity through an otherwise quiescent fluid and obtained the equations governing the behavior of small disturbances, in a form which does not involve the dynamical variables associated with the sphere's rigid body motion. The linear disturbance equations differ from those for the fixed sphere case only in the appearance of the fluid/sphere density ratio ($\beta = \rho_f/\rho_s$) in the boundary conditions.

The problem of the stability of flow past a fixed sphere is exactly recovered when $\beta = 0$.

The methods employed in this investigation of the stability of flow past a sphere can be extended, *via* the use of a body-fitted coordinate system, to other finite axisymmetric bluff bodies such as disks, ellipsoids of revolution, and cones. The onset of instability for each of these has been experimentally investigated (Willmarth, Hawk & Harvey 1964, Goldburg & Florsheim 1966, Stringham, Simons & Guy 1969). Another extension would be to the prediction of the observed shape and trajectory (Magarvey & Bishop 1961a,b, Magarvey & MacLatchy 1965, Winnikow & Chao 1966, and Yeheskel & Kehat 1971) of small droplets and bubbles under the influence of gravity, with an accounting in the nominally steady axisymmetric basic flow for both the internal circulation and the drop's departure from sphericity.

Table 1. Effect of the size of the computational domain for Re = 0.1 with K = L = 20.

a	r_∞	C_D	rel error
1.5	4.48	304.174	2.46×10^{-1}
2.0	7.39	275.089	1.27×10^{-1}
2.5	12.2	260.238	6.58×10^{-2}
3.0	20.1	252.165	3.27×10^{-2}
3.5	33.1	247.753	1.46×10^{-2}
4.0	54.6	245.498	5.41×10^{-3}
4.5	90.0	244.549	1.53×10^{-3}
5.0	148	244.267	3.7×10^{-4}
5.5	245	244.199	9.4×10^{-5}
6.0	403	244.181	2×10^{-5}
6.5	665	244.176	0
7.0	1097	244.176	0

Table 2. Effect of the number of the spectral coefficients for Re = 0.1 with a = 6.5 ($r_\infty = 665$).

K = L	C_D	rel error
2	246.209	8.33×10^{-3}
4	243.340	-3.42×10^{-3}
6	244.402	9.26×10^{-4}
8	244.297	4.96×10^{-4}
10	244.225	2.0×10^{-4}
12	244.190	5.7×10^{-5}
14	244.179	1×10^{-5}
16	244.177	4×10^{-6}
18	244.176	0
20	244.176	0

Table 3. Effect of the size of the computational domain for Re = 40 with K = L = 20.

a	r_∞	C_D	l_s	θ_s	relative error		
					C_D	l_s	θ_s
1.5	4.48	1.767	0.538	35.281	-1.2×10^{-1}	-1.5×10^{-1}	-5.9×10^{-2}
2.0	7.39	1.774	0.561	35.684	-1.1×10^{-1}	-1.2×10^{-1}	-4.8×10^{-2}
2.5	12.2	1.958	0.634	37.252	-2.0×10^{-2}	0	-6.6×10^{-3}
3.0	20.1	2.041	0.633	37.870	2.2×10^{-2}	-2×10^{-3}	9.9×10^{-3}
3.5	33.1	2.009	0.675	37.591	5.5×10^{-3}	6.5×10^{-2}	2.5×10^{-3}
4.0	54.6	1.999	0.650	37.507	5×10^{-4}	2.5×10^{-2}	2×10^{-4}
4.5	90.0	1.998	0.634	37.500	0	0	5×10^{-5}
5.0	148	1.998	0.634	37.498	0	0	0

Table 4. Effect of the number of the spectral coefficients for Re = 40 with a = 5 ($r_\infty = 148$).

K = L	C_D	l_s	θ_s
2	2.593	0.355	52.206
4	2.631	0.000	0.000
6	2.507	0.000	43.156
8	2.289	1.003	22.471
10	2.209	0.583	38.393
12	2.147	0.706	37.842
14	2.096	0.646	37.612
16	2.056	0.652	37.844
18	2.024	0.657	37.616
20	1.998	0.634	37.498
22	1.975	0.629	37.351
24	1.956	0.628	37.222
26	1.940	0.621	37.102
28	1.926	0.613	36.995
30	1.914	0.608	36.899

Table 5. Dependence of C_D on the angular expansion for Re = 40 with K = 20 and a = 5.

L	C_{DP}	C_{DV}	C_D	l_s	θ_s
12	0.820	1.179	1.999	0.683	37.056
14	0.820	1.178	1.998	0.702	37.154
16	0.820	1.178	1.998	0.619	37.535
18	0.820	1.178	1.998	0.647	37.447
20	0.820	1.178	1.998	0.634	37.498

Table 6. Effect of the size of the computational domain for Re = 180 with K = L = 28.

a	r_∞	C_D	l_s	θ_s	relative error		
					C_D	l_s	θ_s
1.5	4.48	0.791	2.836	62.972	-2.0×10^{-1}	7.2×10^{-2}	-1.8×10^{-2}
2.0	7.39	0.861	2.722	63.035	-1.3×10^{-1}	2.9×10^{-2}	-1.7×10^{-2}
2.5	12.2	1.061	2.657	64.883	7.1×10^{-2}	4.5×10^{-3}	1.2×10^{-2}
3.0	20.1	1.007	2.677	64.290	1.6×10^{-2}	1.2×10^{-2}	2.8×10^{-3}
3.5	33.1	0.993	2.637	64.147	2×10^{-3}	-3×10^{-3}	5.5×10^{-4}
4.0	54.6	0.991	2.648	64.114	0	1×10^{-3}	3×10^{-5}
4.5	90.0	0.991	2.645	64.112	0	0	0
5.0	148	0.992	2.645	64.153	1×10^{-5}	0	6.4×10^{-4}

Table 7. Effect of the number of the spectral coefficients for Re = 180 with a = 5 ($r_\infty = 148$).

K, L	C_D	l_s	θ_s
2, 2			
4, 4	1.273	0.478	69.106
6, 6	1.159	0.000	0.000
8, 8	1.198	0.000	0.000
10, 10			
12, 12			
14, 14	1.081	2.645	66.516
16, 16	1.041	2.749	61.591
18, 18	1.048	3.012	63.952
20, 20	1.031	3.009	64.802
22, 22	1.025	2.554	64.240
24, 24	1.008	2.496	64.130
26, 26	1.000	2.571	64.231
28, 28	0.992	2.645	64.153
30, 30	0.983	2.698	64.055
32, 32	0.976	2.719	64.022
34, 34	0.969	2.719	63.973
46, 34	0.934	2.714	63.657
48, 34	0.929	2.714	63.614
50, 34	0.925	2.712	63.573

Table 8. l_s and θ_s near the Reynolds number for separation with a = 6 ($r_\infty = 403$).

Re	K = L	l_s	θ_s	$\theta_{s\infty}$	SD
20	26	0.000	0.000		
	28	0.000	0.000		
	30	0.000	0.000	0.000	
20.5	26	0.017	7.194		
	28	0.015	6.772		
	30	0.013	6.390		
	32	0.011	6.035		
	38	0.007	5.116		
	40	0.006	4.849	0.510	0.0131
21	26	0.033	10.172		
	28	0.031	9.865		
	30	0.028	9.593		
	32	0.026	9.351		
	38	0.017	8.762		
	40	0.015	8.604	5.690	0.0080
22	26	0.067	14.243		
	28	0.064	14.026		
	30	0.062	13.835		
	36	0.053	13.390		
	38	0.051	13.276		
	40	0.050	13.173	11.180	0.0012
24	26	0.136	19.630		
	28	0.133	19.467		
	30	0.132	19.324		
	32	0.131	19.197		
	34	0.129	19.085		
	36	0.128	18.985	17.307	0.0014

Table 9. Effect of the outer boundary
for Re = 20 with K = L = 28.

a	r_∞	C_D	l_s	θ_s
5.0	148	2.817	0.004	3.388
5.5	245	2.816	0.000	0.000
6.0	403	2.816	0.000	0.000

Table 10. Drag coefficient at Re = 0.1.

Authors	C_{DP}	C_{DV}	C_D	Remark
Hamielec et al.			262	
LeClair et al.	81.056	163.445	244.501	$C_{DP} < C_D/3$
Dennis & Walker	81.4	162.8	244.2	$C_{DP} = C_D/3$
Present result	81.395	162.781	244.176	$C_{DP} > C_D/3$

Table 11. Reynolds number for separation obtained by various authors.

Authors	Re_s	Technique	Remarks
Taneda (1956)	24	Experiment	Extrapolation of l_s data for $Re > 25$. Data contains very little scatter.
Kalra & Uhlherr (1973)	20	"	Extrapolation of l_s data for $Re > 27$. Data contains considerable scatter
Kawaguti (1948)	39	Spectral Galerkin	Cited by Hamielec et al. (1967)
Proudman & Pearson (1957)	16	2 term Stokes expansion	
Jenson (1959)	17	Finite difference	Value of Re_s given in abstract. Method of determination unclear.
Hamielec et al. (1967)	22	"	Extrapolation of l_s data at Re = 40 and 100.
Rimon & Cheng (1969)	10	"	
Pruppacher et al. (1970)	20	"	Extrapolation of l_s data at Re = 22, 24, and 30.
Dennis & Walker (1971)	20.5	Series truncation	Linear interpolation between the values at Re = 20 and 40.
Lin & Lee (1973)	20	Finite difference	Their figure 2 shows that the flow is separated at $Re < 20$.
Present work	20.5	Spectral Galerkin	Method of estimation discussed in §2.4

Table 12. Comparison with previous calculations

Authors	r_∞	Re=40		Re=100		Re=120	
		l_s	θ_s	l_s	θ_s	l_s	θ_s
Taneda (1956)		0.61	–	1.80	54.0	2.04	57.4
Kalra & Uhlherr (1973)		0.80	32.0	1.77	49.0	2.06	52.0
Kawaguti (1955)	∞	0.01	15.4	0.65	60.0	–	–
Jenson (1959)	6	0.45	32.0*	–	–	–	–
Hamielec (1967)	15, 7	0.54	38.8	2.04	51.0	–	–
Rimon & Cheng (1969)	20	0.74	39.0	1.64	50.5	–	–
Pruppacher et al. (1970)	12	–	–	1.92	–	–	–
Dennis & Walker (1971)	148	0.60*	35.0	–	–	–	–
Lin & Lee (1973)	20, 12	0.65	37.0	1.91	53.0	–	–
Cliffe & Lever (1983)	37	0.56	37.5	–	–	–	–
Dandy & Leal (1986)	∞	0.62*	36.0*	–	–	2.14*	56.0*
Oliver & Chung (1987)	300	0.68*	36.1	–	–	–	–
Fornberg (1988)	148	–	–	1.747*	52.5	–	–
Proudman & Pearson (1957)		0.70	31.79	1.82	37.81	2.11	38.43
Present results (K,L) in Table 13 extrapolation of θ_s		0.613	37.00 35.59	1.810	54.17 53.81	2.089	57.16 56.79

* numerical values reported by author(s). All other values read from plots.

Table 12. continued

Authors	Re=150		Re=180		Re=200		Remarks
	l_s	θ_s	l_s	θ_s	l_s	θ_s	
Taneda	2.33	60.5	–	63.0	–	64.0	Experiment
Kalra & Uhlherr	2.32	56.0	–	59.0	–	61.0	"
Kawaguti	–	–	–	–	–	–	Spectral Galerkin
Jenson	–	–	–	–	–	–	Finite difference
Hamielec	–	–	–	–	–	–	"
Rimon & Cheng	–	–	–	–	–	–	"
Pruppacher et al.	–	–	–	–	–	–	"
Dennis & Walker	–	–	–	–	–	–	Series truncation
Lin & Lee	–	–	–	–	2.45	60.8	Finite difference
Cliffe & Lever	–	–	–	–	–	–	Finite element
Dandy & Leal	2.7*	59.5*	2.9*	62.0*	–	–	Finite difference
Oliver & Chung	–	–	–	–	–	–	Series truncation
Fornberg	–	–	–	–	2.871*	62.5	Finite difference
Proudman & Pearson	2.51	39.04	2.87	39.45	3.09	39.65	2 term Stokes expansion
Present results (K,L) in Table 13	2.392	60.72	2.712	63.57	2.875	65.20	Spectral Galerkin
extrapolation of θ_s		60.36		63.12		64.90	

Table 13. Size of computational domain and truncation level used in table 12.

Re	a	r_∞	K, L
40	5	148	28, 28
100	5	148	50, 28
120	5	148	50, 28
150	5	148	50, 28
180	5	148	50, 34
200	4.5	90	50, 38

Table 14. Detailed convergence of l_s and θ_s
for Reynolds numbers used in table 12 and 13.

Re	K = L	l_s	θ_s	$\theta_{s\infty}$	SD
40	24	0.628	37.222		
	26	0.621	37.102		
	28	0.613	36.995		
	30	0.608	36.899		
	32	0.610	36.814	35.594	0.0027
100	24	1.829	54.976		
	26	1.818	54.918		
	28	1.813	54.840		
	30	1.815	54.757		
	32	1.813	54.682	53.807	0.0144
120	24	2.102	57.972		
	26	2.111	57.865		
	28	2.095	57.813		
	30	2.085	57.741		
	32	2.084	57.665	56.787	0.0098
150	24	2.340	61.490		
	26	2.402	61.427		
	28	2.441	61.318		
	30	2.449	61.272		
	32	2.440	61.214	60.362	0.0112

Table 14. continued

Re	K = L	l_s	θ_s	$\theta_{s\infty}$	SD
180	26	2.571	64.231		
	28	2.645	64.153		
	30	2.698	64.055		
	32	2.719	64.022		
	34	2.719	63.973	63.116	0.0116
200	28	2.733	65.708		
	30	2.801	65.644		
	32	2.847	65.611		
	34	2.875	65.568		
	36	2.875	65.523	64.901	0.0051

Table 15. Least stable temporal eigenvalue for m = 0 with r_∞ = 148.

Re	I = J = 10	I = J = 14	I = J = 18
50	$-9.638 \times 10^{-4} \pm 9.688 \times 10^{-3}i$	$-8.861 \times 10^{-4} \pm 9.749 \times 10^{-3}i$	$-9.062 \times 10^{-4} \pm 9.740 \times 10^{-3}i$
130	$-6.781 \times 10^{-4} \pm 9.525 \times 10^{-3}i$	$-6.002 \times 10^{-4} \pm 9.670 \times 10^{-3}i$	$-6.301 \times 10^{-4} \pm 9.689 \times 10^{-3}i$
160	$-5.355 \times 10^{-4} \pm 9.524 \times 10^{-3}i$	$-5.127 \times 10^{-4} \pm 9.671 \times 10^{-3}i$	$-5.311 \times 10^{-4} \pm 9.691 \times 10^{-3}i$
170	$-4.804 \times 10^{-4} \pm 9.533 \times 10^{-3}i$	$-4.817 \times 10^{-4} \pm 9.675 \times 10^{-3}i$	$-4.921 \times 10^{-4} \pm 9.695 \times 10^{-3}i$
180	$-4.139 \times 10^{-4} \pm 9.564 \times 10^{-3}i$	$-4.510 \times 10^{-4} \pm 9.677 \times 10^{-3}i$	$-4.612 \times 10^{-4} \pm 9.698 \times 10^{-3}i$
190	$-3.585 \times 10^{-4} \pm 9.615 \times 10^{-3}i$	$-4.175 \times 10^{-4} \pm 9.681 \times 10^{-3}i$	$-4.308 \times 10^{-4} \pm 9.701 \times 10^{-3}i$

Table 16. Least stable temporal eigenvalue for m = 1 with r_∞ = 148.

Re	I = J = 12	I = J = 14	I = 14, J = 16	I = J = 16
160	$-2.153 \times 10^{-4} \pm 0.0986\,i$	$-1.985 \times 10^{-4} \pm 0.0996\,i$	$-2.075 \times 10^{-4} \pm 0.0995\,i$	$-2.095 \times 10^{-4} \pm 0.0996\,i$
170	$-6.428 \times 10^{-5} \pm 0.3111\,i$	$-5.316 \times 10^{-5} \pm 0.3001\,i$	$-5.773 \times 10^{-5} \pm 0.3012\,i$	$-5.937 \times 10^{-5} \pm 0.3004\,i$
175	$-3.041 \times 10^{-6} \pm 0.3113\,i$	$-2.261 \times 10^{-7} \pm 0.3001\,i$	$-1.002 \times 10^{-6} \pm 0.3013\,i$	$-1.052 \times 10^{-6} \pm 0.3004\,i$
175.2	$+1.425 \times 10^{-6} \pm 0.3115\,i$	$+4.458 \times 10^{-7} \pm 0.3000\,i$	$+1.486 \times 10^{-6} \pm 0.3010\,i$	$+1.512 \times 10^{-6} \pm 0.3002\,i$
180	$+8.349 \times 10^{-5} \pm 0.3115\,i$	$+9.453 \times 10^{-5} \pm 0.3000\,i$	$+9.035 \times 10^{-5} \pm 0.3010\,i$	$+8.912 \times 10^{-6} \pm 0.3002\,i$
190	$+2.134 \times 10^{-4} \pm 0.3115\,i$	$+2.012 \times 10^{-4} \pm 0.3000\,i$	$+2.102 \times 10^{-4} \pm 0.3010\,i$	$+2.105 \times 10^{-4} \pm 0.3002\,i$

Table 17. Least stable eigenvalue for m = 1, Re = 175 with r_∞ = 148.

I = J	K = L = 28	K = 28, L = 34	K = 40, L = 28
12	$-3.041 \times 10^{-6} \pm 0.3113\ i$	$-3.050 \times 10^{-6} \pm 0.3110\ i$	$-3.048 \times 10^{-6} \pm 0.3114\ i$
14	$-2.261 \times 10^{-7} \pm 0.3001\ i$	$-2.972 \times 10^{-7} \pm 0.3005\ i$	$-2.756 \times 10^{-7} \pm 0.3002\ i$
16	$-1.052 \times 10^{-6} \pm 0.3004\ i$	$-1.143 \times 10^{-6} \pm 0.3000\ i$	$-1.095 \times 10^{-6} \pm 0.3003\ i$

Table 18. Least stable temporal eigenvalue for m = 2 with r_∞ = 148, I = J = 14.

Re	
160	$-8.116 \times 10^{-4} \pm 0.0\ i$
170	$-8.007 \times 10^{-4} \pm 0.0\ i$
180	$-7.687 \times 10^{-4} \pm 0.0\ i$
190	$-7.439 \times 10^{-4} \pm 0.0\ i$

Table 19. Least stable temporal eigenvalue for Re = 175, with $r_\infty = 148$, I = J = 14.

m	
2	$-7.775 \times 10^{-4} \pm 0.0\ i$
3	$-1.193 \times 10^{-3} \pm 2.348 \times 10^{-2}\ i$
4	$-1.285 \times 10^{-3} \pm 2.377 \times 10^{-2}\ i$
5	$-1.302 \times 10^{-3} \pm 2.375 \times 10^{-2}\ i$

Table 20. Wake oscillation frequencies for previous experimental work, computed using equation (4.3), for Re = 175.1.

Authors	Liquid	Distance Traveled (cm)	U_∞ (cm/sec)	Sphere Radius (cm)	Remarks	Computed f (Hz)
Möller	Water	120	0.286	2.975	Towed	0.00472
	Water	120	0.278	3.050	Towed	0.00449
Taneda	Water	100	0.86	0.991	Towed	0.0425
	Water	100	1.13	0.754	Towed	0.0735
Nakamura	Water	100	1.373	0.619	Falling	0.109
Goldburg & Florsheim	30% glycerol 70% water	120	10.0	0.286	Falling	1.29

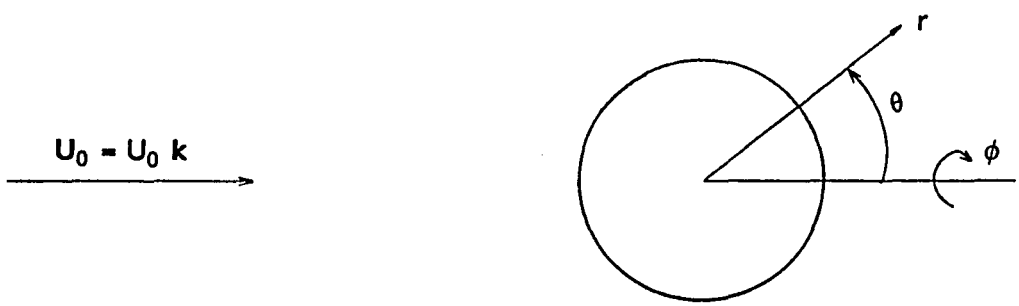

Figure 1. Coordinate system

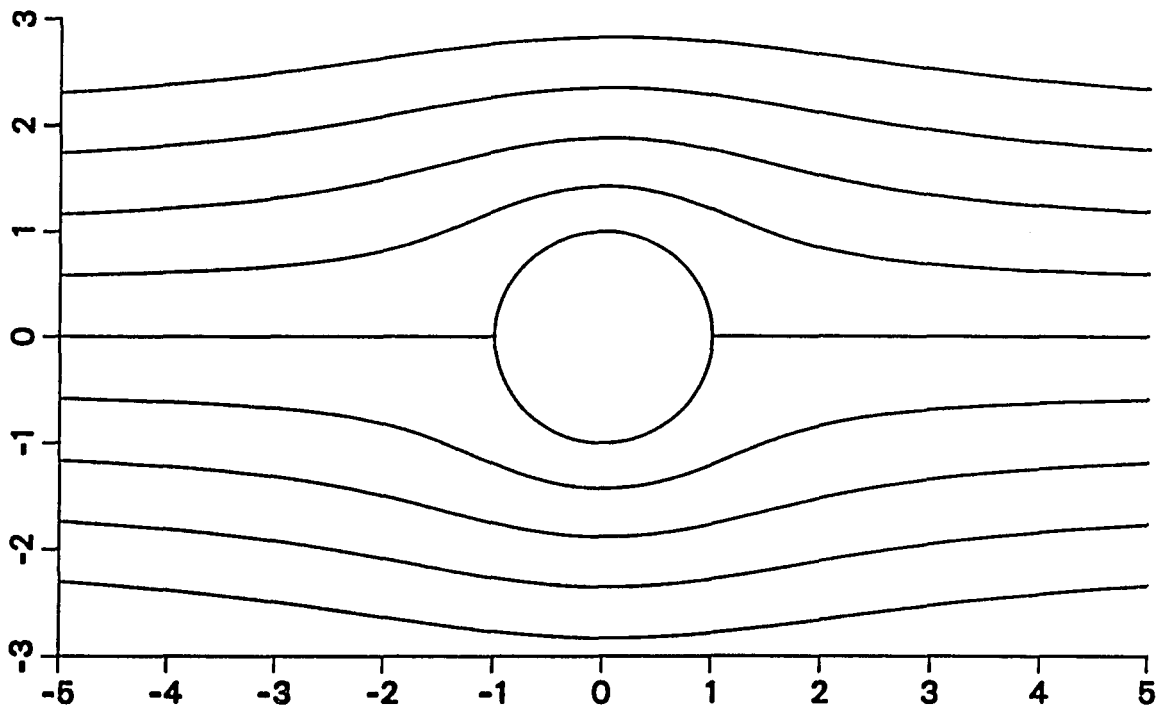

Figure 2. Steady axisymmetric flow past a sphere at Re = 0.1

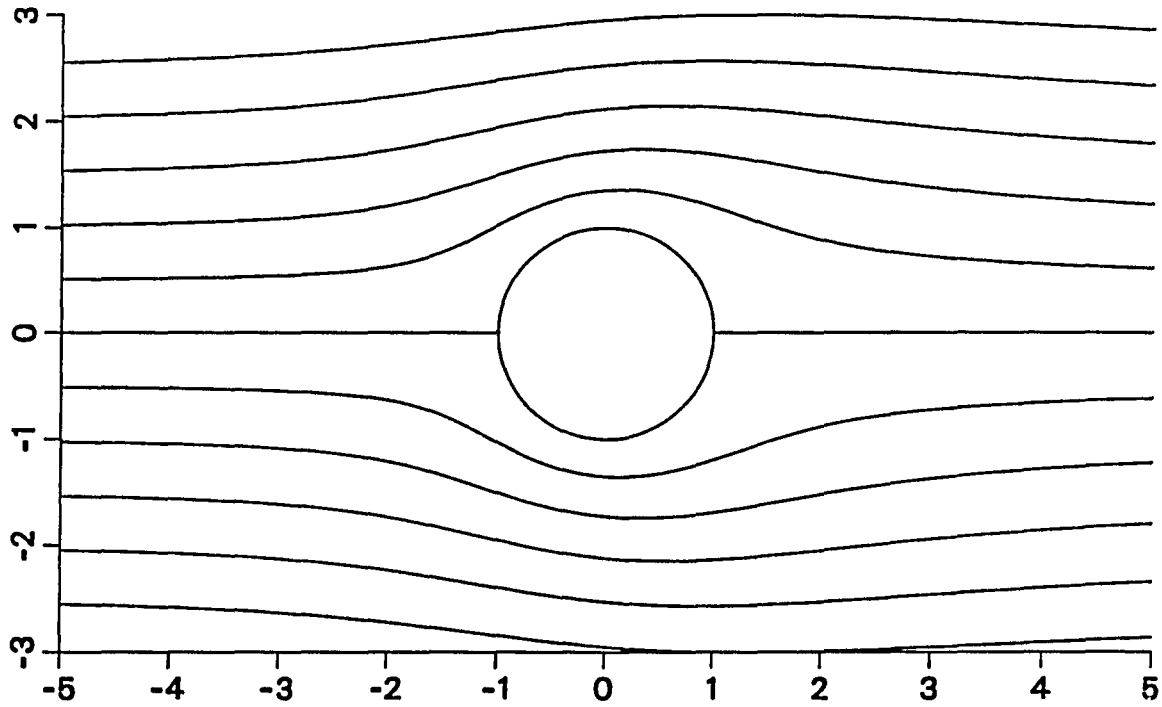

Figure 3. Steady axisymmetric flow past a sphere at Re = 5.

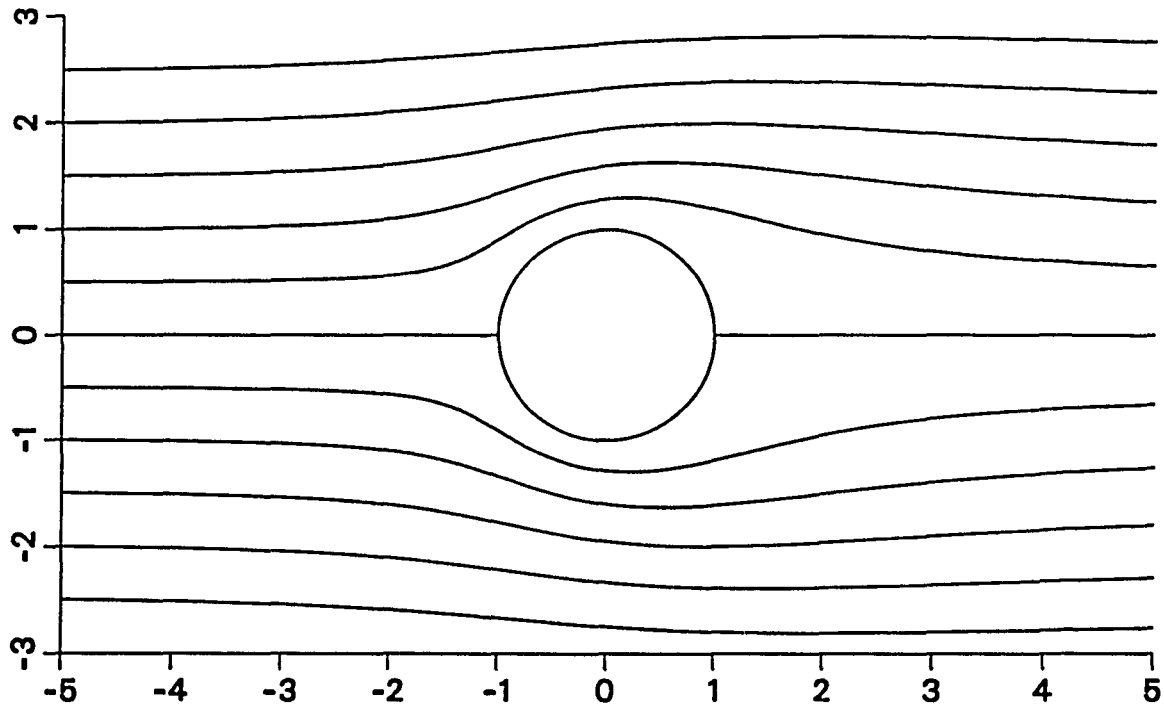

Figure 4. Steady axisymmetric flow past a sphere at Re = 20.

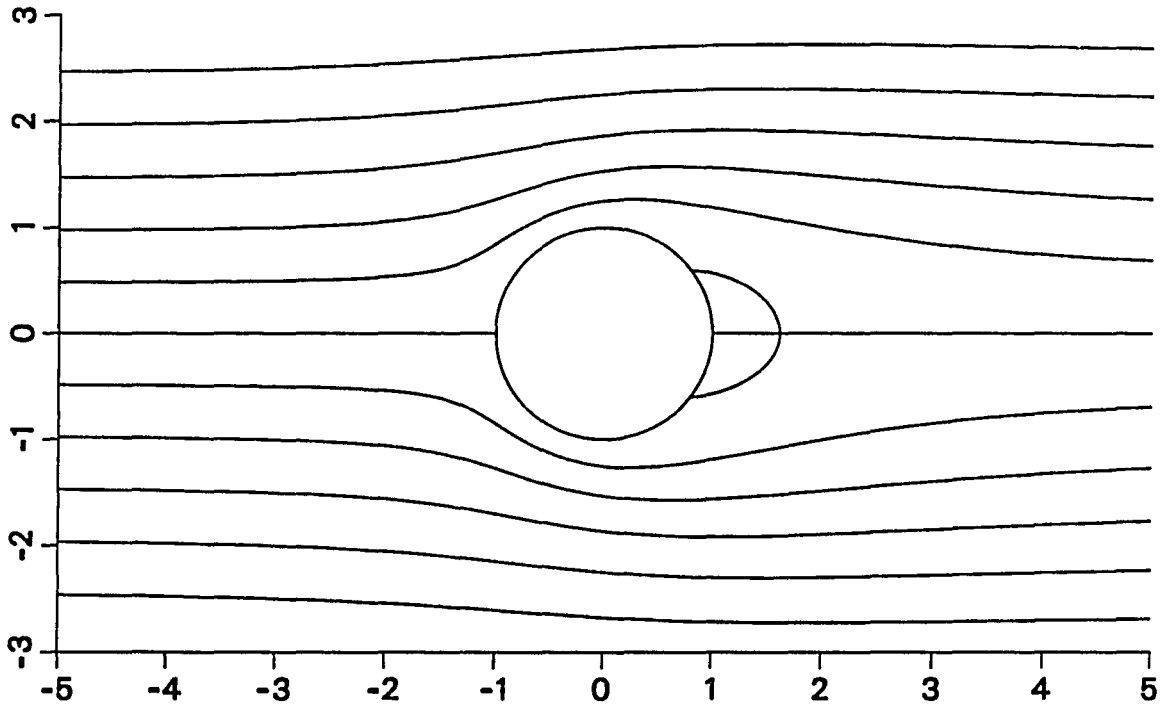

Figure 5. Steady axisymmetric flow past a sphere at Re = 40.

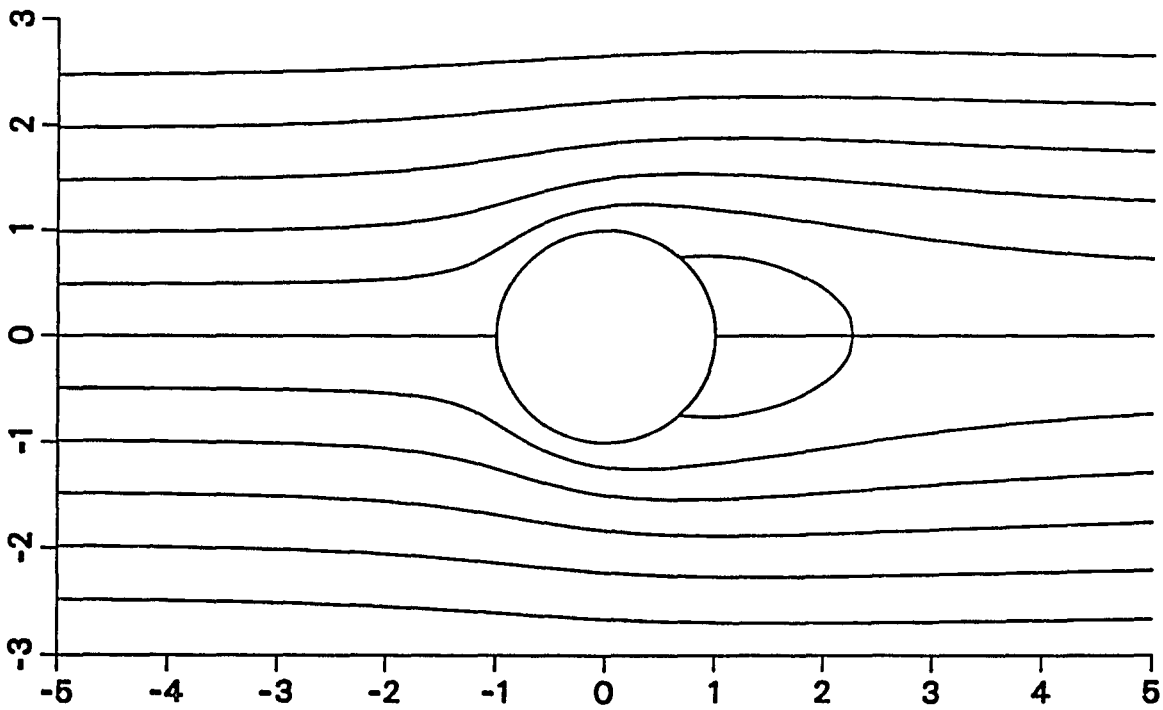

Figure 6. Steady axisymmetric flow past a sphere at Re = 70.

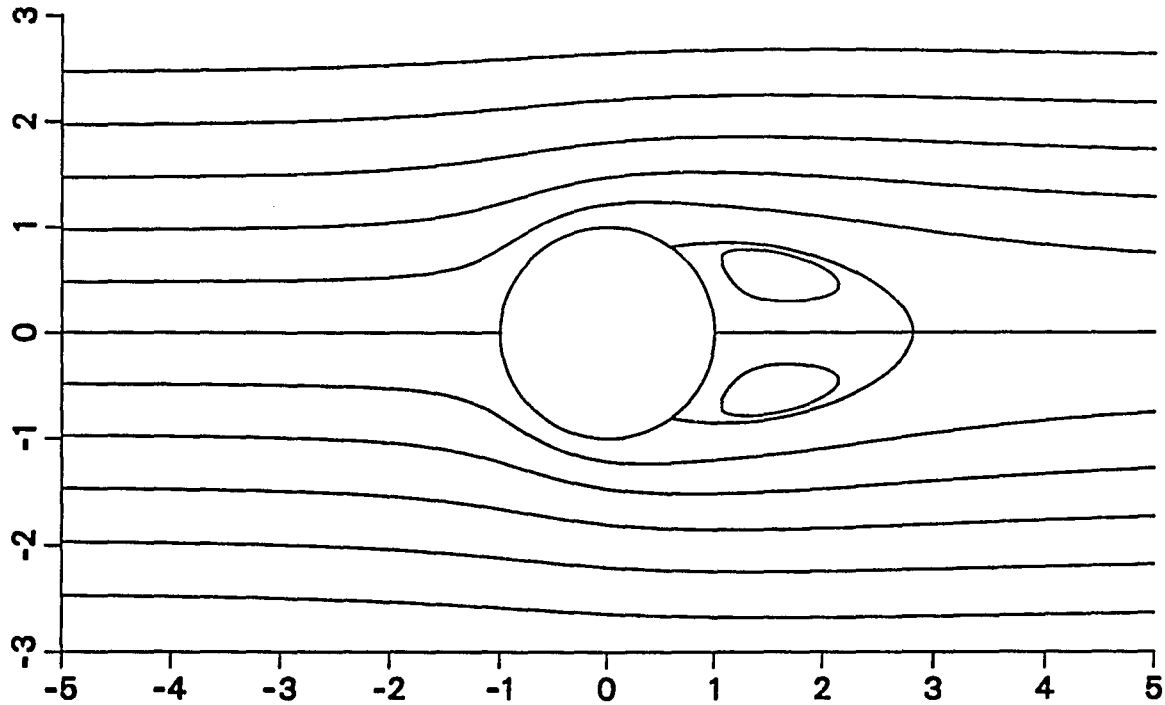

Figure 7. Steady axisymmetric flow past a sphere at Re = 100.

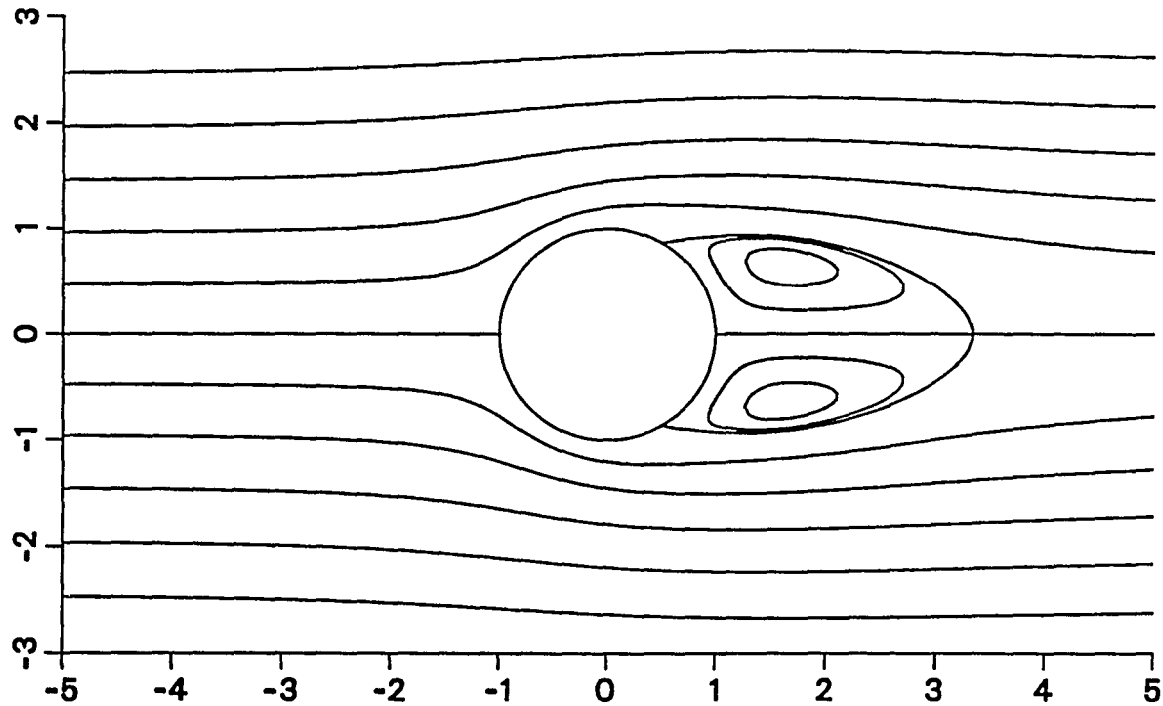

Figure 8. Steady axisymmetric flow past a sphere at Re = 140.

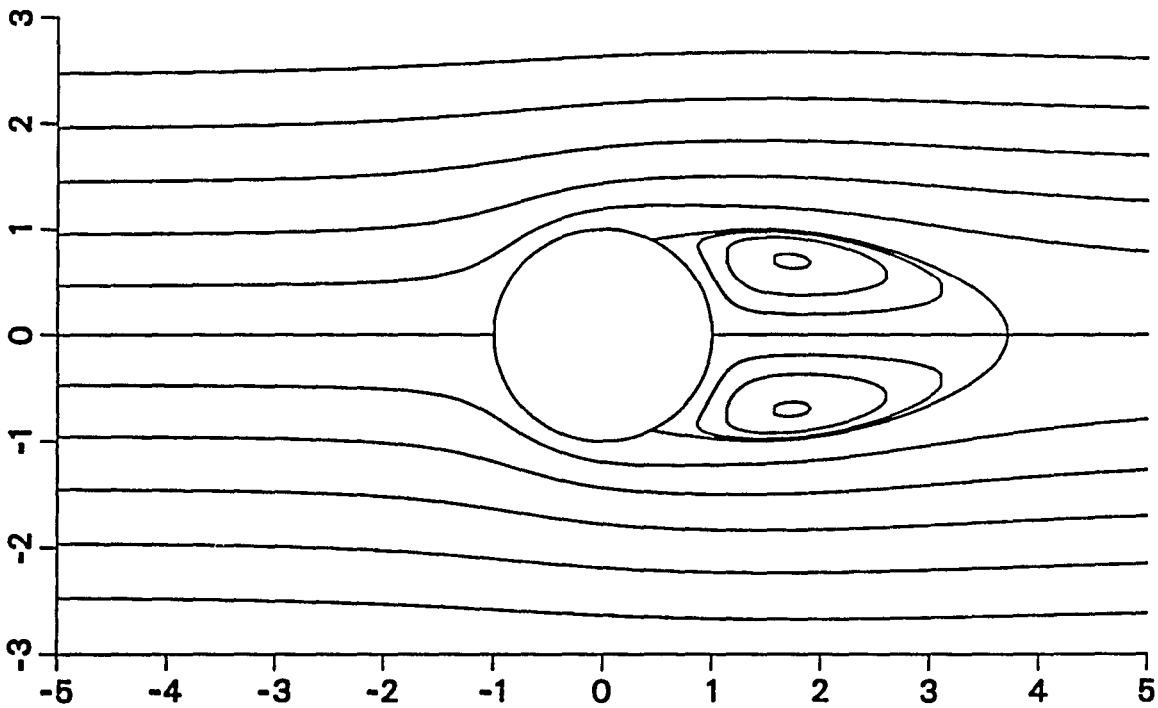

Figure 9. Steady axisymmetric flow past a sphere at Re = 180.

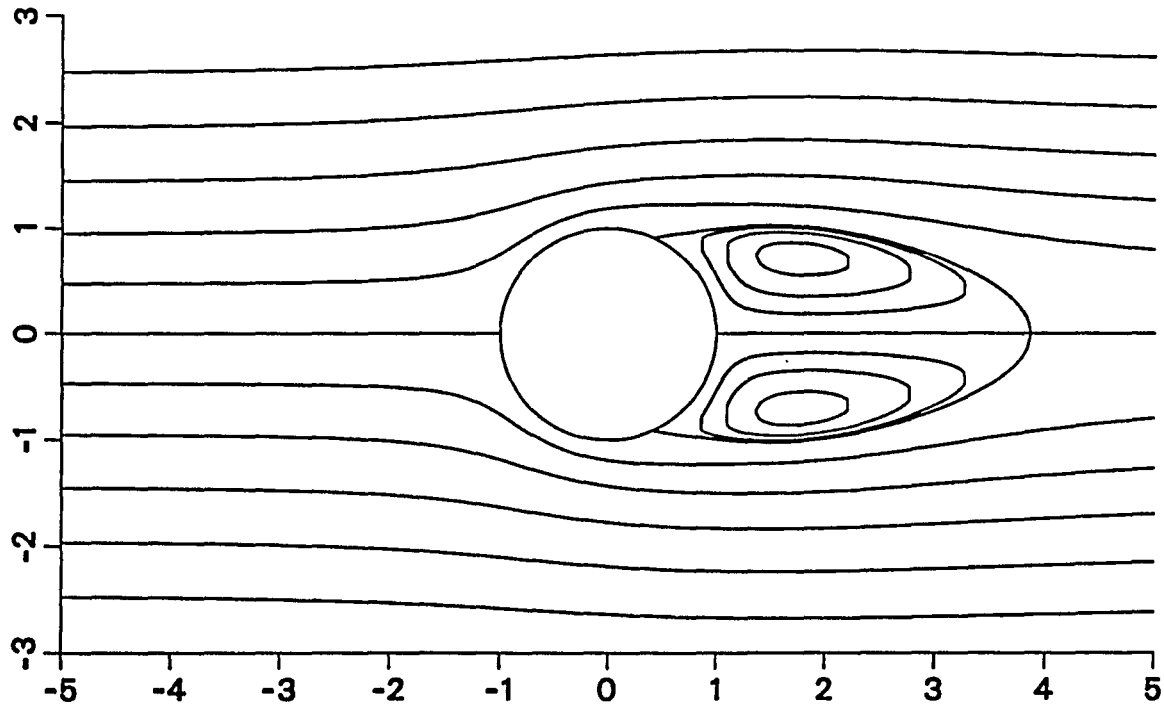

Figure 10. Steady axisymmetric flow past a sphere at Re = 200.

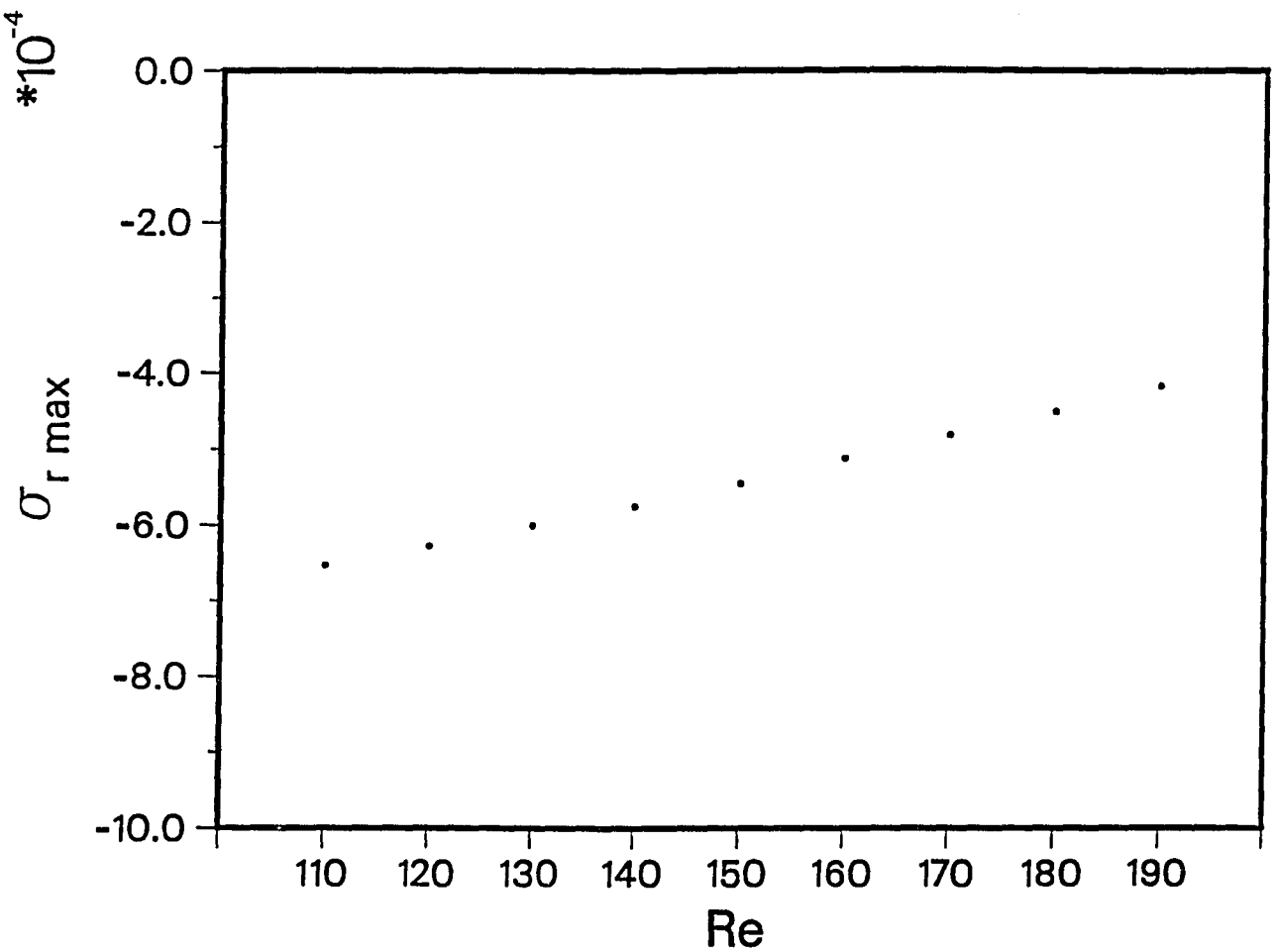

Figure 11. Growth rate versus Re for m = 0

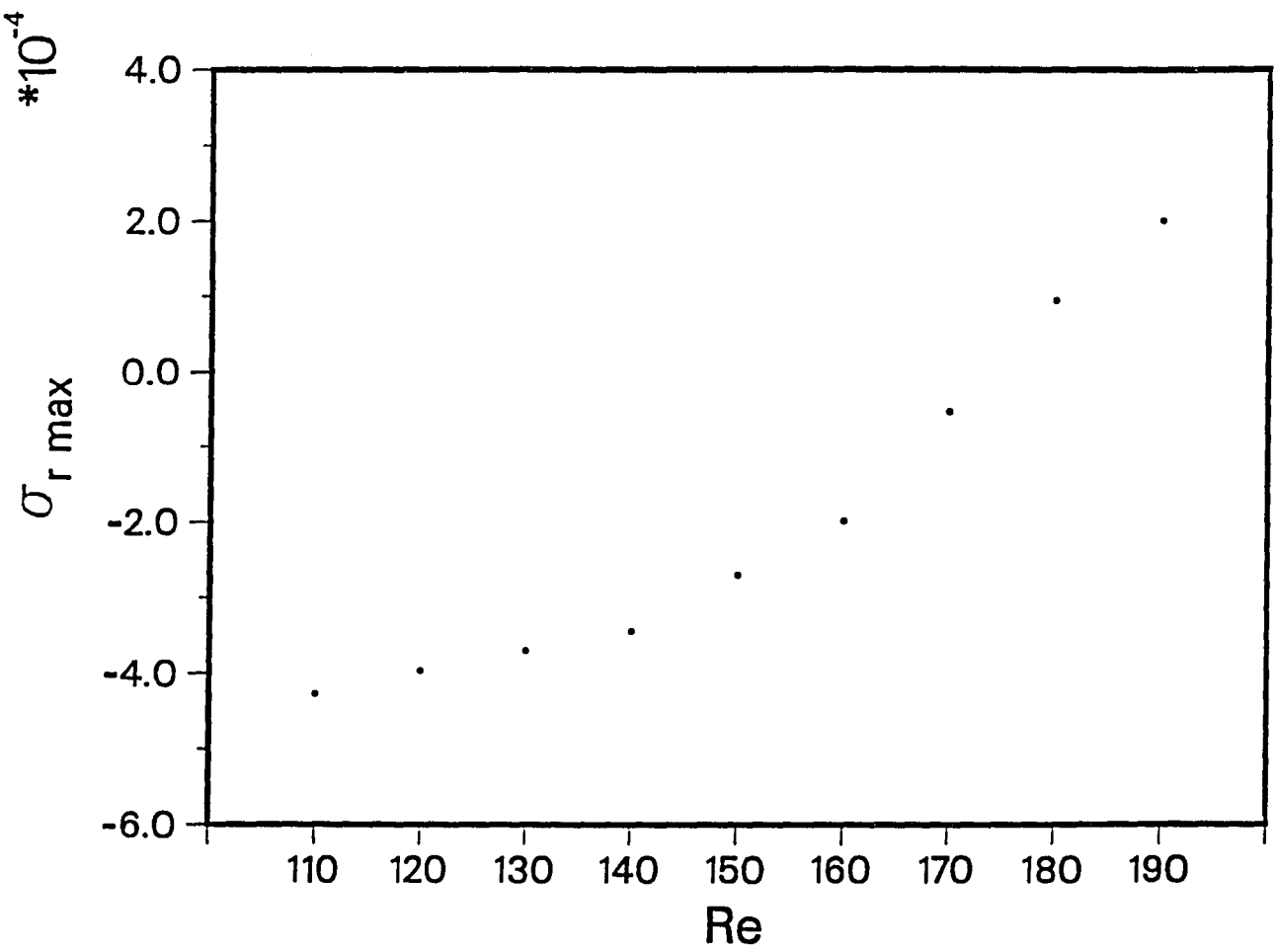

Figure 12. Growth rate versus Re for m = 1

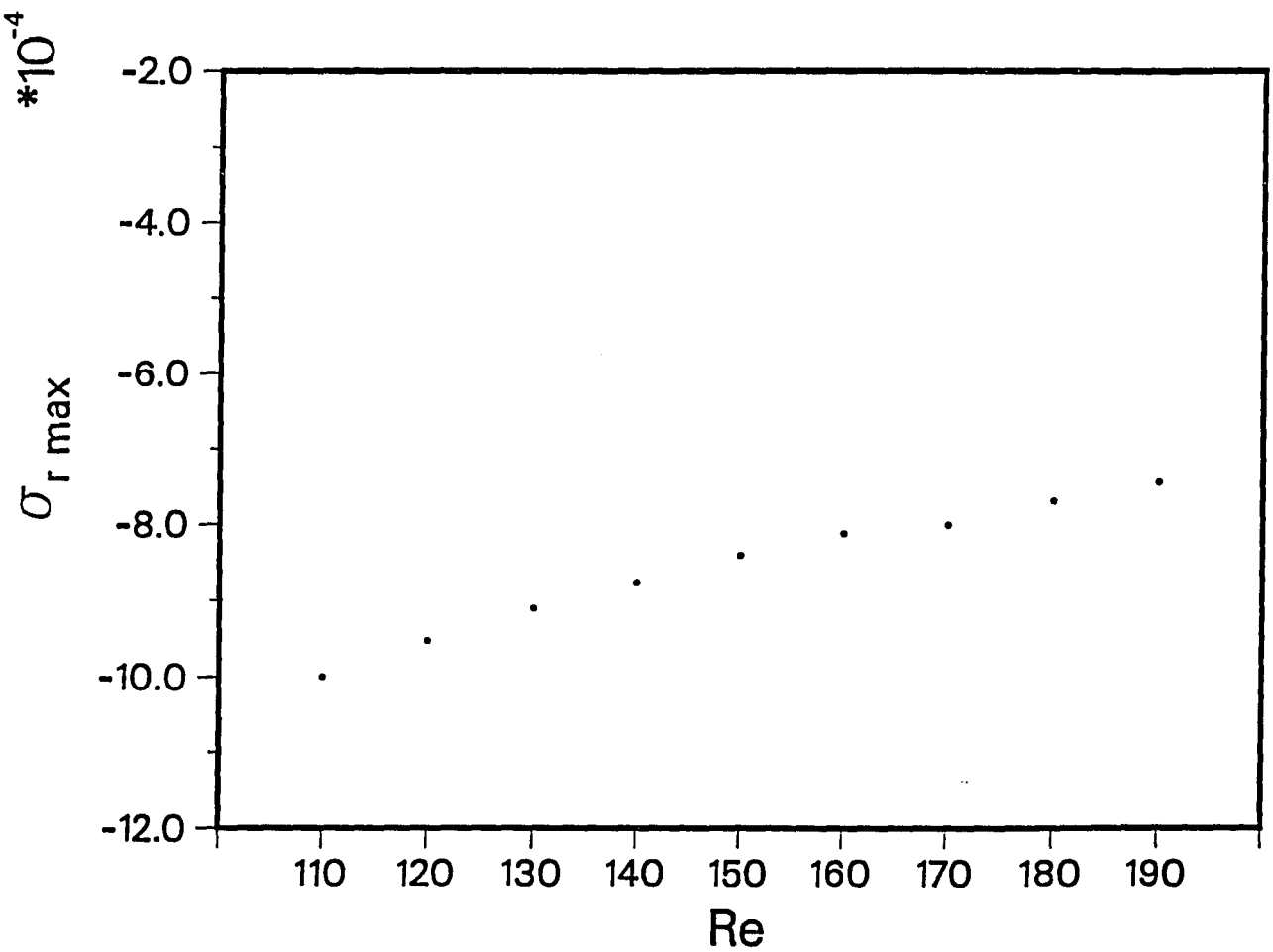

Figure 13. Growth rate versus Re for m = 2

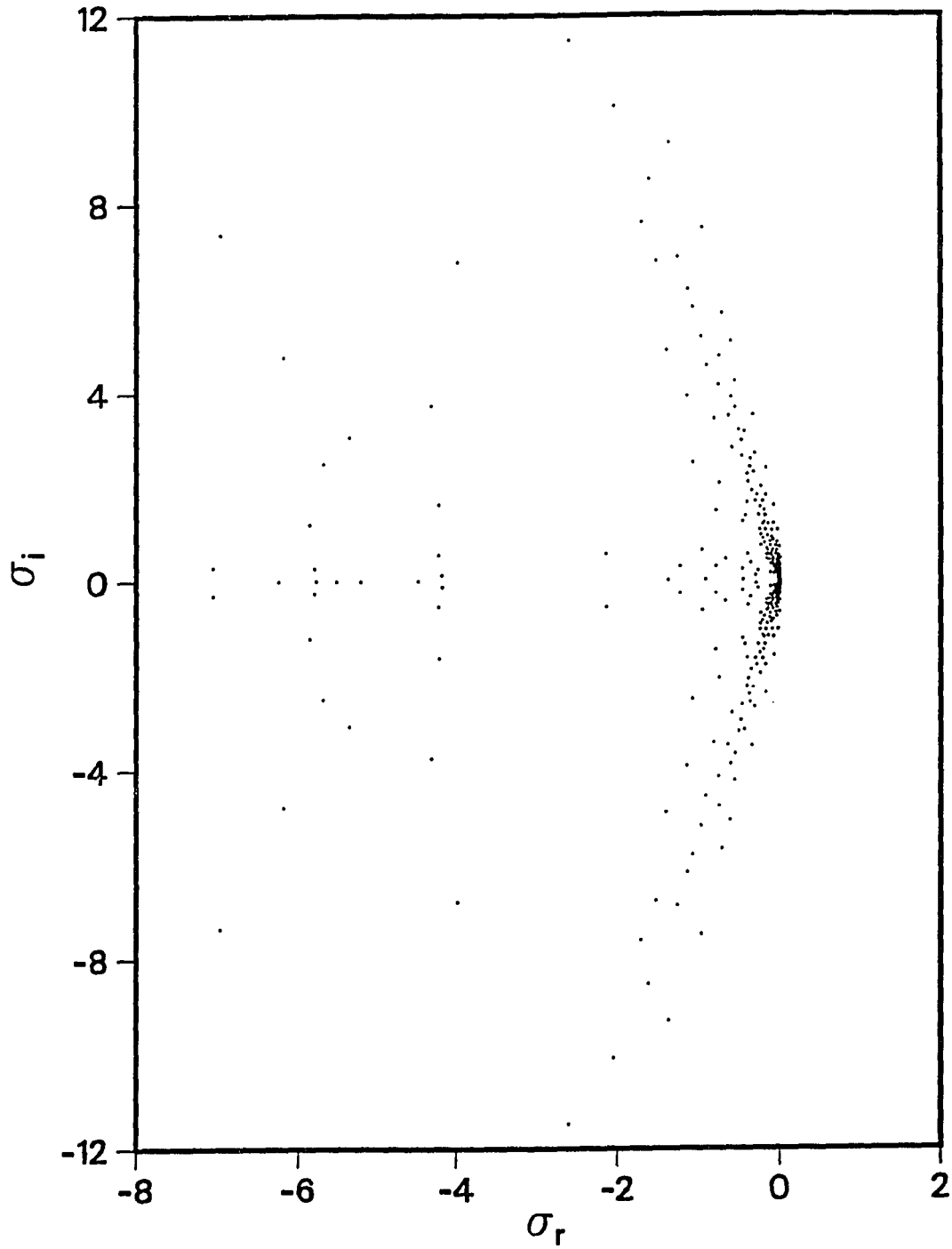

Figure 14.a Distribution of the temporal eigenvalues for m =1 and Re = 175.
All of the temporal eigenvalues.

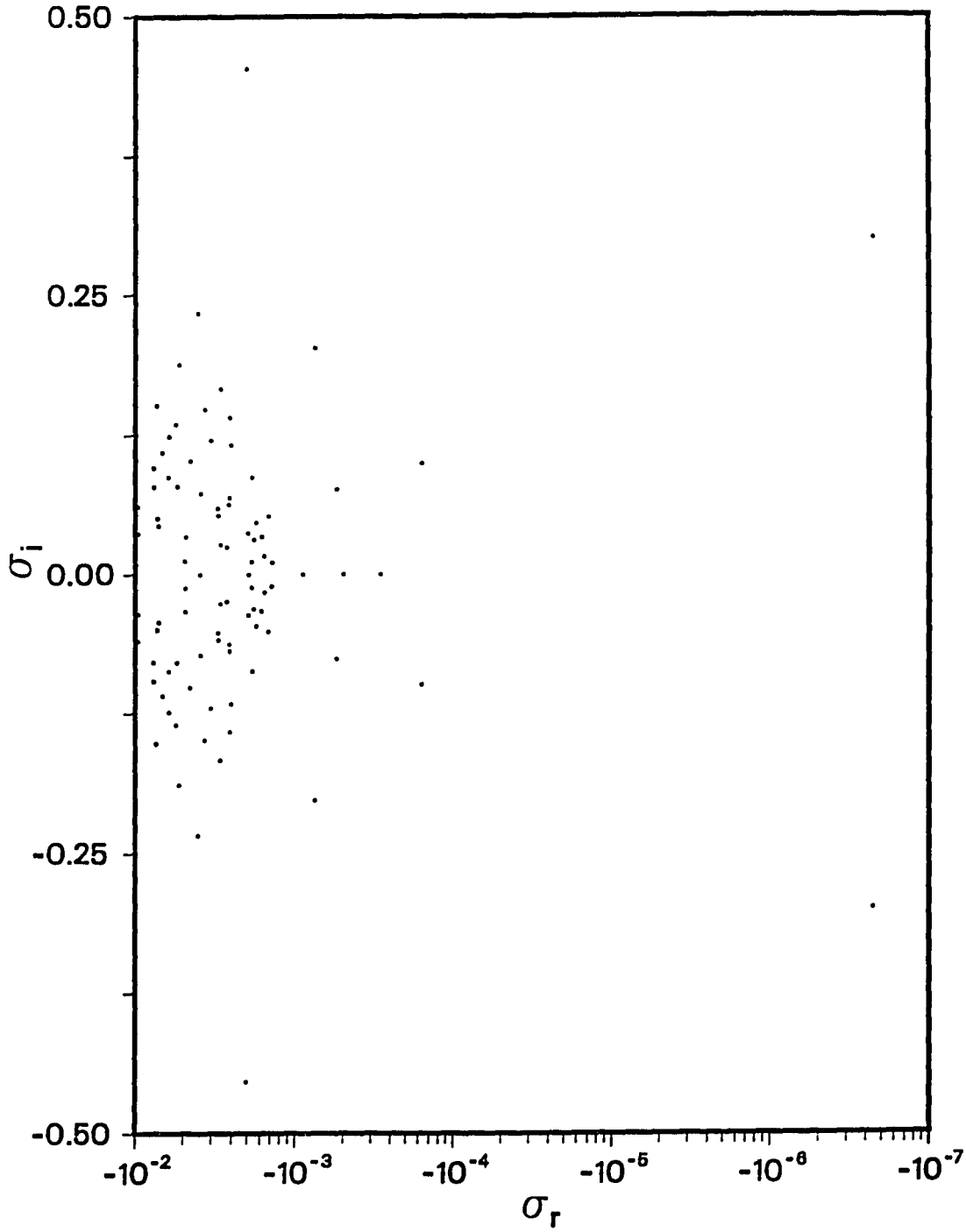

Figure 14.b Distribution of the temporal eigenvalues for m =1 and Re = 175. Detail showing the least stable eigenvalues.

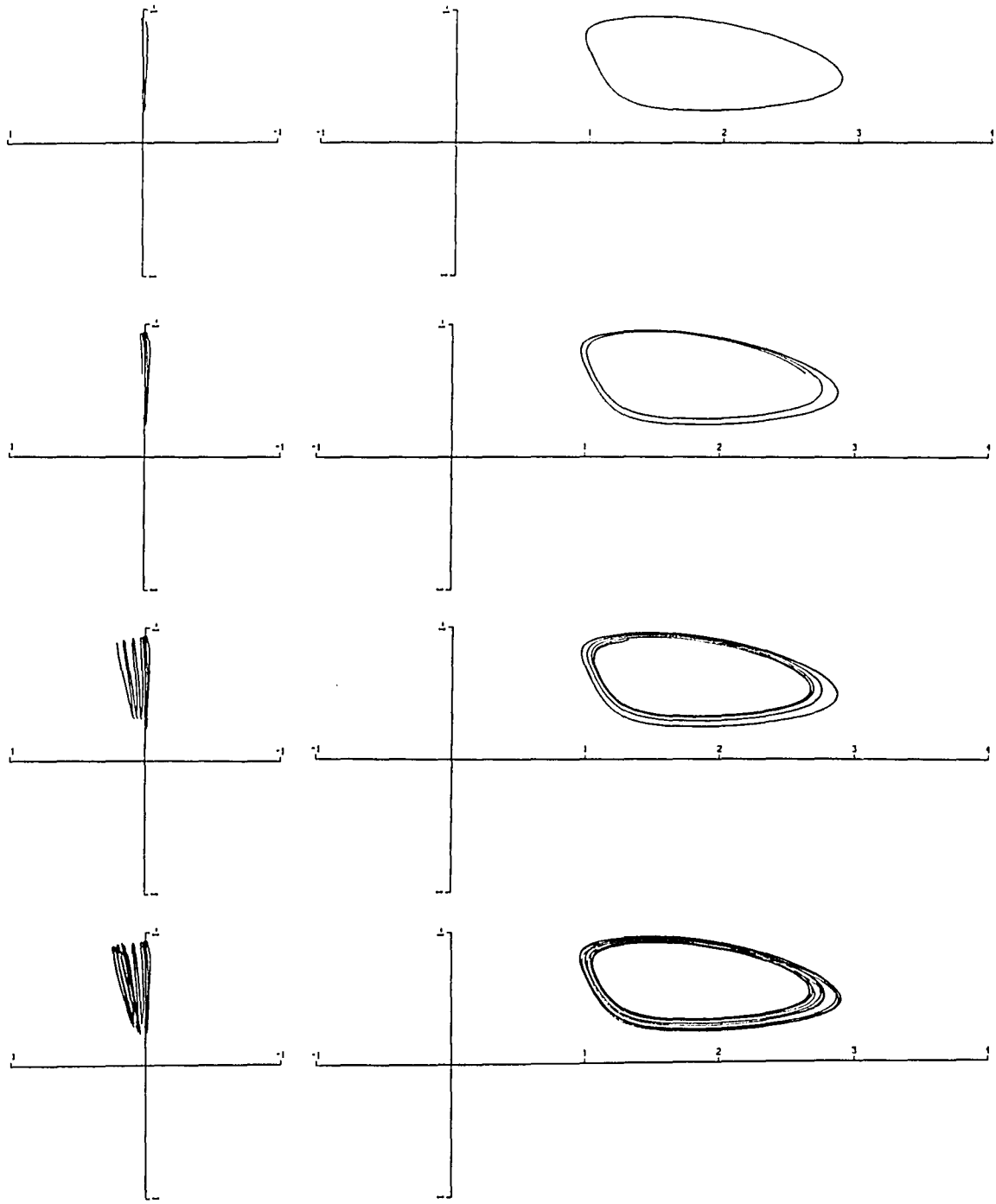

Figure 15. Views of the pathline of a particle beginning at t = 0, r = 1.2, θ = 30°, ϕ = 0. The views on the right are from a point 100 sphere radii above from the plane ϕ = 0. The views on the left are from a point 100 sphere radii upstream of the sphere center. The pathline is shown at t = 30, 60, 120, 240, 480, 960, 1920, and 3840. (See next page for continuation.)

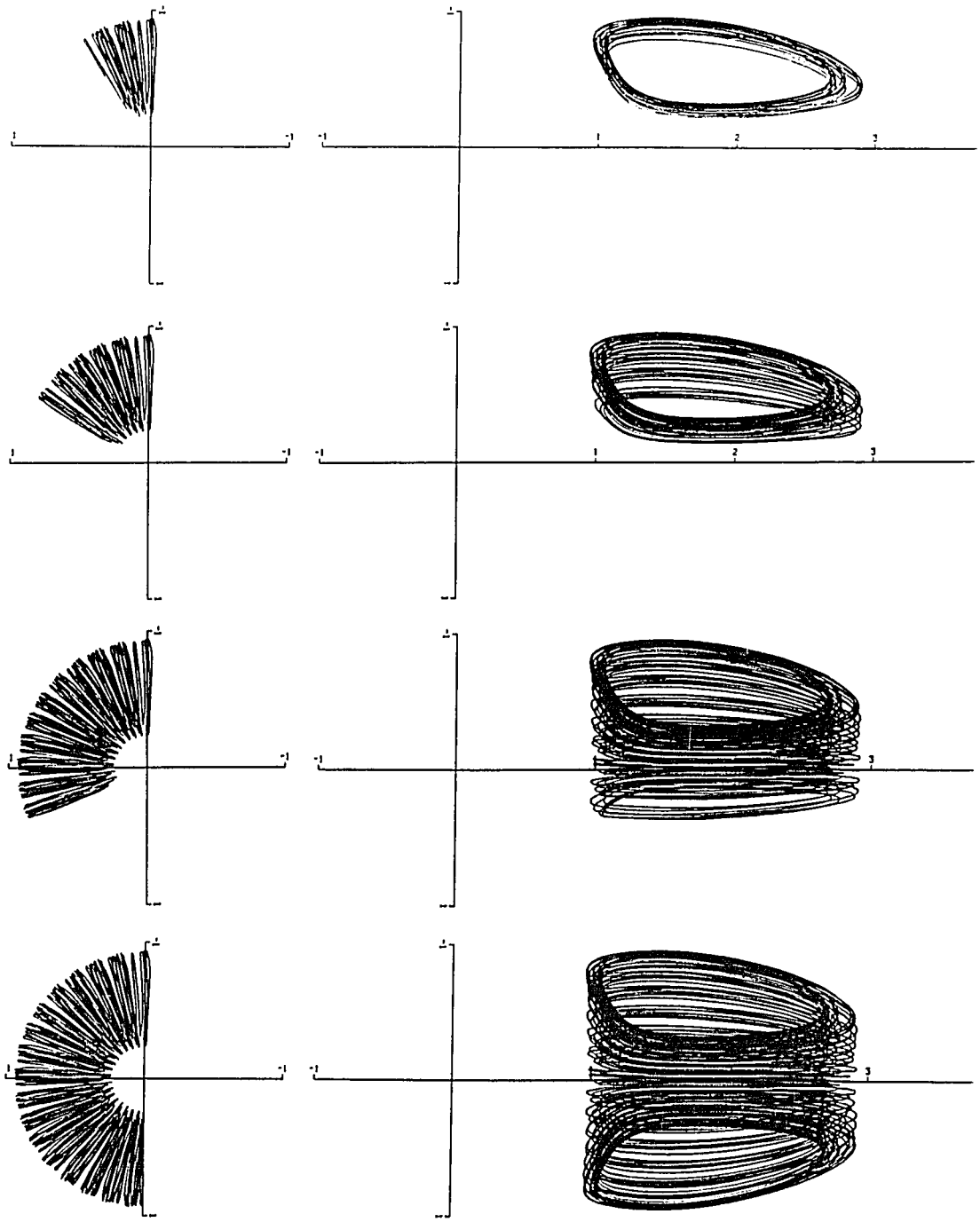

Figure 15. continued

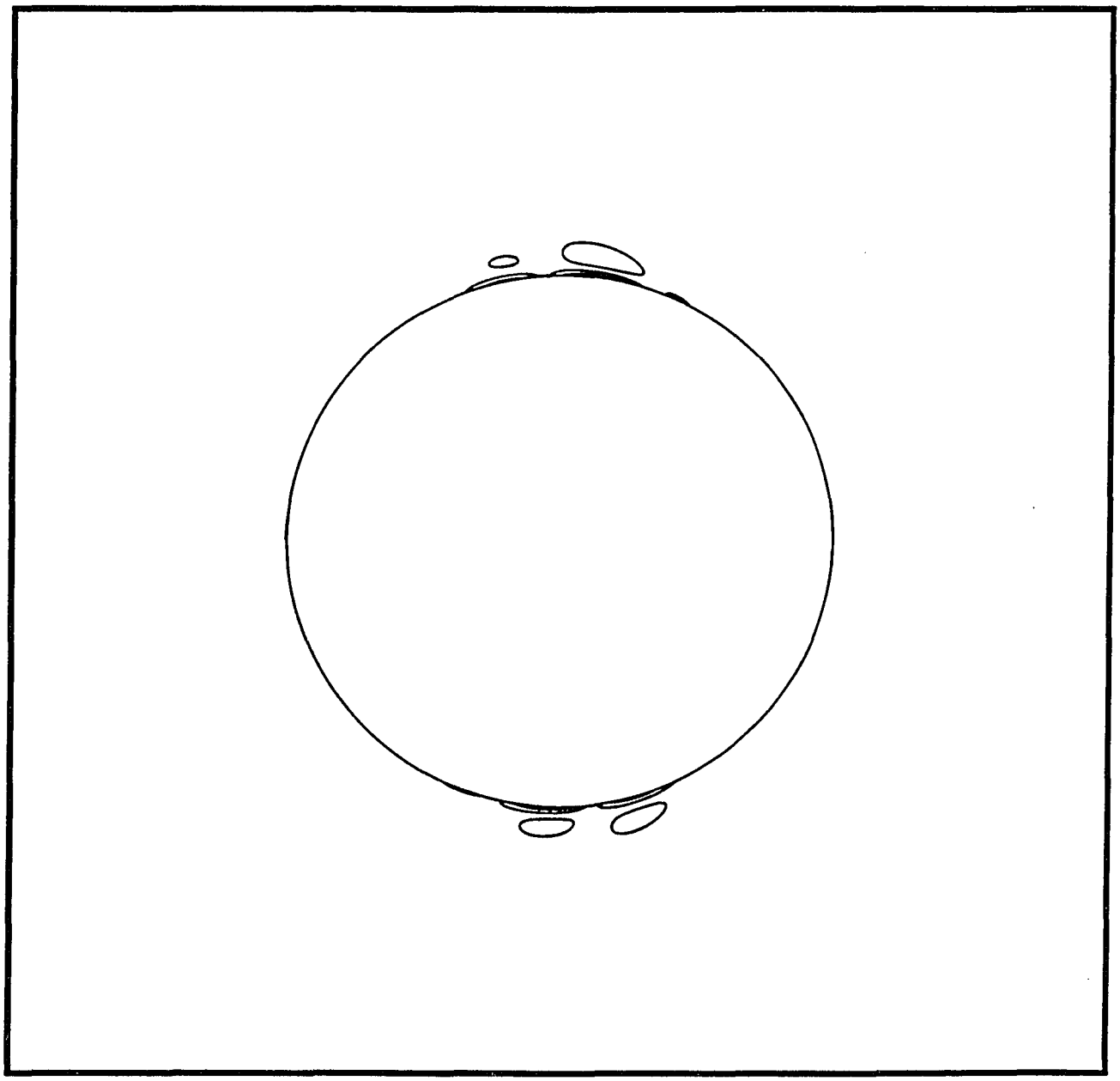

Figure 16.a r-θ dependence of the real and imaginary parts of the ϕ-component of vorticity at Re = 175. The upper and lower halves depict the real and imaginary parts of ω_ϕ.

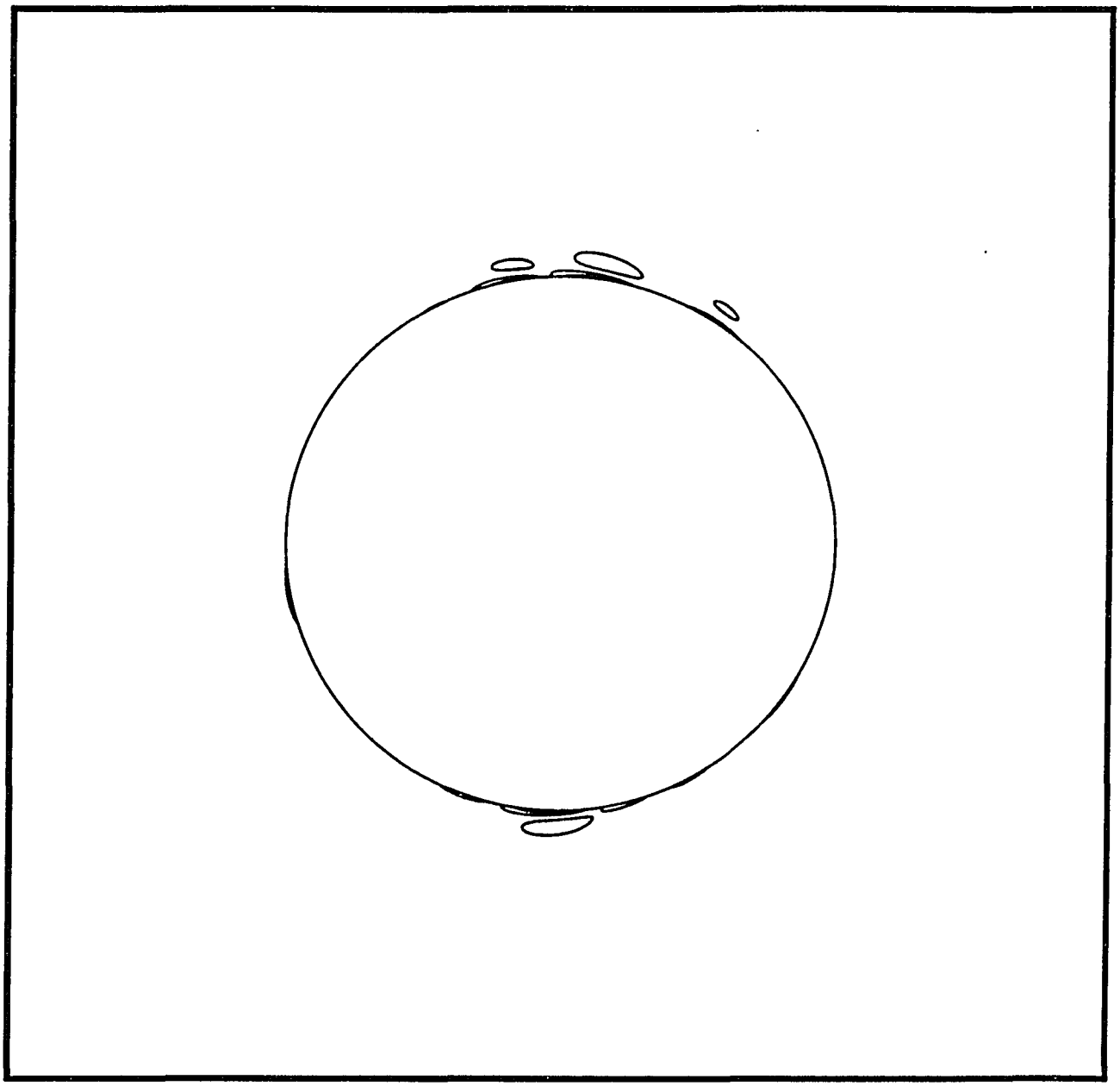

Figure 16.b r-θ dependence of the real and imaginary parts of the θ-component of vorticity at Re = 175. The upper and lower halves depict the real and imaginary parts of ω_θ.

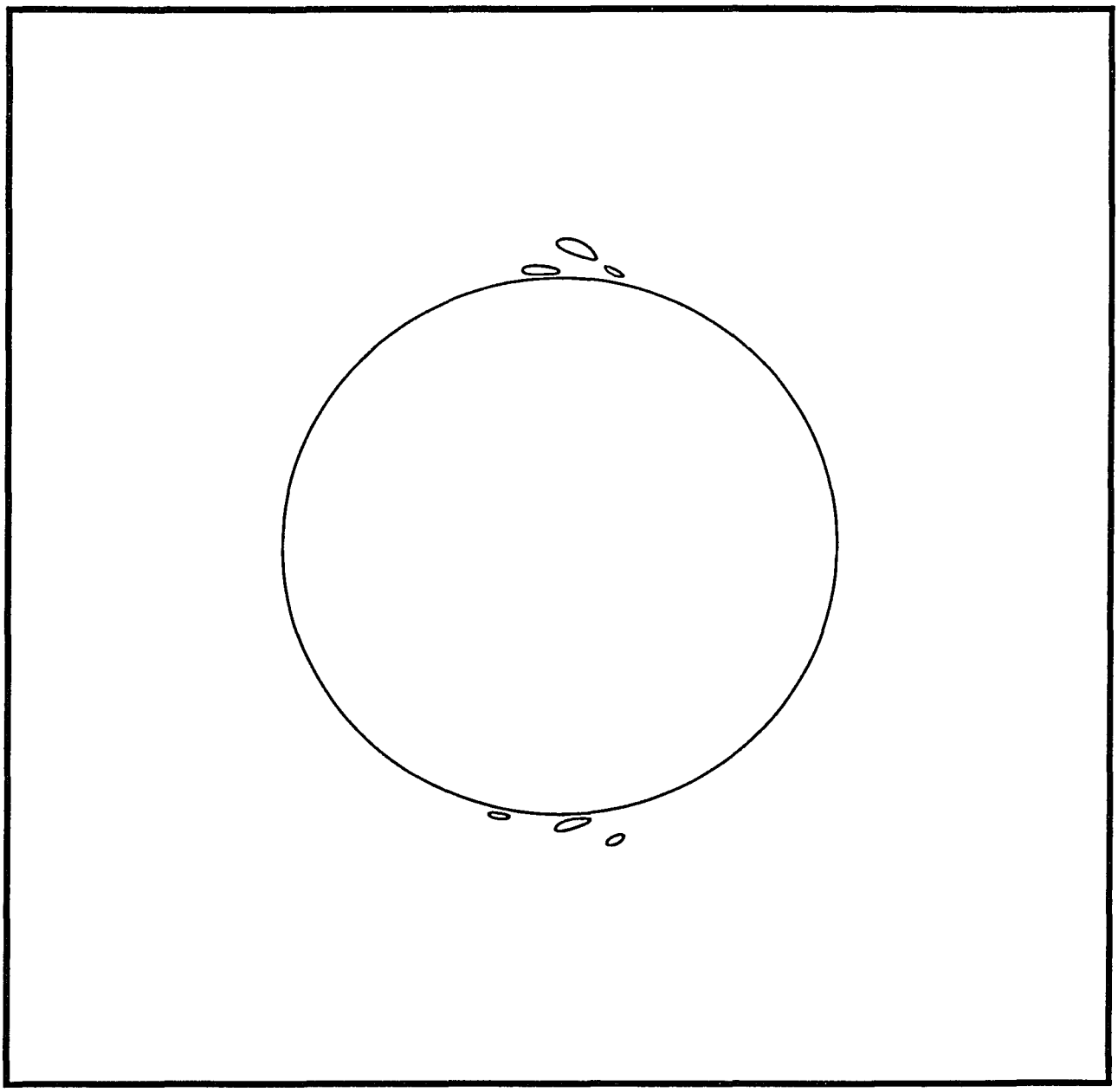

Figure 16.c r-θ dependence of the real and imaginary parts of the r-component of vorticity at Re = 175. The upper and lower halves depict the real and imaginary parts of ω_r.

Appendix

Zebib (1984) used the recurrence formulae

$$2\,T_n(z) = \frac{c_n}{n+1}\,T'_{n+1}(z) - \frac{d_{n-2}}{n-1}\,T'_{n-1}(z)$$

$$2z\,T_n(z) = c_n\,T_{n+1}(z) + d_{n-1}\,T_{n-1}(z)\ ,$$

where $c_n = d_n = 0$ if $n < 0$ and $c_0 = 2$, $d_0 = 1$, $c_n = d_n = 1$ if $n > 0$, to derive the expressions

$$f_{qj}^{(3)} = \delta_{q,j+1}\beta_j^{(3)} + \delta_{q,j-1}\gamma_j^{(3)}$$

$$f_{qj}^{(2)} = \delta_{q,j+2}\beta_j^{(2)} + \delta_{q,j}\gamma_j^{(2)} + \delta_{q,j-2}\delta_j^{(2)}$$

$$f_{qj}^{(1)} = \delta_{q,j+3}\beta_j^{(1)} + \delta_{q,j+1}\gamma_j^{(1)} + \delta_{q,j-1}\delta_j^{(1)} + \delta_{q,j-3}\epsilon_j^{(1)}$$

$$f_{qj}^{(0)} = \delta_{q,j+4}\beta_j^{(0)} + \delta_{q,j+2}\gamma_j^{(0)} + \delta_{q,j}\delta_j^{(0)} + \delta_{q,j-2}\epsilon_j^{(0)} + \delta_{q,j-4}\eta_j^{(0)}\ ,$$

for the coefficients $f_{qj}^{(n)}$, where $\delta_{q,j}$ is the Kronecker delta and the nonzero values of β_j, γ_j, δ_j, ϵ_j, and η_j (for $j \geq 0$ only) are

$$\beta_j^{(3)} = \frac{c_j}{2(j+1)}\ , \qquad \beta_j^{(n-1)} = \frac{\beta_j^{(n)}}{2(j+5-n)}\ ,\ n = 1,2,3,\ j \geq 0$$

$$\gamma_j^{(3)} = \frac{-1}{2(j-1)}\ ,\ j \geq 2\ , \qquad \gamma_j^{(n-1)} = \frac{-\beta_j^{(n)} + \gamma_j^{(n)}}{2(j+3-n)}\ ,\ n = 1,2,3,\ j \geq n-2$$

$$\delta_j^{(2)} = \frac{-\gamma_j^{(3)}}{2(j-2)}\ ,\ j \geq 3\ , \qquad \delta_j^{(n-1)} = \frac{-\gamma_j^{(n)} + \delta_j^{(n)}}{2(j+1-n)}\ ,\ n = 1,2\ j \geq n$$

$$\epsilon_j^{(1)} = \frac{-\delta_j^{(2)}}{2(j-3)}\ ,\ j \geq 4\ , \qquad \epsilon_j^{(0)} = \frac{-\delta_j^{(1)} + \epsilon_j^{(1)}}{2(j-2)}\ ,\ j \geq 3$$

$$\eta_j^{(0)} = \frac{-\epsilon_j^{(1)}}{2(j-4)} \ , \ j \geq 5 \ .$$

The $G_{qj}^{(n)}$ consist of $f_{qj}^{(n)}$ and terms such that ψ satisfies the boundary conditions. These coefficients satisfy the homogeneous version of (3.2a,b) and (3.6a,b) as

$$\sum_{q=0}^{L+1} G_{qj}{}^{(3)} = 0 \qquad \sum_{q=0}^{L+3} G_{qj}{}^{(1)} = 0$$

$$\sum_{q=0}^{L+3} (-1)^q \, G_{qj}{}^{(1)} = 0 \qquad \sum_{q=0}^{L+4} (-1)^q \, G_{qj}{}^{(0)} = 0$$

for $0 \leq j \leq L$. Thus,

$$G_{qj}^{(3)} = f_{qj}^{(3)} - \kappa_j^{(3)} \, \delta_{q,0}$$

$$G_{qj}^{(2)} = f_{qj}^{(2)} - \kappa_j^{(3)} \, \delta_{q,1} - \frac{1}{2} \left[\kappa_j^{(1)} - \nu_j^{(1)}\right] \delta_{q,0}$$

$$G_{qj}^{(1)} = f_{qj}^{(1)} - \frac{1}{4} \kappa_j^{(3)} \, \delta_{q,2} - \frac{1}{2} \left[\kappa_j^{(1)} - \nu_j^{(1)}\right] \delta_{q,1} - \frac{1}{2} \left[\kappa_j^{(1)} + \nu_j^{(1)} - \frac{1}{2} \kappa_j^{(3)}\right] \delta_{q,0}$$

$$G_{qj}^{(0)} = f_{qj}^{(0)} - \frac{1}{24} \kappa_j^{(3)} \, \delta_{q,3} - \frac{1}{8} \left[\kappa_j^{(1)} - \nu_j^{(1)}\right] \delta_{q,2} - \frac{1}{2} \left[\kappa_j^{(1)} + \nu_j^{(1)} - \frac{3}{4} \kappa_j^{(3)}\right] \delta_{q,1}$$

$$- \left[\nu_j^{(0)} + \frac{3}{8} \kappa_j^{(1)} + \frac{5}{8} \nu_j^{(1)} - \frac{1}{3} \kappa_j^{(3)}\right] \delta_{q,0} \ ,$$

where

$$\kappa_j^{(n)} = \sum_{q=0}^{L+4-n} f_{qj}^{(n)} \qquad \nu_j^{(n)} = \sum_{q=0}^{L+4-n} (-1)^q \, f_{qj}^{(n)} \ .$$

The coefficients $B_p^{(n)}$ are determined by the inhomgeneous boundary conditions (3.6a, b) and depend only on the transformation parameter a in (3.5). They are expressed as

$$B_0^{(3)} = 0 \qquad B_1^{(3)} = 0 \qquad B_2^{(3)} = 0$$

$$B_0^{(2)} = \frac{1}{2}\,a \qquad B_1^{(2)} = 0 \qquad B_2^{(2)} = 0$$

$$B_0^{(1)} = -\frac{1}{2}\,a \qquad B_1^{(1)} = \frac{1}{2}\,a \qquad B_2^{(1)} = 0$$

$$B_0^{(0)} = -\frac{5}{8}\,a - 1 \qquad B_1^{(0)} = -\frac{1}{2}\,a \qquad B_2^{(0)} = \frac{1}{8}\,a$$

REFERENCES

Achenbach, E. 1974 Vortex shedding from spheres. *J. Fluid Mech.* **62**, 209-221.

Batchelor, G. K. & Gill, A. E. 1962 Analysis of the stability of axisymmetric jets. *J. Fluid Mech.* **14**, 529-551.

Beard, K. V. 1976 Terminal velocity and shape of cloud and precipitation drops aloft. *J. Atmos. Sci.* 33, 851-864.

Cheremisinoff, N. P. & Cheremisinoff, P. N. 1984 *Hydrodynamics of Gas-Solid Fluidization.* Gulf Publishing Company, Houston, Tex.

Cliffe, K. A. & Lever, D. A. 1983 *Proc. 3rd Int. Conf. on Numerical Methods in Laminar and Turbulent Flow.* (Taylor, C., Johnson, J. A., & Smith, W. R., Eds.) Pineridge, Swansea, 25-36.

Cliffe, K. A. & Lever, D. A. 1986 A comparison of finite-element methods for solving flow past a sphere. *J. Comput. Phys.* **62**, 321-330.

Clift, R., Grace, J. R., & Weber, M. E. 1978 *Bubbles, Drops and Particles.* Academic Press, New York.

Dandy, D. S. & Leal, L. G. 1986 Boundary-layer separation from a smooth slip surface. *Phys. Fluids.* **29**, 1360-1366.

Dennis, S. C. R. & Walker, J. D. A. 1971 Calculation of the steady flow past a sphere at low and moderate Reynolds numbers. *J. Fluid Mech.* **48**, 771-789.

Domb, C. & Sykes, M. F. 1957 On the susceptibility of a ferromagnetic above the Curie point. *Proc. Roy. Soc. London,* A **240**, 214-228.

Flumerfelt, R. W. & Slattery, J. C. 1965 A widely applicable type of variational integral-II. *Chem. Eng. Sci.* **20**, 157-163.

Fornberg, B. 1980 A numerical study of steady viscous flow past a circular cylinder. *J. Fluid Mech.* **98**, 819-855.

Fornberg, B. 1988 Steady viscous flow past a sphere at high Reynolds numbers. *J. Fluid Mech.* **190**, 471-489.

Fuchs, H. V., Mercker, E. & Michel, U. 1979 Large-scale coherent structures in the wake of axisymmetric bodies. *J. Fluid Mech.* **93**, 185-207.

Garbow, B. S., Boyle, J. M., Dongarra, J. J. & Moler, C. B. 1977 *Matrix Eigensystem Routines - EISPACK Guide Extension* (Springer-Verlag, New York).

Garner, F. H., Jenson, V. G. & Keey, R. B. 1959 Flow pattern around spheres and the Reynolds analogy. *Trans. Inst. Chem. Engrs.* **37**, 191-197.

Gold, H. 1963 Stability of laminar wakes. Ph.D. Dissertation, Calif. Inst. Tech.

Goldburg, A. & Florsheim, B. H. 1966 Transition and Strouhal number for the incompressible wake of various bodies. *Phys. Fluids.* **9**, 45-50.

Gottlieb, D. & Orszag, S. A. 1977 Numerical Analysis of Spectral Methods. SIAM, Philadelphia.

Hama, F. R. & Peterson, L. F. 1976 Axisymmetric laminar wake behind a slender body of revolution. *J. Fluid Mech.* **76**, 1-15.

Hama, F. R., Peterson, L. F., de la Veaux, S. C. & Williams, D. R. 1977 Instability and transition in axisymmetric wakes. *Proc. Conf. Laminar-Turbulent Transition*, AGARD-CP-224.

Hamielec, A. E., Hoffman, T. W. & Ross, L. L. 1967 Numerical studies of the Navier-Stokes equation for flow past spheres. *A.I.Ch.E.J.* **13**, 212-219.

Harms, V. W. & Wiegel, R. L. 1979 Dye-vector flow visualization -- cooling water model. *J. Waterway, Port, Coastal and Ocean Division ASCE.* **105**, 293-312.

Harpole, G. M. 1981 Droplet evaporation in high temperature environments. *J. Heat Transfer.* **103**, 86-91.

Jackson, C. P. 1987 A finite-element study of the onset of vortex shedding in flow

past variously shaped bodies. *J. Fluid Mech.* **182**, 23-45.

Jayaweera, K. O. L. F. & Mason, R. J. 1965 The behavior of freely falling cylinders and cones in a viscous fluid. *J. Fluid Mech.* **22**, 709-720.

Jenson, V. G. 1959 Viscous flow round a sphere at low Reynolds numbers. *Proc. Roy. Soc.* **A 249**, 346-366.

Kalra, T. R. & Uhlherr, P. H. T. 1973 Geometry of bluff body wakes. *Can. J. Chem. Eng.* **51**, 655-658

Kawaguti, M. 1955 The critical Reynolds number for the flow past a sphere. *J. Phys. Soc. Jap.* **10**, 694-699.

Kendall, J. M. 1964 The periodic wake of a sphere. *Space Programs Summary* No. 37-25, Volume IV, Jet Propulsion Laboratory, Pasadena, Calif.

Kim, H. J. & Durbin, P. A. 1988 Observations of the frequencies in a sphere wake and of drag increase by acoustic excitation. *Phys. Fluids.* **31**, 3260-3265.

Kim, I. & Pearlstein, A. J. 1989 Stability of the flow past a sphere. *J. Fluid Mech.* accepted for publication.

Kim, I. & Pearlstein, A. J. 1989 Flow past a sphere at low and intermediate Reynolds numbers. *J. Fluid Mech.*, to be submitted.

Le Clair, B. P., Hamielec, A. E. & Pruppacher, H. R. 1970 A numerical study of the drag on a sphere at low and intermediate Reynolds numbers. *J. Atmos. Sci.* **27**, 308-315.

Lessen, M. & Singh, P. J. 1973 The stability of axisymmetric free shear layers. *J. Fluid Mech.* **60**, 433-457.

Letan, R. & Kehat, E. 1968 The mechanism of heat transfer in a spray column heat exchanger. *A.I.Ch.E. J.* **14**, 398-405

Lin, C. L. & Lee, S. C. 1973 Transient state analysis of separated flow around a

sphere. *Computers and Fluids.* **1**, 235-250.

Lin, C. L., Pepper, D. W., & Lee, S. C. 1976 Numerical methods for separated flow solutions around a circular cylinder. *AIAA J.* **14**, 900-907.

MacCready, P. B. & Jex, H. R. 1964 Study of sphere motion and balloon wind sensors. NASA TM X-53089.

Masliyah, J. H. 1972 Steady wakes behind oblate spheroids: flow visualization. *Phys. Fluids*, **15**, 1144-1146.

Maxworthy, T. 1965 Accurate measurement of sphere drag at low Reynolds numbers. *J. Fluid Mech.* **23**, 369-372.

Möller, W. 1938 Experimentelle Untersuchengen zur Hydrodynamik der Kugel. *Phys. Z.* **39**, 57-80.

Monkewitz, P. A. & Nguyen, L. N. 1987 Absolute instability in the near-wake of two-dimensional bluff bodies. *J. Fluids and Structures*, **1**, 165-184.

Monkewitz, P. A. 1988a The absolute and4 convective nature of instability in two-dimenional wakes at low Reynolds numbers. *Phys. Fluids*, **31**, 999-1006.

Monkewitz, P. A. 1988b A note on vortex shedding from axisymmetric bluff bodies. *J. Fluid Mech.* **192**, 561-575.

Nakamura, I. 1976 Steady wake behind a sphere. *Phys. Fluids*, **19**, 5-8.

Natarajan, R. 1974 Some experimental observations of rotation, oscillation, spinning and swerving of falling burning drops. *Can. J. Chem. Eng.* **52**, 835-837.

Oliver, D. L. R. & Chung J. N. 1987 Flow about a fluid sphere at low to moderate Reynolds numbers. *J. Fluid Mech.* **177**, 1-18.

Peterson, L. F. & Hama, F.R. 1978 Instability and transition of the axisymmetric wake of a body of revolution. *J. Fluid Mech.* **88**, 71-96.

Preukschat, A. W. 1962 Measurements of drag coefficients for falling and rising

spheres in free motion. Aeronautical Engineering Thesis, Calif. Inst. Tech.

Proudman, I. & Pearson, J. R. A. 1957 Expansions at small Reynolds numbers for the flow past a sphere and a circular cylinder. *J. Fluid Mech.* **2**, 237-262.

Provansal, M., Mathis, C. & Boyer, L. 1987 Benard-von Karman instability: transient and forced regimes. *J. Fluid Mech.* **182**, 1-22.

Pruppacher, H. R., Le Clair, B. P. & Hamielec, A. E. 1970 Some relations between drag and flow pattern of viscous flow past a sphere and a cylinder at low and intermediate Reynolds numbers. *J. Fluid Mech.* **44**, 781-790.

Rimon, Y. & Cheng S. I. 1969 Numerical solution of a uniform flow over a sphere at intermediate Reynolds numbers. *Phys. Fluids.* **12**, 949-959.

Roos, F. W. 1968 An experimental investigation of the unsteady flows about spheres and disks. Ph.D. Dissertation, Univ. Michigan.

Roos, F. W. & Willmarth, W. W. 1971 Some experimental results on sphere and disk drag. *AIAA J.* **9**, 285-291.

Sato, H. & Okada, O. 1966 The stability and transition of an axisymmetric wake. *J. Fluid Mech.* **26**, 237-253.

Sayegh, N. N. & Gauvin, W. H. 1979 Calculation of variable property heat transfer to spheres. *A.I.Ch.E. J.* **25**, 522-534.

Segur, J. B. & Oberstar, H. E. 1951 Viscosity of glycerol and its aqueous solutions. *Ind. Eng. Chem.* **43**, 2117-2120.

Shafrir, U. 1965 Horizontal oscillations of falling spheres. AFCRL-65-141.

Sheth, R. B. 1970 Secondary motion of freely falling spheres. M.S. Thesis, Brigham Young University, Provo, Utah.

Stringham, G. E. , Simons, D. B. & Guy, H.P. 1969 The behavior of large particles falling in quiescent liquids. U.S. Geol. Survey Prof. Paper 562C.

Taneda, S. 1956 Studies on wake vortices (III). Experimental investigation of the wake behind a sphere at low Reynolds numbers. *Reports of Research Institute for Applied Mechanics, Kyushu Univ.* **4**, 99-105. (See also *J. Phys. Soc. Jpn.* **11**, 1104-1108.)

Thoman, D. C. & Szewczyk, A. A. 1969 Time-dependent flow over a circular cylinder. *Phys. Fluids, Supp. II*, 76-87.

Tiwary, R. & Reethof, G. 1986 Hydrodynamic interaction of spherical aerosol particles in a high intensity acoustic field. *J. Sound Vib.* **108**, 33-39.

Torobin, L. B. & Gauvin, W. H. 1959 Fundamental aspects of solids-gas flow. Part II. The sphere wake in steady laminar flow. *Can. J. Chem. Eng.* **37**, 167-176.

Toulcova, J. & Podzimek, J. 1968 Contribution to the question of the catching of aerosol particles in the wake of falling water droplets. *J. de Rech. Atmos.* **3**, 89-95.

Van Dyke, M. 1975 *Perturbation Methods in Fluid Mechanics, Annotated Edition.* Parabolic Press, Stanford, Calif.

Vardelle, M., Vardelle, A. Fauchais, P. & Boulos, M. I. 1983 Plasma-particle mass and heat transfer. *A.I.Ch.E. J.* **29**, 236-243.

Viets, H. 1971 Accelerating sphere-wake interaction. *AIAA J.* **9**, 2087-2089.

Viets, H. & Lee, D. A. 1971 Motion of freely falling spheres at moderate Reynolds number. *AIAA J.* **9**, 2038-2042.

Wang, P. K. & Pruppacher, H. R. 1977 An experimental determination of the efficiency with which aerosol particles are collected by water drops in subsaturated air. *J. Atmos. Sci.* **34**, 1664-1669.

Willmarth, W. W., Hawk, N. E., & Harvey, R. E. 1964 Steady and unsteady motions and wakes of freely falling disks. *Phys. Fluids*, **7**, 197-208.

Zarin, N. A. 1970 Measurement of non-continuum and turbulence effects on subsonic sphere drag. NASA CR-1585.

Zarin, N. A. & Nicholls, J. A. 1971 Sphere drag in solid rockets -- Noncontinuum and turbulence effects. *Comb. Sci. Tech.* 3, 273-285.

Zebib, A. 1984 A Chebyshev method for the solution of boundary value problems. *J. Comput. Phys.* 53, 443-455.

Zebib, A. 1987 Stability of viscous flow past a circular cylinder. *J. Engr. Math.* 21, 155-165.

Zikmundova, J. 1970 Experimental investigation of the wake behind a sphere and a spheroid for Reynolds numbers from 44 to 495. *J. de Rech. Atmos.* 4, 7-18.